AD-A081 315 NATIONAL BUREAU OF STANDARDS WASHINGTON DC NATIONAL E--ETC F/G 17/7
A STANDARD FOR RF MODULATION FACTOR,(U)
SEP 79 W G ARTHUR, G R REEVE
UNCLASSIFIED NBS-TN-1016 FAA-RD-79-94 NL

1 OF 1
AD
A081315

END
DATE FILMED
4-80
DDC

Report No. FAA-RD-79-94

LEVEL II 12

A Standard For RF Modulation Factor

M. G. Arthur
G. R. Reeve

Electromagnetic Fields Division
National Engineering Laboratory
National Bureau of Standards
Boulder, Colorado 80303

September 1979

Prepared for

U.S. DEPARTMENT OF TRANSPORTATION
FEDERAL AVIATION ADMINISTRATION
Systems Research & Development Service
Washington, D.C. 20590

NOTICE

This document is disseminated under the sponsorship of the Department of Transportation in the interest of information exchange. The United States Government assumes no liability for its contents or use thereof.

NBS-114A (REV. 8-78)

U.S. DEPT. OF COMM. BIBLIOGRAPHIC DATA SHEET	1. PUBLICATION OR REPORT NO. NBS-TN-1016 FAA-RD-79-94	

4. TITLE AND SUBTITLE

A STANDARD FOR RF MODULATION FACTOR

5. Publication Date: Sept 79

6. AUTHOR(S)

M. G. Arthur G. R. Reeve

8. Performing Organ. Report No.

9. PERFORMING ORGANIZATION NAME AND ADDRESS

NATIONAL BUREAU OF STANDARDS
DEPARTMENT OF COMMERCE
WASHINGTON, DC 20234

11. Contract/Grant No.

12. SPONSORING ORGANIZATION NAME AND COMPLETE ADDRESS (Street, City, State, ZIP)

Federal Aviation Administration
800 Independence Avenue, S. W.
Washington, D. C. 20591

13. Type of Report & Period Covered

15. SUPPLEMENTARY NOTES

☐ Document describes a computer program; SF-185, FIPS Software Summary, is attached.

16. ABSTRACT (A 200-word or less factual summary of most significant information. If document includes a significant bibliography or literature survey, mention it here.)

A modulation factor standard has been developed to support the Federal Aviation Administration's requirements for a measurement capability for the ILS and VOR navigation systems. The standard consists of both a precision modulation meter and a stable amplitude-modulated signal source. Although designed primarily for ILS and VOR signals, it has general purpose capabilities within an rf range of 10 MHz to 500 MHz and an af range of 20 Hz to 20 kHz. Measurement uncertainty is less than 0.11 percent modulation below 90 percent modulation for ILS/VOR tones of 90 Hz and above, and is somewhat greater at 30 Hz. Included are a circuit description and an error analysis.

18. FAA-RD

19. 79-94

17. KEY WORDS (six to twelve entries; alphabetical order; capitalize only the first letter of the first key word unless a proper name; separated by semicolons)

Amplitude modulation; instrument landing system (ILS); measurement instrumentation; measurement standard; modulation; modulation factor; modulation meter; Newton-Raphson method; percent modulation; signal generator; vhf omnidirectional radio range (VOR).

18. AVAILABILITY	19. SECURITY CLASS (THIS REPORT)	21. NO. OF PRINTED PAGES
☒ Unlimited	UNCLASSIFIED	92
☐ For Official Distribution. Do Not Release to NTIS		
☐ Order From Sup. of Doc., U.S. Government Printing Office, Washington, DC 20402,	20. SECURITY CLASS (THIS PAGE)	22. Price
☒ Order From National Technical Information Service (NTIS), Springfield, VA. 22161	UNCLASSIFIED	

USCOMM-DC

411010

CONTENTS

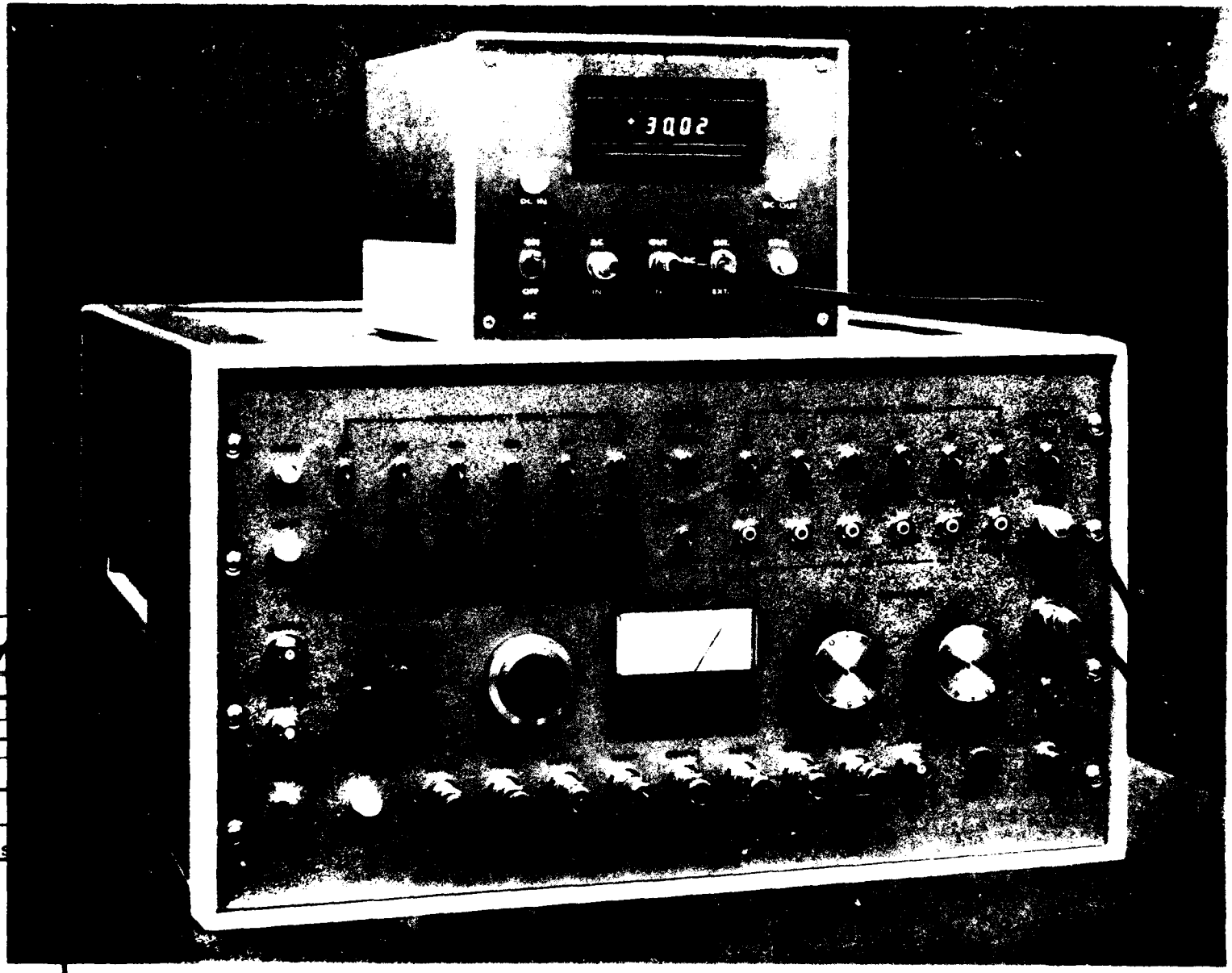

Fig. 1. NBS modulation factor standard

A Standard For RF Modulation Factor

M. G. Arthur
G. R. Reeve

Abstract

A modulation factor standard has been developed to support the Federal Aviation Administration's requirements for a measurement capability for the ILS and VOR navigation systems. The standard consists of both a precision modulation meter and a stable amplitude-modulated signal source. Although designed primarily for ILS and VOR signals, it has general purpose capabilities within an rf range of 10 MHz to 500 MHz and an af range of 20 Hz to 20 kHz. Measurement uncertainty is less than 0.11 percent modulation below 90 percent modulation for ILS/VOR tones of 90 Hz and above, and is somewhat greater at 30 Hz. Included are a circuit description and an error analysis.

Key words: Amplitude modulation; instrument landing system (ILS); measurement instrumentation; measurement standard; modulation; modulation factor; modulation meter; Newton-Raphson method; percent modulation; signal generator; vhf omnidirectional radio range (VOR).

1. Introduction

This report describes a modulation standard which the National Bureau of Standards (NBS) developed at the request of the Federal Aviation Administration (FAA) in support of their air navigation programs. This standard is intended as a laboratory instrument for use at the highest echelon of measurement accuracy. It provides two capabilities, viz., (1) an amplitude-modulated radiofrequency signal of known modulation factor, and (2) a meter for measuring the modulation factor of an amplitude-modulated signal. Figure 1 is a photograph of this instrument.

Although this standard was developed primarily for use with air navigation systems, it has measurement capabilities beyond those specifically required by such systems. Therefore, it can serve a wider variety of applications than was originally specified.

The basic specifications of the standard are as follows:

I. Modulation Meter

a. RF Frequency Range: 10 MHz to 500 MHz
b. AF Frequency Range: 20 Hz to 20 kHz
c. Modulation Factor Range: 0.10 to 0.90 (at stated accuracy)
d. RF Operating Level: 1.8 volts rms minimum
e. Input Impedance: 50Ω nominal
f. Accuracy: $\pm$ 0.0011 (modulation factor units) or better for modulation tones above 90 Hz. $\pm$0.0012 at 30 Hz and 30 percent modulation. See figure 17, and tables 5 and 6.
g. Resolution: 0.0001 (modulation factor units)
h. AF Bandpass Filters: 30 Hz, 90 Hz, 150 Hz, 9960 Hz

II. Signal Source

a. RF Frequency Range: 10 MHz to 500 MHz with external generator; 108 MHz, 110 MHz, 112 MHz, 115 MHz, 118 MHz, 328 MHz, 332 MHz, 336 MHz internal oscillators, crystal-controlled
b. AF Frequency Range: 20 Hz to 20 kHz with external generator; 90 Hz and 150 Hz internal oscillators, crystal-controlled or phase-locked to 60 Hz line frequency.
c. Modulation Factor Range: 0.00 to 1.00
d. Output Level: -8 dBm to +12 dBm. Output adjustable in 1 dB steps
e. Output Impedance: 50Ω nominal
f. Accuracy: Unspecified (derives accuracy from modulation meter)

2. Background

2.1. Purpose

The two navigation systems which the modulation standard supports are (1) the Instrument Landing System (ILS), and (2) the Very High Frequency Omnidirectional Radio Range (VOR) system. Each system requires careful adjustment of electronic system parameters in order to assure safe operations for their users.

FAA test equipment includes both modulation meters and signal generators. Therefore, the NBS standard is designed to calibrate both types of devices; i.e., it contains a signal source for calibrating modulation meters, and separately, a modulation meter for calibrating generators or measuring the amplitude modulation factor of other sources.

In the NBS standard, the meter serves as the precision instrument and has been thoroughly evaluated. The signal source, although of high quality, is not intended as an independent source of known characteristics. Its "calibration" is provided continuously by the companion precision modulation meter.

2.2. Characteristics of Air Navigation Signals

The essential characteristics of ILS and VOR navigation signals, as related to this work, are given below. More complete information is contained in standard reference sources on this subject [1].

2.2.1. ILS

The ILS provides landing guidance to aircraft by means of amplitude-modulated radiofrequency signals. Lateral guidance information is provided by the Localizer signal which operates in the 108 MHz to 112 MHz band. Vertical guidance (angle of descent) information is provided by the Glide Slope signal, operating in the 328 to 336 MHz band.

Each rf carrier is amplitude modulated by two audiofrequency tones of 90 Hz and 150 Hz. Equal amounts of modulation received at the aircraft indicate an on-course condition; unequal amounts indicate an off-course condition in proportion to the difference in depth of modulation (DDM) of the two tones.

The Localizer on-course depth of modulation at the aircraft is 0.20 (i.e., 20 percent modulation), plus or minus 0.01 for Category III (highest precision) localizers. Full scale indication on the aircraft's cross-pointer meter occurs for a DDM of 0.155. The corresponding figures for the Glide Slope modulation are 0.40 ± 0.025, and 0.175 DDM.

Inasmuch as guidance information is provided specifically by the DDM of the two tones, the accurate measurement of modulation factor is essential to the accurate functioning of the system.

2.2.2. VOR

The VOR system provides enroute navigation guidance by means of radio signals operating in the 112 MHz to 118 MHz band. Bearing information is contained in the phase relationship between two 30 Hz tones, one of which (the variable phase tone) amplitude modulates the rf carrier directly, and the other (the reference phase tone) frequency modulates a 9960 Hz subcarrier which in turn amplitude modulates the rf carrier. The depth of modulation of the rf carrier by each of these two tones (30 Hz variable phase and 9960 Hz subcarrier) is 0.30 ± 0.02.

Note that in the VOR system depth of modulation is not critical to the navigation accuracy of the system.

2.3. Accuracy Considerations

Two accuracy considerations are discussed in this section: (1) Operational accuracies of the ILS and VOR systems, and (2) measurement accuracies needed at the topmost level of the measurement hierarchy to support these systems.

2.3.1. ILS and VOR Operational Accuracies

The required spatial alignment accuracy of the ILS Localizer signal for a Category III installation corresponds to a DDM accuracy of ± 0.00435. For the Glide Slope signal, it is ± 0.035. There is no equivalent accuracy requirement for modulation factor for the VOR system inasmuch as its navigation guidance derives from a phase difference as stated above. However, it is good operating practice to maintain modulation factor to well within the ± 0.02 tolerance.

Thus, the Localizer accuracy requirement, being the most stringent, determines the accuracy requirement of the NBS modulation standard.

2.3.2. Measurement Accuracy

By mutual agreement with FAA, NBS set a target accuracy of ± 0.00125 for its modulation meter for modulation factor values between 0.20 and 0.80 (i.e., ± 0.125 percent modulation between 20 and 80 percent modulation). This figure is obtained as follows: The FAA desired its instruments to have a measurement uncertainty no worse than ± 0.005. The NBS instrument used to calibrate the FAA instruments must have a greater accuracy; a factor of 4:1 has been found suitable based upon previous studies of error propagation [2]. Thus, $0.005 \div 4 = 0.00125$.

2.4. Measurement Requirements

Considering the foregoing discussions, the modulation standard's basic measurement requirements for navigation signals are as follows:

a. RF Range: 108 to 118 MHz; 328 to 336 MHz
b. AF Tones: 30, 90, 150, 9960 Hz
c. Modulation Factor Range: 0.20 to 0.80
d. Accuracy: ± 0.00125

3. Amplitude Modulation

3.1. Introduction

"Amplitude modulation is the process, or the result of the process, whereby the amplitude of one electrical quantity is varied in accordance with some selected characteristic of a second quantity, which need not be electrical in nature." (IEEE Std. 100-1977, 2nd Edition)

The subject of amplitude modulation has been adequately covered in the open literature and reference textbooks [3]. This section contains a brief description of selected aspects of amplitude modulation that pertain to the design of the NBS modulation standard.

3.2. Modulation Factor

"Modulation factor (amplitude-modulated wave) is the ratio (usually expressed in percent) of the peak variation of the envelope from its reference value, to the reference value. Notes: (1) For modulating functions having unequal positive and negative peaks, both positive and negative modulation factors are defined, respectively, in terms of the positive or negative peak variations. (2) The reference value is usually taken to be the amplitude of the unmodulated wave..." (IEEE Std. 100-1977, 2nd Edition)

Depth of modulation is specified by either of two terms, modulation factor or percent modulation. It is a dimensionless ratio and, in principle, does not derive from any of the international system (SI) of units of measurement. However, it has been customary (but not essential) to consider it as the ratio of two voltages.

Consider an ideal amplitude-modulated signal waveform, $v(t)$, that is produced when the amplitude, V_c, of a sinusoidal voltage, $v_c(t)$, is varied by a second sinusoidal voltage, $v_m(t)$, in accordance with the following formula:

$$\text{Varying amplitude of } v(t) = V_c + v_m(t). \tag{1}$$

Thus, if

$$v_c(t) = V_c \cos 2\pi f_c t \tag{2}$$

and

$$v_m(t) = V_m \cos 2\pi f_m t, \tag{3}$$

then

$$v(t) = (V_c + V_m \cos 2\pi f_m t) \cos 2\pi f_c t, \tag{4}$$

where V_c and V_m are constants. This ideal model represents the type of modulation process used to generate the navigation signals under consideration in this report.

Equation (4) may be written as

$$v(t) = V_c(1 + m \cos 2\pi f_m t) \cos 2\pi f_c t. \tag{5}$$

The factor m, where

$$m = \frac{V_m}{V_c}, \tag{6}$$

is the modulation factor of v(t). Percent modulation is derived from m as follows:

$$\text{Percent modulation} = m \times 100 \text{ percent}. \tag{7}$$

Modulation factor and percent modulation describe the degree of modulation of v(t) when the modulating waveform, $v_m(t)$, has the same peak amplitude in both the positive and negative directions. Otherwise, a single value for m is inadequate to describe the degree of modulation because it may be different in the positive direction as compared with the negative direction. In such cases, it is useful to speak of the modulation factor in the positive or "upward" direction as the ratio of the positive peak amplitude of the modulating waveform to the amplitude of the carrier voltage, and the modulation factor in the negative or "downward" direction as the ratio of the negative peak amplitude of the modulating waveform to the amplitude of the carrier voltage.

Alternatively, inasmuch as any arbitrary waveform can be analyzed into a set of sinusoidal components by the method of Fourier analysis, each sinusoidal component of $v_m(t)$ has a definite amplitude and hence a definite modulation factor associated with it. In the case of the navigation signals under consideration, each component (e.g., 90 Hz) has a definite modulation factor associated with it regardless of what other modulating components may be present, either by intent or by unintended consequences (e.g., distortion products).

Thus, modulation factor may be viewed in two ways: First, as a characteristic of the amplitude-modulated waveform; and second, as a measure of the relative amplitude of a given modulation component. For a sinusoidal modulation, $v_m(t)$, these two concepts become one and the same.

3.3. Range of Modulation Factor

If the modulating waveform, $v_m(t)$, has equal positive and negative peak amplitudes, the maximum amplitude of v(t), from eq (5), is

$$V_c(1 + m),$$

and the minimum amplitude of the envelope of v(t) is

$$V_c(1 - m).$$

The ratio, R, of these two quantities is the dynamic range of the envelope of v(t).

$$R = \frac{1 + m}{1 - m}. \tag{8}$$

Table 1 shows R as a function of m. The large size of R for large m necessitates an adequate dynamic range in a modulation meter if it is to provide accurate measurements.

Table 1. Ratio of maximum to minimum envelope amplitude as a function of modulation factor

m	R	R(dB)
0.10	1.222	1.74 dB
0.20	1.500	3.52
0.30	1.857	5.38
0.40	2.333	7.36
0.50	3.000	9.54
0.60	4.000	12.04
0.70	5.666	15.07
0.80	9.000	19.08
0.90	19.000	25.58
0.99	199.000	45.98

4. Measurement of Modulation Factor

4.1. Introduction

Of the many modulation factor measurement methods (references [4] through [14] provide a sampling) that have been employed since the advent of amplitude-modulated radio transmission, the following are considered to be potentially capable of the accuracy required of a national standard:

a. RF RMS Method
b. RF Demodulator Method
c. Spectrum Analyzer Method
d. Oscilloscopic Methods (three)
e. Sampling Method

A brief description of each of these methods is given below. The rf demodulator method was chosen for the NBS standard and is described in section 4.2. A general discussion of modulation meter requirements has been given by Gaudernack [15]. A brief discussion of the major shortcomings of the above methods completes this introductory section.

4.1.1. RF RMS Method

The root-mean-square value, v(rms), of the voltage v(t), eq (5), is given by the equation

$$v(\text{rms}) = \frac{V_c}{\sqrt{2}}\left(1 + \frac{m^2}{2}\right)^{1/2} . \qquad (9)$$

A modulation meter based on this relationship has appeal because it can employ highly accurate square-law devices. Strafford [7] described such a meter in 1934. However, this method does not discriminate against multiple modulation components of the signal, and if more than one component is present, the method yields an "average" modulation factor.

4.1.2. RF Demodulator Method

If the voltage v(t) is applied to an ideal detector (see sec. A.2.), the output voltage $v_o(t)$, is given by the equation

$$v_o(t) = kV_c(1 + m \cos 2\pi f_m t) \tag{10}$$

where k is a proportionality constant. By well-known techniques of filtering and voltage measurement, the ac component of $v_o(t)$, that is,

$$\text{ac component} = kV_c m \cos 2\pi f_m t,$$

and the dc component, that is,

$$\text{dc component} = kV_c ,$$

can be separated and their amplitude ratio, R_a, can be measured. Thus,

$$R_a = \frac{kV_c m}{kV_c} = m. \tag{11}$$

This method is the basis of many of the techniques described in the papers of references [4] through [14]. In 1929, Jolliffe of NBS [5] described a modulation meter based on this method in which he used a slide-back technique to determine the ac and dc components of $v_o(t)$. A modern and highly accurate version of this method has been described by Sorger [14].

4.1.3. Spectrum Analyzer Method

Equation (5) can be written as

$$v(t) = V_c \cos 2\pi f_c t + \frac{mV_c}{2} [\cos 2\pi(f_c - f_m)t + \cos 2\pi(f_c + f_m)t] \tag{12}$$

which clearly shows that the amplitude of the sidebands at frequencies $(f_c - f_m)$ and $(f_c + f_m)$ is $mV_c/2$. A spectrum analyzer can be used to measure the voltage ratio R_v, where

$$R_v = \frac{mV_c/2}{V_c} ; \tag{13}$$

therefore,

$$m = 2R_v . \tag{14}$$

This method has the ability to discriminate against amplitude distortion products, but the measurement accuracy may be limited by resolution and accuracy of critical circuits [16].

4.1.4. Oscilloscopic Methods

The oscilloscope can be employed in several different ways to measure modulation factor directly [12]. In addition, it has been used as a component of other methods, such as the rf demodulator method and the spectrum analyzer method. Three direct-measurement methods are described below.

4.1.4.1. Envelope Method

If the voltage v(t) is applied to the oscilloscope's vertical input port and a suitable linear ramp voltage to the horizontal input port, the outline of the resulting display, as shown in figure 2, represents the envelope of v(t). Modulation factor can be calculated

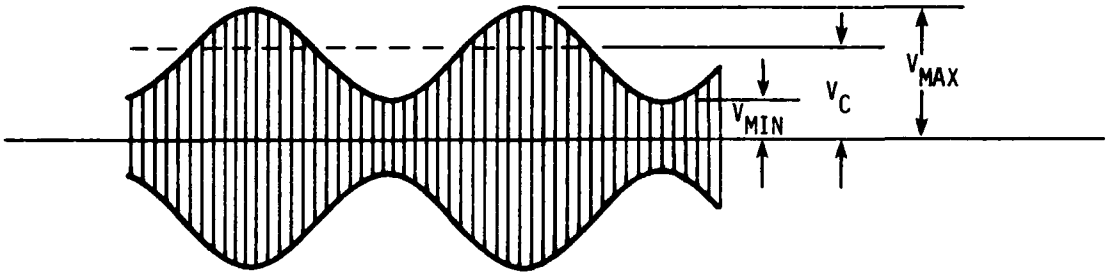

Fig. 2. Envelope waveform for envelope oscilloscopic method

from the dimensions of this pattern. For example, for equal positive and negative modulation, the carrier amplitude will be given by

$$V_c = \frac{V_{max} + V_{min}}{2} \tag{15}$$

where V_{max} and V_{min} are the maximum and minimum amplitudes, respectively, of the envelope pattern. Then,

$$m = \frac{V_{max} - V_c}{V_c} , \tag{16}$$

or

$$m = \frac{V_c - V_{min}}{V_c} , \tag{17}$$

or

$$m = \frac{V_{max} - V_{min}}{V_{max} + V_{min}} . \tag{18}$$

4.1.4.2. Ring-Pattern Method

If the voltage v(t) is applied to a resistance-capacitance phase splitter, as shown in figure 3, an elliptical pattern is produced from which modulation factor can be calculated.

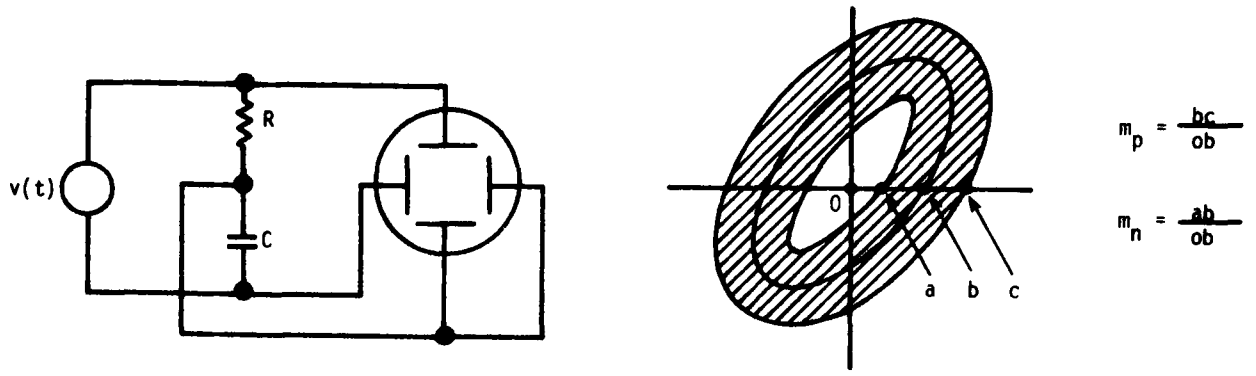

Fig. 3. Schematic diagram and elliptical pattern for ring-pattern oscilloscopic method

The ellipse that cuts the horizontal axis at b is produced by voltage V_c. The shaded area within and without this ellipse is produced by voltage $v_m(t)$. Thus the outer ellipse that cuts the axis at c represents the crest of the envelope of v(t), and the inner ellipse that cuts the axis at a represents the trough of v(t). Positive and negative modulation factors, m_p and m_n, are given by the equations

$$m_p = \frac{bc}{ob} , \tag{19}$$

$$m_n = \frac{ab}{ob} . \tag{20}$$

4.1.4.3. Trapezoid Method

When the modulation voltage, $v_m(t)$, is available, it can be applied to the horizontal deflection plates which, with the modulated voltage, v(t), applied to the vertical plates, will produce the trapezoidal pattern as shown in figure 4. For symmetrical modulation, the modulation factor is calculated from the vertical dimensions of the trapezoid by the equation

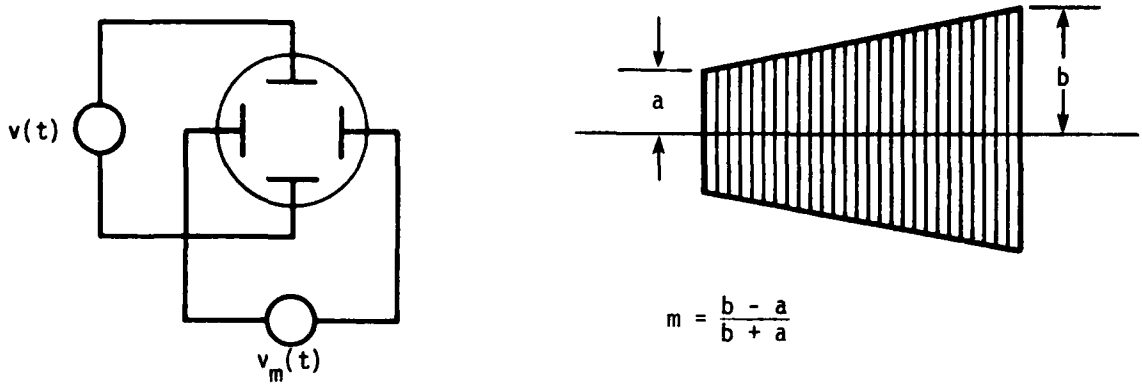

Fig. 4. Schematic diagram and trapezoidal pattern for trapezoidal oscilloscopic method

$$m = \frac{b - a}{b + a} , \tag{21}$$

where a and b are defined in figure 4.

4.1.5. Sampling Method

The sampling method is based on a technique by which the peak power, P_1, at the crest of the envelope of v(t), is measured, and then the peak power, P_2, at the bottom of the trough of v(t)'s envelope is measured, both measurements being made in a very narrow time interval. This is similar in concept to the oscilloscopic envelope method. The basic instrumentation for making these measurements has been described by Hudson et al. [17]. The modulation factor is related to the power ratio, R_p, by the equation

$$m = \frac{1 - \sqrt{R_p}}{1 + \sqrt{R_p}} \tag{22}$$

where

$$R_p = \frac{P_2}{P_1} . \tag{23}$$

4.1.6. Comparative Evaluation of Measurement Methods

The relative merits of these seven methods were examined in terms of the following factors:

a. Potential accuracy
b. Realizability
c. Development cost
d. Maintenance cost

The following is a brief summary of the conclusions drawn from this examination.

First, there appears to be no fundamental technical reason that any of these methods could not be developed to the point of meeting the requirements listed in section 2.4, given enough time and money. However, some methods would require much more effort than others.

Here are the major technical problems of each method. The rf rms method requires complicated and state-of-the-art filtering techniques to measure the modulation factor of complex waveforms. The rf demodulator method requires a highly linear rf detector, or else a detector whose transfer characteristic is well known. The spectrum analyzer method requires significant improvements in circuit accuracy and stability and in cathode-ray tube design to reduce its measurement uncertainty below the ± 2.54 dB uncertainty typically achieved with present commercial equipment [16]. Note especially that the VOR signal requires large frequency stability and sharp filters to accurately resolve the 30 Hz tone from the carrier frequency. As for the oscilloscopic methods, both the envelope and the ring-pattern methods suffer a severe sensitivity and accuracy loss at small values of modulation factor, and the trapezoid method does likewise at large values. One commercial firm has produced a refined instrument based upon the envelope method for which they claim a "consistency of measurement" of 0.02 percent "statistically," but no clear accuracy statement is made. This instrument does, however, suggest that further development of this method could be fruitful. The sampling method requires the careful design of low-jitter gating circuits and very low-noise detectors. These are within the state of the art, however.

In addition to these major problems, each method has its own distinctive set of secondary technical problems that must be solved, such as are related to optimizing the circuits for the particular characteristics of ILS and VOR signal waveforms and devising test schemes to evaluate the actual performance of the fabricated instrument. No method appears to have fewer or less formidable technical problems than another.

At the time this work began, the relative development cost was judged to be lowest for the rf demodulator method because the techniques it employs have been widely used and proven in electronic instruments and require no new component development. The approximate development cost of some of the other methods was difficult to determine because of new designs that would be necessary to evolve.

The relative maintenance cost is difficult to judge because the final form of some of the unselected methods is not known. However, the rf rms method may be the simplest to maintain because it should be basically less complex than the other methods. The maintenance cost of the other methods should be approximately similar to one another, and should not be excessive.

4.2. NBS Modulation Meter

The NBS modulation meter design is based directly on the definition of modulation factor, eq (6).

$$m = \frac{V_m}{V_c} \tag{6}$$

Figure 5 shows a minimal block diagram of the meter. A detailed circuit description is in section 5.

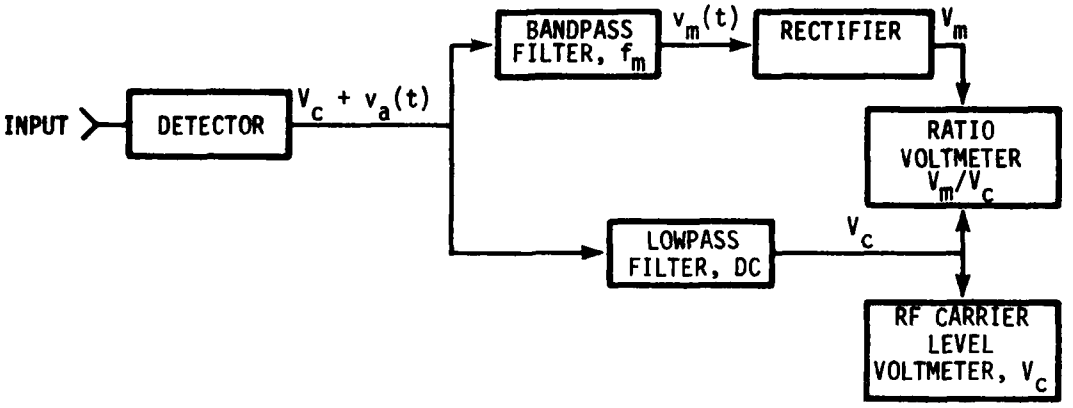

Fig. 5. Block diagram of modulation meter

4.2.1. Ideal Operation

The amplitude-modulated signal is rectified by an envelope detector. Ideally, the detector output voltage is the sum of (a) dc voltage V_c, which is proportional to the unmodulated rf carrier level; and (b) ac voltage $v_a(t)$, which is proportional to the modulation waveform of the amplitude-modulated rf signal. Voltage V_c is separated from $v_a(t)$ by a low-pass filter. The band pass filter selects the audiofrequency component, $v_m(t)$, at frequency f_m. The rectifier output is a dc voltage, V_m, proportional to the amplitude of $v_m(t)$. The ratio, V_m/V_c, is measured and displayed by the ratio voltmeter. The several proportionality constants (voltage gains) are adjusted to make this ratio numerically equal to the modulation factor for modulation frequency f_m.

4.2.2. Actual Operation

No measurement system is ideal, and the above description must be modified accordingly. In general, components and circuits have a limited dynamic range and bandwidth over which their transfer characteristics are independent of impressed voltage or frequency. Also, other deviations from ideality may exist, such as sensitivity to changes in supply voltages or environmental conditions.

The NBS meter is designed, constructed, and operated so as to reduce the effects of supply voltage and temperature variations to insignificance. However, circuit nonlinearities and bandwidth limitations must be carefully accounted for in an instrument of this quality. This is done by measuring these characteristics, determining their effects

upon the voltage ratio, M, indicated by the instrument, and applying the necessary corrections to obtain a precise value for m.

Thus, the NBS technique for measuring modulation factor involves two steps. First, a measurement is made with the NBS modulation meter. Then, the meter reading, M, is corrected for known errors associated with the meter circuits. (An alternate technique for ILS tones and for the lower VOR tone eliminates one source of error in the second step; this is discussed in Appendix B.) Three corrections are applied to the modulation meter's ratio voltmeter reading: (1) Audiofrequency response correction, (2) post-detector nonlinearity correction, and (3) detector nonlinearity correction. These are given below. Voltage, V_c, measured by a separate voltmeter, is required for the latter correction. Refer to Appendix A for a detailed description of these corrections and how they are determined.

4.2.2.1. Audiofrequency Response Correction

The modulation meter's audiofrequency measurement bandwidth is limited primarily by the post-detector networks. Here, bandwidth refers to the range of modulation frequencies, f_m, that can be measured, and not to the bandwidth of the audiofrequency bandpass filters. Figure 6 and table 2 show the relative gain as a function of frequency of the post-detector ac channel, operating in the wideband mode (see sec. 5.2.1.3). These data are used to calculate the frequency response correction by the following formula (see sec. A.4):

$$\Delta m_f = M(f_m) \cdot \frac{1 - g(f_m)}{g(f_m)} \qquad (24)$$

where

Δm_f = frequency response correction
$M(f_m)$ = ratio voltmeter reading at frequency f_m
$g(f_m)$ = relative gain at frequency f_m.

Δm_f is to be added to the ratio voltmeter reading before the detector nonlinearity correction is calculated.

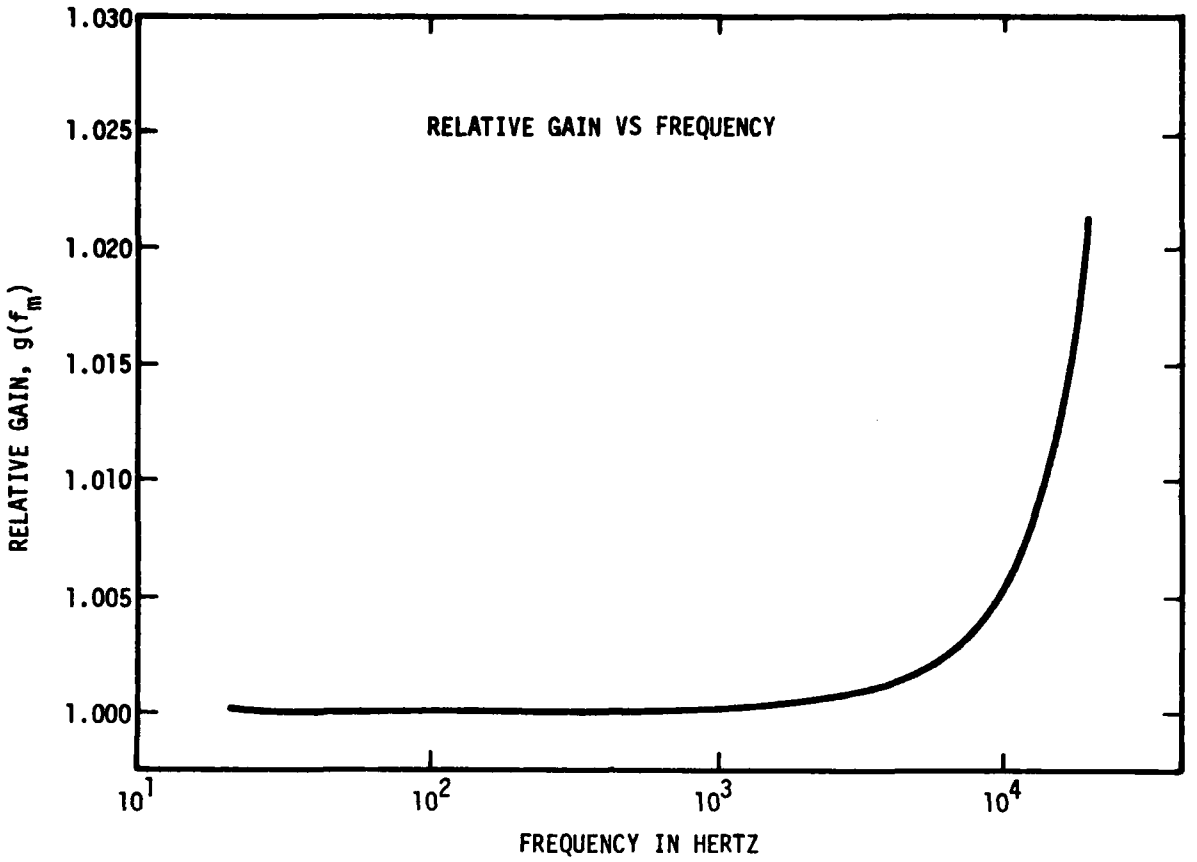

Fig. 6. Relative gain versus frequency

Table 2. Relative audiofrequency gain, $g(f_m)$, at selected frequencies

Frequency, Hz	Relative gain $g(f_m)$	Frequency, Hz	Relative gain, $g(f_m)$
20	1.0002	900	1.0002
30	1.0001	1000	1.0002
40	1.0000	1500	1.0003
50	1.0000	2000	1.0005
60	1.0000	3000	1.0008
70	1.0000	4000	1.0012
80	1.0000	5000	1.0017
90	1.0000	6000	1.0022
100	1.0000	7000	1.0028
150	1.0000	8000	1.0035
200	1.0000	9000	1.0043
300	1.0001	10000	1.0053
400	1.0001	12000	1.0076
500	1.0001	14000	1.0104
600	1.0001	16000	1.0136
700	1.0001	18000	1.0173
800	1.0002	20000	1.0215

4.2.2.2. Post-Detector Nonlinearity Correction

Tests of the post-detector networks reveal amplitude nonlinearities primarily in two circuits: (1) The audiofrequency bandpass filters, and (2) the audiofrequency rectifier. Table 3 shows the post-detector nonlinearity corrections, Δm_n, as a function of frequency for selected values of ratio voltmeter reading, M. Figure 7 shows plots of these data. Δm_n is to be added to the ratio voltmeter reading before the detector nonlinearity correction is calculated.

Table 3. Post-detector nonlinearity correction, Δm_n

M	30 Hz	90 Hz	150 Hz	9960 Hz	Unfiltered
0.1000	0.0005	0.0000	0.0004	0.0002	0.0002
0.2000	0.0003	-0.0001	0.0008	0.0002	0.0002
0.3000	-0.0029	-0.0002	0.0009	0.0001	0.0001
0.4000	-0.0047	-0.0003	0.0010	0.0001	0.0001
0.5000	-0.0046	-0.0004	0.0010	0.0000	0.0000
0.6000	-0.0033	-0.0003	0.0009	0.0000	0.0000
0.7000	-0.0021	-0.0002	0.0008	0.0000	0.0000
0.8000	-0.0010	-0.0001	0.0006	0.0000	0.0000
0.9000	-0.0005	0.0000	0.0003	0.0000	0.0000

4.2.2.3. Detector Nonlinearity Correction

Because it was not possible within the time and cost constraints of this project to design a demodulator to have both sufficient linearity and bandwidth to completely meet the accuracy goals without correction, the decision was made to build a conventional, stable detector network, carefully measure its nonlinearity characteristic, and, from this information, calculate a corrected value of modulation factor for each measured value, M, given by the ratio voltmeter.

In practice, the calculation is performed on a programmable computer in which the nonlinearity information is stored. However, to illustrate the corrections that result from this process, table 4 shows selected values of modulation factor, m, the corresponding ratio voltmeter corrected readings, M_c (i.e., corrected for post-detector effects), and the resulting detector correction, Δm_d. Figure 8 is a plot of this data.

Table 4. Typical corrections for detector nonlinearity, Δm_d

m	M_c	Δm_d
0.1000	0.1034	-0.0034
0.2000	0.2068	-0.0068
0.3000	0.3102	-0.0102
0.4000	0.4136	-0.0136
0.5000	0.5168	-0.0168
0.6000	0.6199	-0.0199
0.7000	0.7225	-0.0225
0.8000	0.8249	-0.0249
0.9000	0.9264	-0.0264

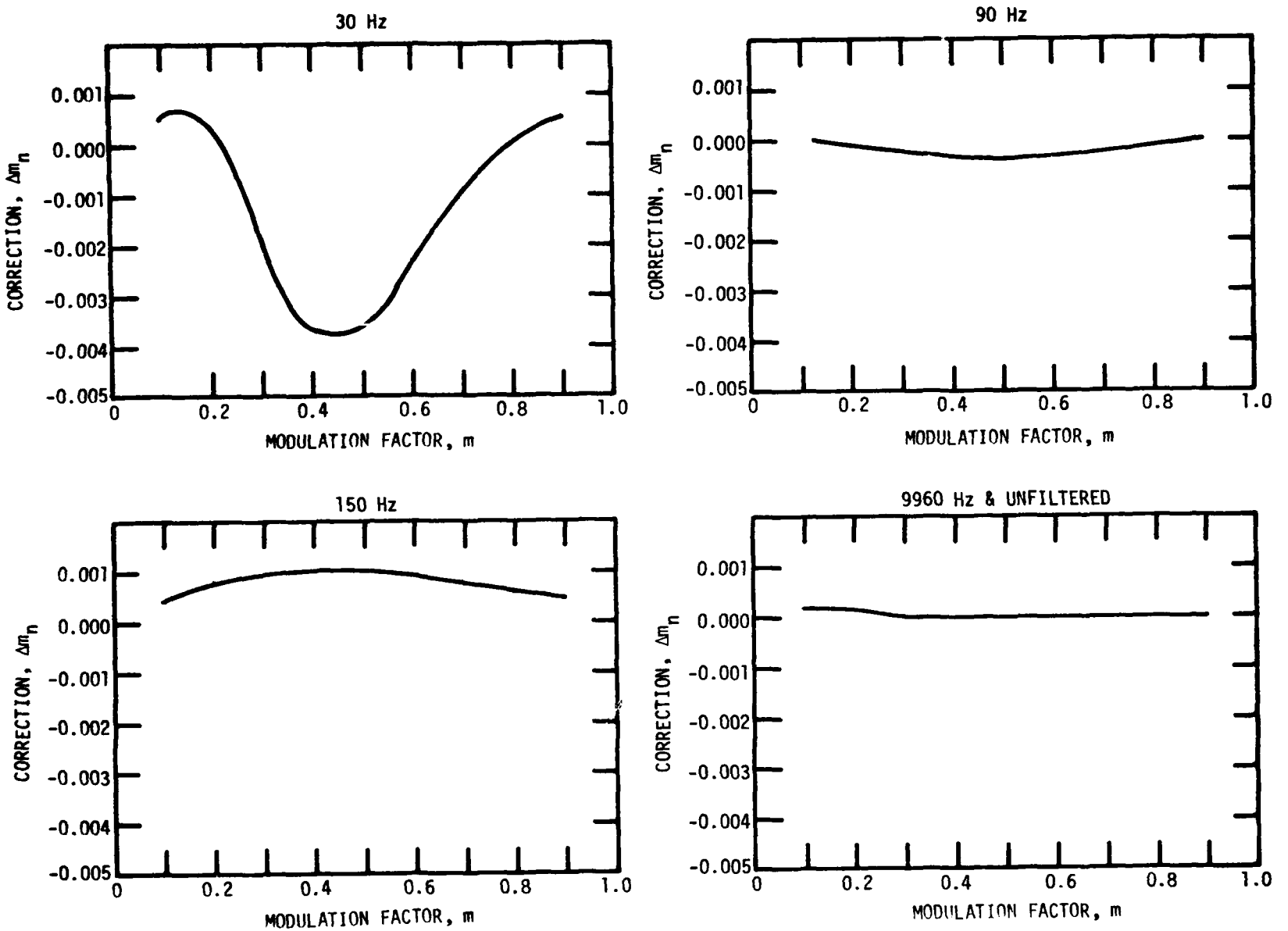

Fig. 7. Post-detector nonlinearity corrections

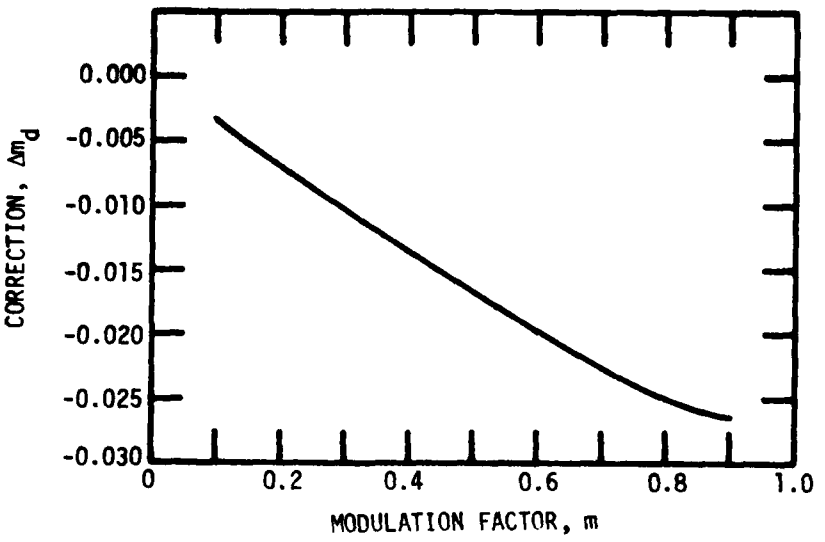

Fig. 8. Detector nonlinearity correction

4.3. Summary of Measurement Corrections

The three corrections to the ratio voltmeter reading, M, are made in this order:

a. Correction for post-detector frequency response: Use the tabulated data of table 2, or figure 6, and the formula of eq (24).

b. Correction for post-detector nonlinearity: Use the tabulated data of table 3, or figure 7.

c. Correction for rf detector nonlinearity: Use the computational procedure described in section A.2.2. For approximate corrections, use the tabulated data of table 4, or figure 8.

Note that the first two corrections are independent of each other and may be made in reverse order. However, the correction for rf detector nonlinearity must be made after these corrections are made because the detector correction pertains only to the detector output voltage.

4.4. Measurement Examples

Suppose a 150 Hz modulation tone is measured and produces a ratio voltmeter reading, M, of 0.4137.

$$M = 0.4137$$

From table 2 and eq (24), the correction for post-detector frequency response is zero. From table 3, the correction for post-detector nonlinearity is

$$\Delta m_n = +0.0010.$$

Thus, the corrected value of M is

$$M_c = 0.4137 + 0.0010 = 0.4147.$$

Using the procedure of section A.2.2 to further correct M_c for rf detector nonlinearity yields

$$m = 0.4011$$

as the measured value of m. Alternatively, from table 4,

$$\Delta m_d = -0.0136$$

so that

$$m = 0.4147 - 0.0136 = 0.4011.$$

If the modulation tone had been 12 kHz, the frequency response correction would be

$$\Delta mf = 0.4137 \cdot \frac{1 - 1.0076}{1.0076}$$

$$= -0.0031.$$

Thus, the corrected value of M would be

$$M_c = 0.4137 - 0.0031 + 0.0010 = 0.4116,$$

and the measured value of m would be

$$m = 0.4116 - 0.0136 = 0.3980.$$

5. Circuit Description of the NBS Modulation Standard

5.1. Introduction

The NBS modulation standard consists of two parts; viz., (1) a precision modulation meter, and (2) a stable signal source. A brief overview description follows below. A detailed description is in section 5.2.

5.1.1. Precision Modulation Meter

A functional block diagram of the modulation meter is shown in figure 9. The amplitude-modulated signal whose modulation factor is to be measured is applied to an envelope detector. The detector's output voltage passes through lowpass (dc) and bandpass or wideband af filters to gain-setting networks. The filtered dc voltage is applied to the reference port of a dual-slope digital voltmeter. Also, an expanded-scale suppressed-zero analog panel meter displays this voltage to the operator. The filtered ac voltage is applied to a precision rectifier network whose dc output voltage is filtered and applied to the measurement port of the voltmeter.

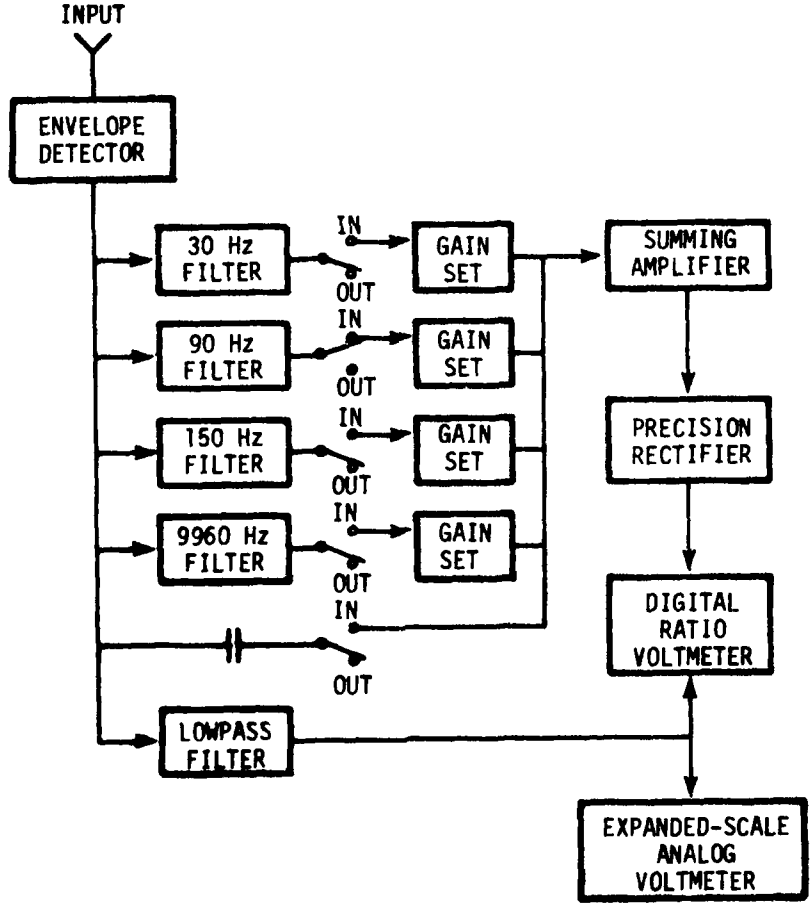

Fig. 9. Functional block diagram of modulation meter

Two or more of the voltages from the af filters may be applied simultaneously to the precision rectifier. In this case, the indicated modulation factor is the average of the positive and negative values of the composite waveform (i.e., the sum of the individual waveforms) from the filters.

5.1.2. Stable Signal Source

A functional block diagram of the signal source is shown in figure 10. The rf carrier voltage is supplied either by one of eight internal crystal-controlled oscillators or by an

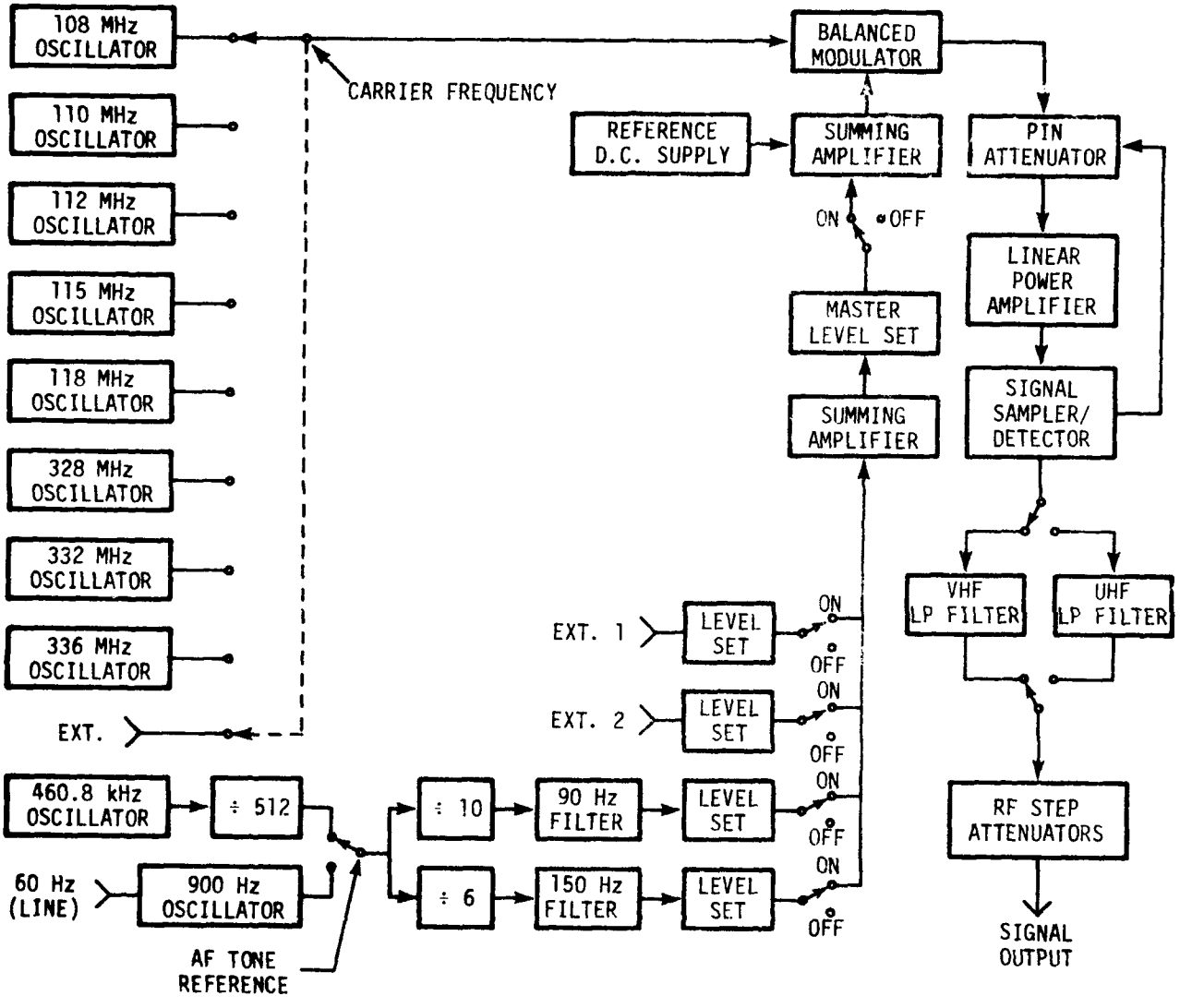

Fig. 10. Functional block diagram of signal source

external signal generator. Similarly, af tone voltages are available from either internal and/or external sources. Internally, 90 Hz and 150 Hz tones are derived either from a crystal-controlled oscillator or from the 60 Hz line voltage, in which case the resulting af tones are phase-locked to the line frequency. For the crystal-controlled case, a 460.8 kHz voltage is divided by 512 to produce a 900 Hz voltage. For the 60 Hz line-derived case, a phase-locked loop oscillator generates a 900 Hz voltage that is synchronized to the line. The 90 Hz and 150 Hz voltages are obtained by frequency division of the 900 Hz voltage, followed by filtering through bandpass filters. Phase adjustment, not shown in figure 10, is also provided.

VOR tones (30 Hz and 9960 Hz) are not generated internally and are obtained from an external VOR af signal generator. Two ports are provided for inputting up to two external signals, which may have any frequency between approximately 20 Hz and 20 kHz.

Each tone channel has an individual voltage level control and on/off switch to control the voltage amplitudes in any desired manner. The af voltages are combined in a summing amplifier which also has a gain control and on/off switch. The composite af voltage is combined with a dc voltage for rf carrier level control, and this final combination is applied to the modulation port of a double-balanced mixer.

RF carrier voltage from one of the sources mentioned above is applied to the mixer's carrier input port. The amplitude-modulated rf signal from the mixer's output port is applied to a voltage-controlled PIN diode attenuator, then to a broadband linear rf power amplifier, followed by VHF and UHF lowpass filters and output attenuators. An overload protection circuit, located between the power amplifier output and lowpass filter input, provides a shut-off voltage to the PIN diode attenuator.

5.1.3. Physical Arrangement

The modulation standard is constructed in two parts; viz., (1) the total electronic package less the ratio voltmeter, and (2) the ratio voltmeter. See figure 1. A two-package design may not have been necessary, but an early decision for this approach was made to minimize a possible undesirable heating effect on the voltmeter circuitry.

The interior construction of the two packages uses the circuit board and frame technique. Circuits requiring shielding and filtering are built into totally closed aluminum boxes. Patch cords are used extensively to interconnect the individual subassemblies.

Along the top of the front panel of the main package, toward the left side, are located the controls for the af portion of the signal source. To the right are located the selection switches and gain set controls (behind-the-panel screwdriver adjust) for the modulation meter's af channel. The DC ZERO control is not used. To the left of the centrally located rf carrier level meter are the voltage control potentiometer (RF LEVEL) for the PIN attenuator and the selector switch for the rf carrier frequency. To the right are the two output attenuators, connected in tandem, each consisting of a 10 dB step attenuator with 1 dB step intervals. Above the meter are a switch used in calibrating the ac channel relative gain (see sec. 5.2.1.3), and a switch to select between the crystal-controlled and the line-controlled sources of 90 Hz and 150 Hz modulation tones. Along the bottom of the panel are a series of BNC connectors and patch cables which permit access to various points in the system for testing purposes. The right-hand connector is the signal source output port which electrically connects directly to the rf attenuators above it. The second connector from the right, i.e., the RF ATTENUATOR INPUT connector, provides direct input to the modulation meter. Vertically along the left side of the front panel are BNC connectors for external af voltage input to the modulation circuits of the signal source, and an output port for monitoring the af voltage applied to the modulator.

The CARRIER MONITOR OUTPUT connector is not used. Vertically along the right side are BNC connectors for connecting the modulation meter's ac and dc output signal voltages to the external ratio voltmeter package. Above these connectors is a second switch used in calibrating ac channel relative gain; below these connectors are the rf lowpass filter selector switch and the push-to-reset switch for the overload protection circuit. Indicator lamps for the overload circuit and for primary power (next to the power switch at lower left) complete the front panel controls.

On the rear panel are located the line cord receptacle, power supply fuses, and a BNC connector for inputting an external source of rf carrier voltage.

Front panel controls on the ratio voltmeter package are, counterclockwise from top left, as follows: Input port to the precision rectifier for calibration adjustment; power supply switch; input port for the ac signal voltage from the modulation meter; BNC connector that serves the dual purpose of (1) input port for the dc signal voltage from the modulation meter and (2) output port to monitor the dc reference voltage internal to the ratio voltmeter package; an internal/external switch to select between the two roles of the previous connector; output port to monitor the trigger (synchronization) period of the ratio voltmeter; and, at the upper right, an output port to monitor the dc output of the precision rectifier. The zero set control for the ratio voltmeter (located at top center) is accessible from the front by removing the meter's optical filter plate.

5.2. Detailed Circuit Description

The purpose of this detailed circuit description is to provide an operational understanding of those electronic networks that are special to the modulation standard, either in the sense that they are not widely found in other electronic devices or that they have been specifically selected to accomplish the objectives of this work. Therefore, little, if any, discussion is given to networks whose function and performance are generally well known, such as dc power supplies, operational amplifiers, digital logic, etc. Enough information is given to provide an overall picture, however.

This description is not intended to provide information for the purposes of instrument fabrication or maintenance. This is a one-of-a-kind instrument designed as a national standard for use at the National Bureau of Standards laboratories. Therefore, no lists of component parts, parts location layouts, interconnecting cable drawings, connector terminal schedules, drawings of specially fabricated structures, adjustment and calibration procedures, or any other information needed to manufacture or service this instrument are provided. However, with the information given here, those skilled in the art should be able to achieve comparable results in a similar instrument of their own design.

Note: Certain integrated circuits are identified by commercial part numbers in order to identify the units actually used. In no case does such identification imply recommendation by the National Bureau of Standards, nor does it imply that they are necessarily the best available for the purpose.

5.2.1. Precision Modulation Meter

5.2.1.1. RF Detector Network

The amplitude-modulated rf signal at the RF ATTENUATOR INPUT port is applied through resistor R1 to the anode terminal of Schottky barrier diode CR1. See figure 11, page 30. Capacitor C1, inductor L1, and resistor R2 provide an RLC termination at the diode's cathode. Field effect transistor Q1 and resistor R3 provide a constant current of approximately 7uA to forward bias CR1. Biasing the diode this way reduces its temperature coefficient and its inherent distortion, but also reduces its rectification efficiency. The

bias value chosen compromises between these latter two effects. The dc return is through the external termination (nominally 50 ohms) at the input port.

Note: In order for the performance analysis of the modulation meter to be valid, the rf carrier voltage level applied to the detector diode is always adjusted to a standard value whenever a measurement is made. Otherwise, the accuracy specification given in this report does not apply. This standard value is that value which produces +2.50 volts dc output at the cathode terminal of the detector diode. Thus, at that point, the instantaneous voltage may be as large as +4.75 volts (for 90 percent peak positive modulation), or as small as +0.25 volt (for 90 percent peak negative modulation). The front-panel RF CARRIER LEVEL meter is used to indicate when this standard level is achieved.

The diode output voltage is applied to operational amplifier IC-1 through R2. This stage has resistive feedback (R7 and R8) to produce a gain of approximately unity. Resistor R5 adjusts the output voltage at pin 6 to zero when the rf input voltage is zero, thus compensating for the approximately 0.2 volt bias at pin 2 caused by the constant current circuit (Q1).

Amplifier IC-1 connects to operational amplifier IC-2 through R9. Resistive feedback (R11) around IC-2 produces a gain of two. Resistor R12 adjusts the output voltage at pin 6 to zero when the input voltage is zero.

Note: Amplifier stages IC-1 and IC-2 are treated as part of the detector network when evaluating the detector's transfer characteristic (sec. 7.2) but are treated as part of the ac channel when evaluating the ac channel gain and frequency characteristics (see sec. 7.3).

Terminal points A, B, and C relate to the modulated subcarrier feedback detector circuit discussed in Appendix B.

5.2.1.2. DC Channel Networks

Amplifier IC-2 connects to operational amplifier IC-3 through R13 and R15. See figure 11. Resistive feedback (R17) around IC-3 produces a gain of unity at zero frequency. Capacitive feedback (C4) produces a gain near zero at frequencies above approximately one hertz. Thus, this stage serves as a lowpass filter to remove the af voltages from the dc channel.

Amplifier IC-3 connects to operational amplifier IC-4 through R19 and R20. Resistive feedback (R20 and R21) around IC-4 produces a nominal gain of two. Gain control R20 is used to calibrate the dc channel gain to obtain a direct reading of modulation index on the ratio voltmeter.

Resistors R24, R25, and R26 form a divider network which, along with the -15 VDC source and the microammeter M, constitute an expanded-scale suppressed-zero voltmeter network to indicate the RF CARRIER LEVEL.

Amplifier IC-4 connects to operational amplifier IC-101 in the ratio voltmeter package through a coaxial cable, switch S101A, and resistor R101. See figure 12. Resistive feedback (R103) around IC-101 produces a gain of unity. Switch S101B selects between either the output voltage of IC-101 (EXT position) or a -10 VDC internal reference voltage source for the ratio voltmeter reference input voltage.

Potentiometers R18, R22, and R104 permit IC-3, IC-4, and IC-101 to be zeroed under no-signal conditions.

5.2.1.3. AC Channel Networks

Amplifier IC-2 connects to the input ports of the bandpass filters (FL1 through FL5) and the wideband path through R13 and relay K1 when K1 is in the OPERATE position. See figure 11. In the CALIBRATE position, K1 connects an audio tone voltage from the internal signal source (see fig. 14) to the filter input line. The filter output ports connect through switches S1, S2, S3, S4, and S5 to GAIN SET controls R27, R29, R31, R33, and R35, and then through resistors R28, R30, R32, R34, and R36 to operational amplifier IC-5. The wideband path consists of dc blocking capacitors C5 and C6, their polarizing diodes CR2 and CR3, switch S6, and resistors R37 and R38. Filter FL4 (1020 Hz) is included to permit measurement of the 1020 Hz identification tone, should this be desired.

Resistive (R40 and R41) and capacitive (C8) feedback around IC-5 produces a nominal gain of unity. When relay K1 is in the CALIBRATE position, the voltage gain from K1 to the junction of R40 and R41 can be made very close to unity by alternately switching switch S7 between the MODE 1 and MODE 2 positions, and adjusting each GAIN SET control until the same AC OUTPUT voltage reading is obtained. This process compensates for gain drifts in active filters FL1 through FL5. When K1 is in the OPERATE position, switch S7 should be in the MODE 2 position for normal operation.

Amplifier IC-5 connects to precision rectifier buffer amplifier IC-102 through a coaxial cable and capacitor C101. See figure 12. Diodes CR101 and CR102 protect IC-102 from voltage overloading. Resistor R106, along with feedback resistors R107, R109, and R110, and capacitors C102 and C103 produce a gain of two from zero to 10 kHz.

Positive voltages at pin 6 of IC-102 reach the input port of operational amplifier IC-104 via two paths. Path one is through resistors R114 and R115. For this path, IC-104 has a gain of minus 1.5708 (adjusted by R115). Path two is through R111 to operational amplifier IC-103 which, for positive voltages, has a gain of approximately minus one at the junction of R116 and R117 because diode CR103 is forward biased. Therefore, the composite gain of IC-103 and IC-104, for positive voltages via path two is plus 3.1416 (adjusted by R118). The net effect of these two paths is a gain of plus 1.5708 from pin 6 of IC-102 to pin 6 of IC-104.

Negative voltages at pin 6 of IC-102 reach the input port of IC-104 via path one only, for which IC-104 has a gain of minus 1.5708. Path two via IC-103 has zero gain because diode CR104 is forward biased for negative voltages.

The net result of this operation is that the network from pin 6 of IC-102 to pin 6 of IC-104 functions as a fullwave rectifier with a gain of plus 1.5708. Furthermore, feedback capacitor C104 averages the fullwave-rectified waveform to produce a dc output voltage that, for a sinusoidal input voltage, is equal to its amplitude. This dc voltage is applied to the signal input port of the ratio voltmeter.

Potentiometers R108, R113, and R121 permit IC-102, IC-103, and IC-104 to be zeroed under no-signal conditions. BNC connectors labeled CALIBRATE DC IN and CALIBRATE DC OUT permit R115 and R118 to be precisely adjusted for the correct gain values using precision dc instruments.

5.2.1.4. Ratio Digital Voltmeter

The ratio voltmeter is a 4 1/2-digit commercial unit designed to use an external reference voltage. The dc voltage from amplifier IC-101 is connected to the voltmeter reference port through switch S101B when placed in the EXT position. See figure 12. A -10 VDC internal reference voltage can be applied to the voltmeter by placing S101B in the INT position, converting the voltmeter to a general purpose, single range, digital voltmeter. Simultaneously, this reference voltage is made available at the DC REF IN/OUT connector through resistor R122 and switch S101A.

The internal reference source consists of operational amplifier IC-105, zener diode VR101, and resistors R123, R124, R125, R126, and R127. Potentiometer R125 permits the voltage to be adjusted precisely to -10VDC.

A trigger voltage that is synchronous with the 60 Hz line frequency is provided by the network beginning with rectifier diode CR105 and ending with monostable multivibrator IC-110. This establishes a voltmeter sampling rate of three samples per second. Diode CR105, transistor Q101, and gates IC-106A and IC-106B provide a very steep squarewave voltage to decade counter IC-107. The 6 Hz squarewave voltage from IC-107 is further divided by a factor of 2 by flip-flop IC-108 and gate IC-106C. This 3 Hz voltage is converted to a 30μsec negative pulse by IC-110. A 3 Hz, 0.25 sec square pulse is generated by IC-109 and made available at the SYN OUT connector, but is not required for use in the modulation meter.

Synchronizing the voltmeter sampling rate with the line frequency eliminates the cyclic variation in voltmeter reading that can result from line frequency ripple entering the voltmeter. Any residual offset reading is removed with the voltmeter zeroing control.

5.2.2. Modulated RF Signal Source

5.2.2.1. RF Carrier Generator Networks

The VHF crystal-controlled oscillators are of conventional design. See figure 13. Quartz crystal units are excited at their fifth overtone in a harmonic oscillator circuit. The UHF sources have the same oscillator circuit, followed by a frequency tripler network and buffer amplifier consisting of transistors Q201 and Q202 and other associated components. Each crystal-controlled oscillator is a complete module to which dc supply voltage is switched by the front-panel CARRIER FREQUENCY control. Its rf output is connected to following circuits either directly or through the tripler/buffer network by means of a matrix of coaxial relay switches (K201 through K208). Lowpass filters FL201 and FL202 remove harmonics from the rf voltages.

5.2.2.2. AF Tone Generator Networks

The crystal-controlled source of 90 Hz and 150 Hz af tones uses a Colpitts oscillator circuit. See figure 14. A quartz crystal unit is excited at its fundamental frequency of 460.800 kHz. The use of a low-Q inductive load (L301 and R303) plus shunt diode CR301 produces a clipped sinusoid waveform that is compatible with the subsequent CMOS logic. The 460.8 kHz frequency is divided by a factor of two in flip-flop IC-301, again by two in flip-flop IC-302, and finally by a factor of 128 in binary divider IC-303 for a total division of 516. Thus a 900 Hz squarewave voltage is delivered to gate IC-304A.

The 60 Hz line voltage source of af tones uses a 900 Hz phase-locked-loop oscillator, IC-305, which obtains the 60 Hz synchronizing voltage through resistor R307 and capacitor C308. The other 60 Hz voltage to the phase comparator in IC-305 is obtained by use of divider IC-307, along with gate IC-308 and buffers IC-306C through IC-306E, which are

located in the feedback path between buffer IC-306A and pin 15 of IC-305. This branch provides a division factor of 15. The 900 Hz voltage from IC-305 is thus phase locked to the 60 Hz line. Buffer IC-306B applies this voltage to gate IC-304B.

Switch S301 selects which of gates IC-304A or IC-304B will pass a 900 Hz signal to gates IC-304C and IC-304D for further frequency division.

The 90 Hz af tone is generated by phase-locked-loop oscillator IC-310 and waveform generator IC-311. This voltage is synchronized to the 900 Hz signal from IC-304D by dividing it by a factor of 10 in divider IC-309 and applying the resulting 90 Hz squarewave voltage through R317 and C317 to pin 12 of IC-310. IC-311 delivers a nearly-sinusoidal ($\sim$ 2 percent distortion) 90 Hz voltage to follower amplifier IC-312. Operational amplifier IC-313, along with resistors R320, R321, R322, and capacitor C324, provide a constant-voltage phase-shift network to permit phase adjustment of the 90 Hz tone. This voltage is filtered in active bandpass filter FL301, and passes through level set potentiometer R342, on/off switch S302, capacitor C336, and resistor R347 to summing amplifier IC-320.

The 150 Hz af tone is generated by phase-locked loop oscillator IC-316 and waveform generator IC-317. This voltage is sychronized to the 900 Hz signal from IC-304D by dividing it by a factor of 6 in divider IC-314 plus gate IC-315, and applying the resulting 150 Hz squarewave voltage through R324 and C327 to pin 12 of IC-316. IC-317 delivers nearly sinusoidal ($\sim$ 2 percent distortion) 150 Hz voltage to follower amplifier IC-318. Operational amplifier IC-319, along with resistors R338, R339, R340, and capacitor C334, provide a constant-voltage phase-shift network for phase adjustment of the 150 Hz tone. IC-318 can be made either inverting or non-inverting by the location of the input jumper so that the phase of the 150 Hz tone may be adjusted through a full 360 degrees. This voltage is filtered in active bandpass filter FL302, and passes through level set potentiometer R343, switch S303, capacitor C337, and resistor R348 to summing amplifier IC-320.

Up to two external af signals can also be applied to IC-320 via input connectors EXT. 1 and EXT. 2. Each has a level set control and on/off switch. Provision has been made for a fifth input at 1020 Hz via active filter FL303, but this is not presently used.

The output voltage from summing amplifier IC-320 is adjusted by MASTER LEVEL SET control R354. It is then applied through switch S307, capacitor C341, and resistor R355 to buffer amplifier IC-321. The output of IC-321 connects to three points: (1) The modulator driver circuit, figure 15, (2) the CALIBRATE/OPERATE relay, K1, figure 11, and (3) the AF TONE MONITOR OUTPUT connector.

5.2.2.3. Modulator Networks

Radiofrequency carrier voltage is applied to the balanced modulator, DBM401, via the MODULATOR INPUT connector. See figure 15. DBM401 is a double-balanced mixer of conventional design, having the following specifications:

Frequency Range:	RF and LO ports: 0.2-600 MHz IF port: DC-600 MHz
Conversion Loss:	8.0 dB (maximum)
Isolation:	LO-RF: 30 dB (minimum) LO-IF: 25 dB (minimum) RF-IF: 20 dB (minimum)
Total Input Power:	50 mW, maximum
IF Port DC Current:	50 mA, maximum
Nominal Level, LO:	+7 dBm
RF Level for 1 dB Compression:	+2 dBm

Modulated rf output voltage is applied directly to the MODULATOR OUTPUT connector.

Audiofrequency tone voltage and dc voltage are applied to the intermediate frequency (IF) port of DBM401 through a Howland [18] voltage-to-current converter circuit. The basic Howland circuit consists of operational amplifier IC-401 and resistors R403, R405, R406, and R408. Resistor R402 and capacitors C402 and C403 are added to improve audiofrequency response. Clamping diode CR401 and blocking diode CR402 assure that only negative current flows into the doubly balanced mixer. Choke coil L401 provides a high rf impedance to the mixer for improved performance. Audiofrequency voltage from IC-321 is applied to the Howland circuit through capacitor C401. DC voltage from operational amplifier IC-403 is applied through resistor R405. This dc voltage determines the rf carrier level at the output of the doubly balanced mixer under zero-modulation conditions.

IC-403 obtains its dc input voltage from an internal reference source that consists of operational amplifier IC-402, zener diode VR401, and resistors R409, R410, R411, R412, and R413. Potentiometer R411 permits the voltage at pin 6 of IC-402 to be adjusted precisely to +10VDC. Inverting amplifier IC-403 has a gain of minus one-half to supply -5VDC to IC-401.

5.2.2.4. PIN Diode Attenuator Networks

Modulated rf voltage at the RF AMPLIFIER INPUT connector is applied to an adjustable attenuator network consisting of PIN diodes CR403 and CR404, capacitors C408, C409, C410, C411, and C412, inductors L402, L403, L404, and L405, and resistors R426 and R427. See figure 15. PIN diode CR404 is supplied with an adjustable direct current from Howland circuit IC-405 through inductor L404 to provide manual control of the modulated rf signal level. Adjustable dc voltage from RF LEVEL control R418 is applied to buffer amplifier IC-404, thence to the non-inverting port of IC-405 for conversion to PIN diode control current. Diode CR404's rf attenuation range is approximately 25 dB or greater, depending upon carrier frequency.

PIN diode CR403 is normally forward biased with current from transistor Q402, and presents a low rf impedance to the modulated input voltage. However, when the amplifier overload protection circuit is activated, as discussed below, diode CR403 is back biased and provides a minimum of approximately 30 dB attenuation to the rf signal.

5.2.2.5. RF Amplifier Networks

The rf output voltage from the PIN diode attenuator passes through 6 dB attenuator A401 to rf amplifier U401. See figure 15. Amplifier specifications are as follows:

Frequency Range:	10 MHz to 500 MHz
Linear Gain:	49 dB (minimum)
Power Output:	4 watts (rated)
Compression (4w):	0.8 dB (maximum)
Noise Figure:	<7 dB
Input VSWR:	<2:1
Output VSWR:	<3:1

Amplified rf voltage is applied through directional coupler DC401 to the RF AMPLIFIER OUTPUT connector.

Coupler DC401 is part of a protection circuit that prevents damage to amplifier U401 in the event that its rf output voltage exceeds approximately 150 percent of the normal rf voltage level. The protection circuit (1) reduces the input voltage to U401 by 30 dB minimum within approximately 30 µs of the overvoltage condition, and (2) turns off the 24VDC power supply to U401 within approximately 8 ms. This is accomplished as follows:

Radiofrequency voltage from the side arm of DC401 is rectified by diode CR407, filtered by capacitors C417 and C418 and a ferrite bead, and the resulting dc voltage is applied to the non-inverting input port of operational amplifier IC-406. IC-406 is operated as a bi-stable multivibrator by virtue of zener diodes VR402 and VR403 in the feedback path between the output and inverting input ports, and resistors R433 and R434 and diode CR406 in the feedback path between the output and non-inverting input ports. Under normal conditions, the positive voltage on pin 3 is smaller than the positive voltage on pin 2, and IC-406 is driven to saturation, limited by VR402. This produces approximately -7VDC at pin 6. Diode CR406 prevents this voltage from back-biasing detector diode CR407 under these conditions. When a positive voltage from CR407 exceeds the positive voltage on pin 2, IC-406 is rapidly driven to saturation in the opposite direction because of positive feedback through R433, R434, and CR406. Saturation is limited by VR403, producing aproximately +7VDC at pin 6. Feedback conditions to pin 3 are such that IC-406 remains in this latter saturation condition even when the positive voltage from CR407 falls to zero. In order to reset IC-406 to the original saturation state for normal operation, the junction of R433 and R434 is grounded through PUSH TO RESET switch S401. This drops the positive voltage on pin 3 to less than that on pin 2, and the original conditions return.

When pin 6 on IC-406 is at -7VDC (normal condition), the current supplied through transistor Q402 to PIN diode CR403 forward-biases CR403 to a low impedance condition. When pin 6 is at +7VDC (overload condition), CR403 is back-biased to produce the high impedance required to reduce the rf voltage to U401. Simultaneously, transistor Q401 passes current to OVERLOAD indicator lamp P401. Also, the +7VDC is coupled through diode CR405 to place transistor Q403 in an off state; this switches off the 24-volt power supply to U401 by means of solid-state relay SR401. Normally, Q403 is on, and SR401 is closed.

5.2.2.6. Post-Amplifier Networks

The rf output signal from directional coupler DC401 is applied to either lowpass filter FL401 or FL402 through the LOW-PASS FILTER INPUT connector and relay K401A. See figure 15. Relay K401B connects the filtered output voltage to the LOW-PASS FILTER OUTPUT connector, which is connected by a coaxial link to the RF ATTENUATOR INPUT connector. This connector is wired to both the rf detector network (see sec. 5.2.1.1), and to a 6 dB attenuator. Two 0 to 10 dB step attenuators are connected in tandem to the RF ATTENUATOR OUTPUT connector. This is the output port of the modulated rf signal source.

5.2.3. DC Power Supplies

Nine dc power supplies are used in the modulation standard. Figure 16 shows in block diagram form the voltages and currents supplied. Note that supply PS6 is switched off by solid-state relay SR401, figure 15, when an overload condition exists in rf amplifier U401.

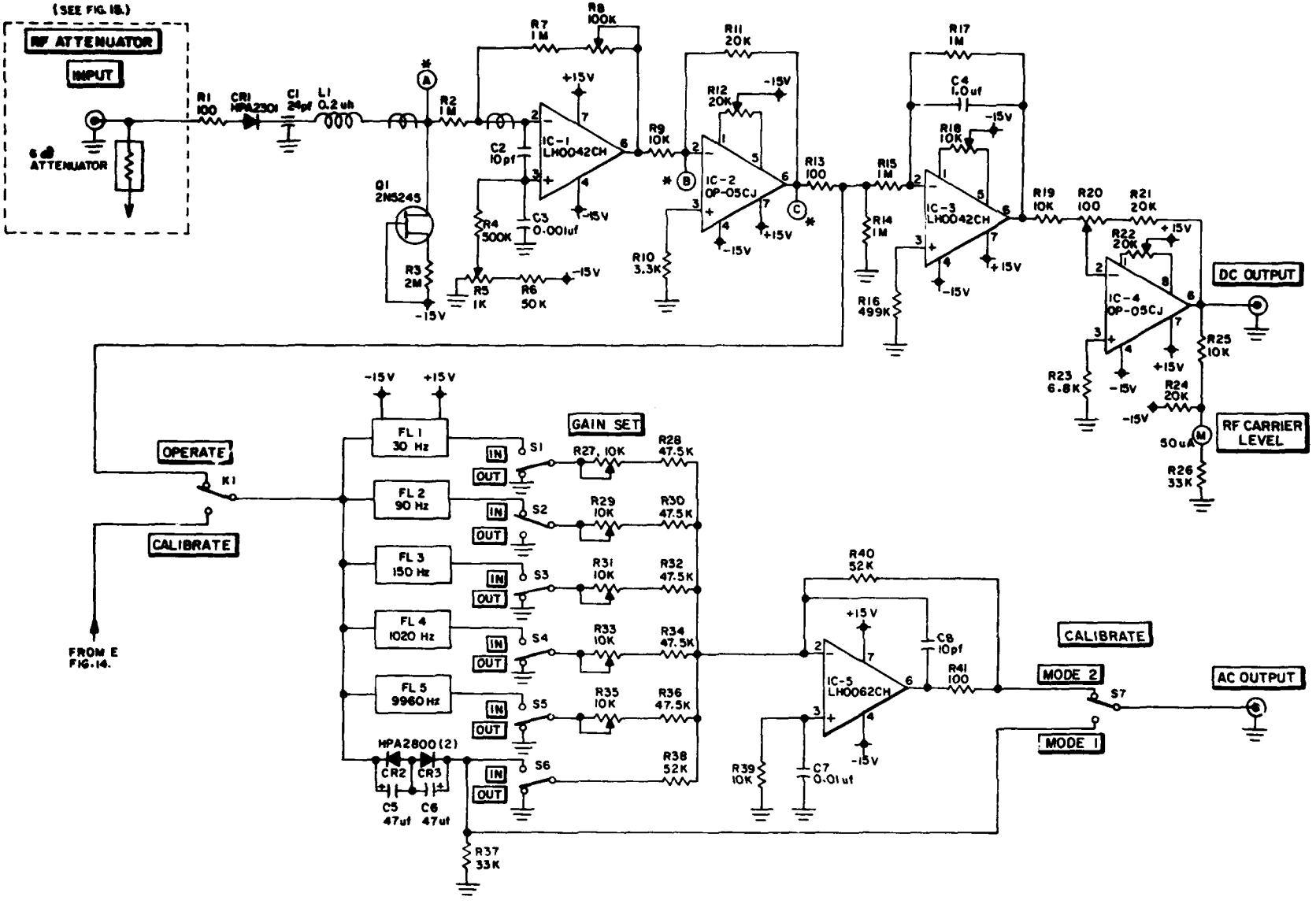

▭ = FRONT PANEL NOMENCLATURE
* = SEE FIG. 8.3.
⌒ = FERRITE BEAD

FIGURE 11. SCHEMATIC DIAGRAM OF MODULATION STANDARD.
DRAWING 1 OF 5

NOTE:
RELAY COIL WIRING NOT SHOWN.

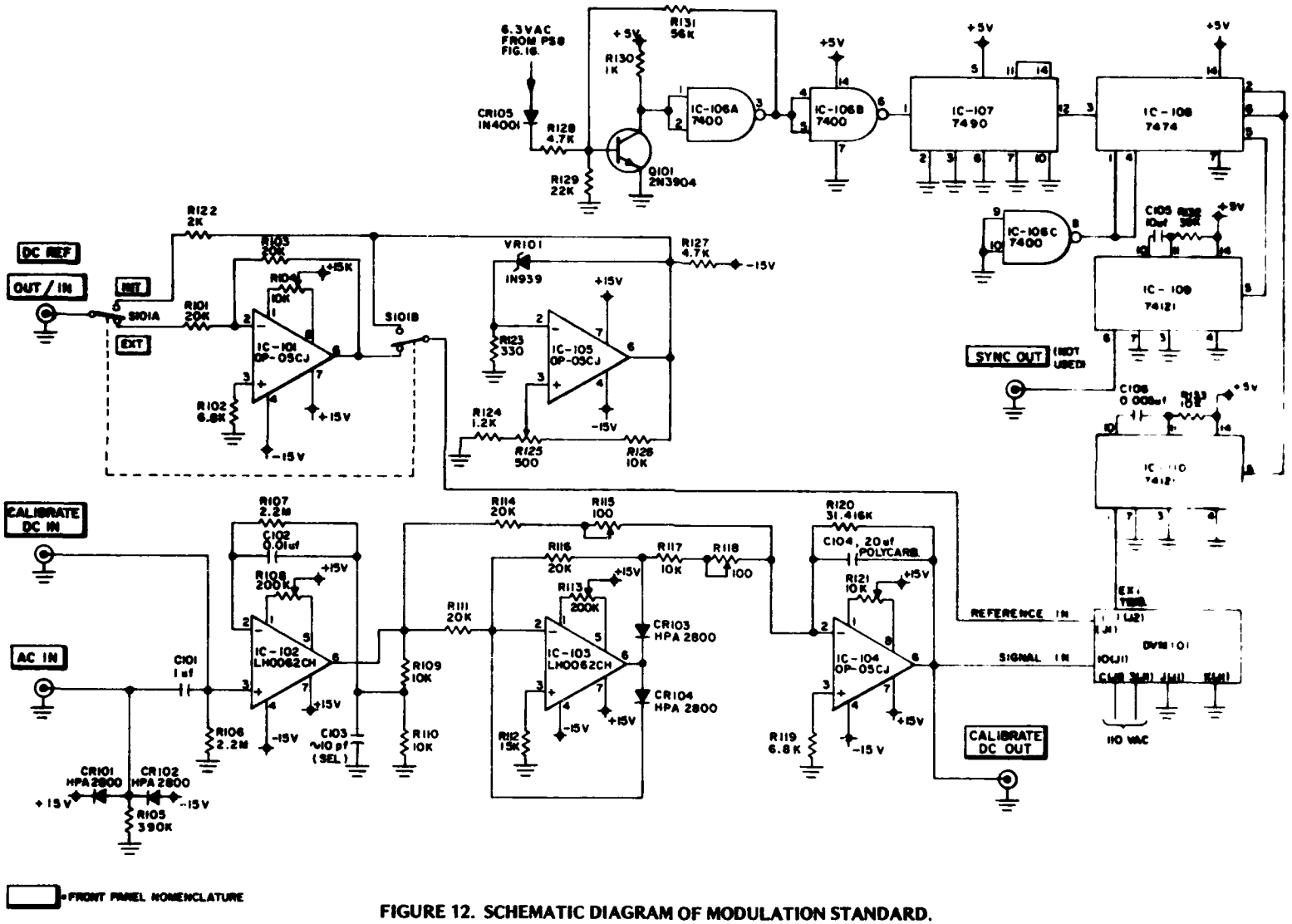

FIGURE 12. SCHEMATIC DIAGRAM OF MODULATION STANDARD. DRAWING 2 OF 5.

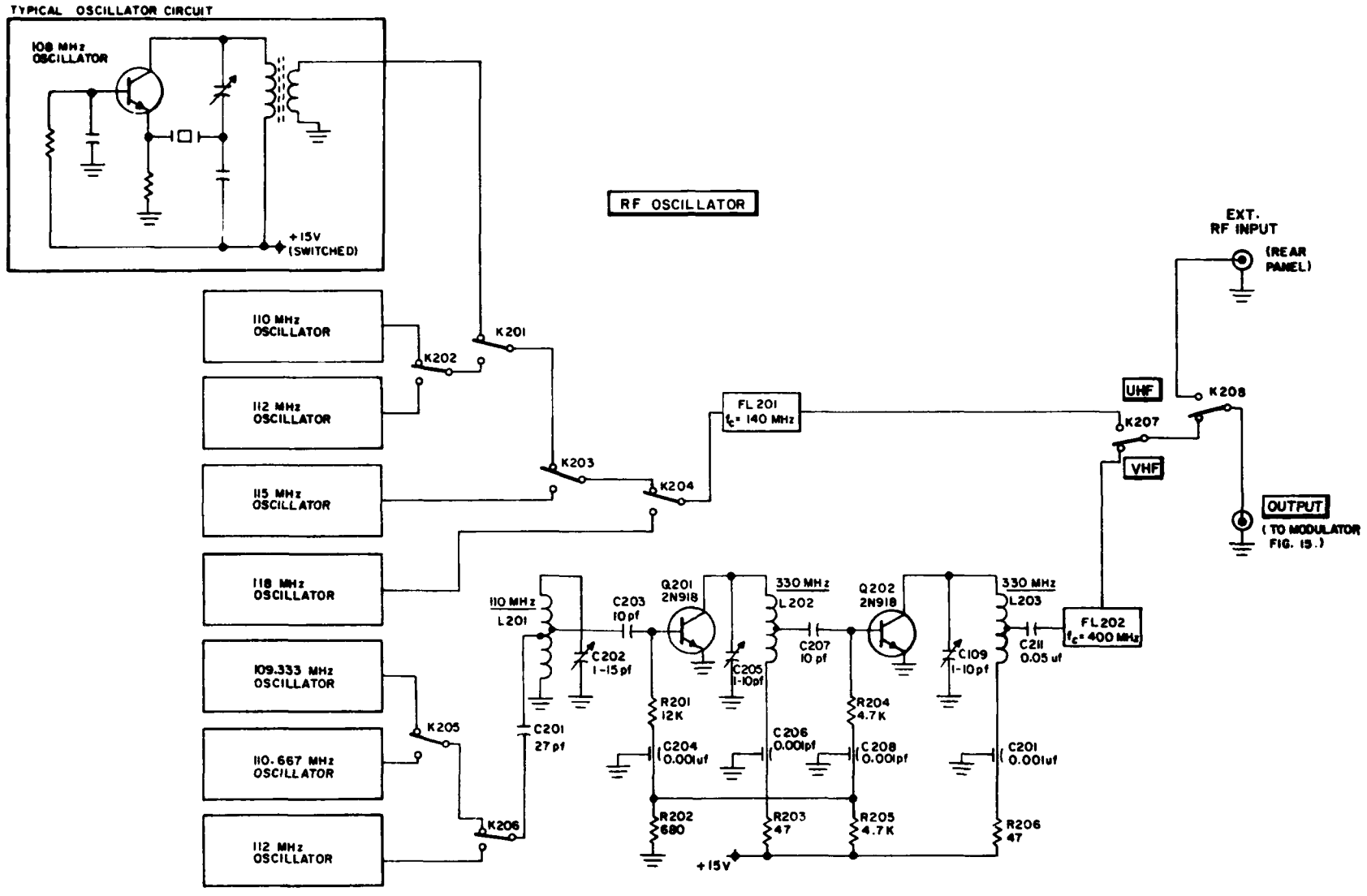

* FRONT PANEL NOMENCLATURE

FIGURE 13. SCHEMATIC DIAGRAM OF MODULATION STANDARD. DRAWING 3 OF 5

NOTE:
RELAY COIL WIRING NOT SHOWN

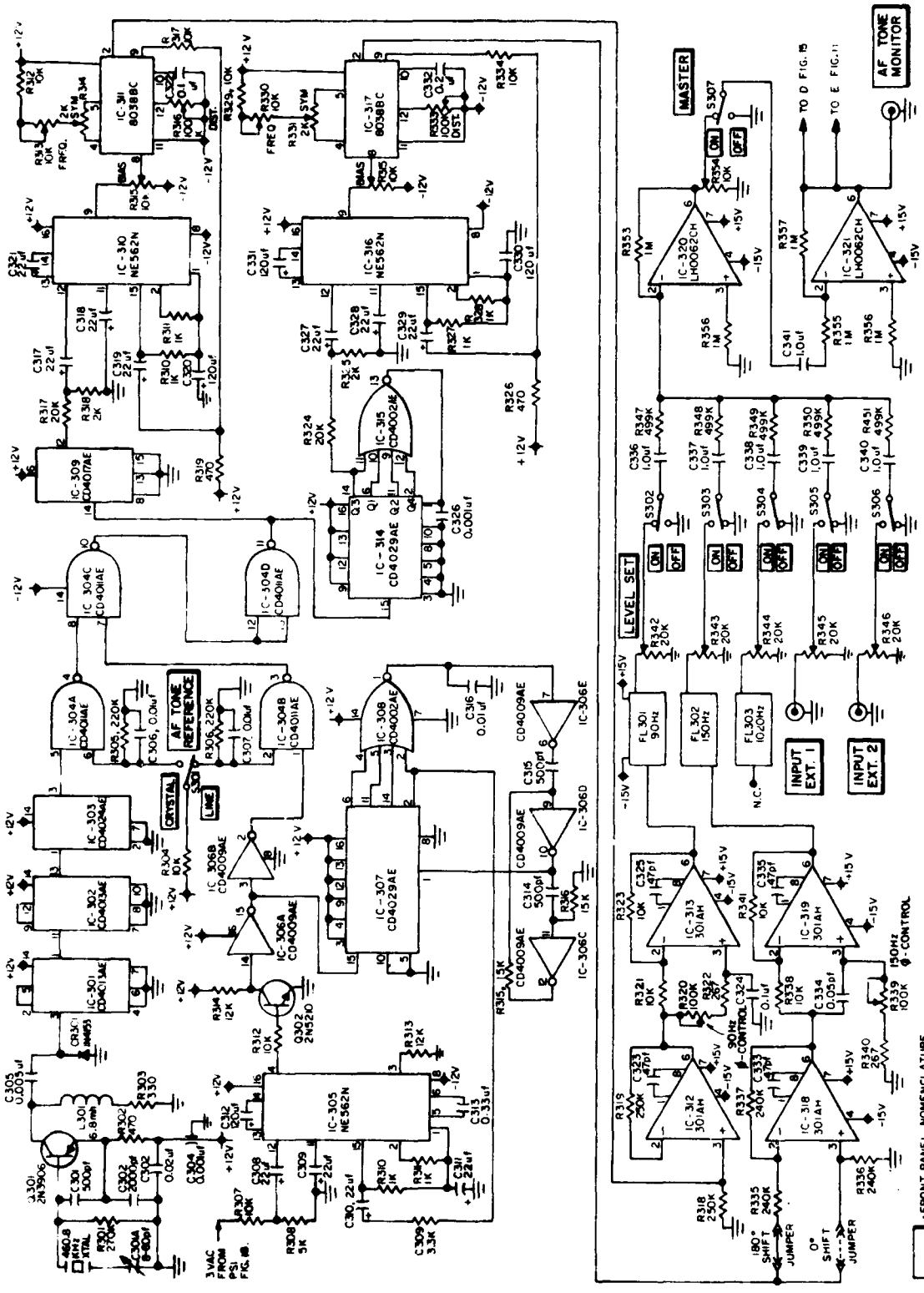

FIGURE 14. SCHEMATIC DIAGRAM OF MODULATION STANDARD. DRAWING 4 OF 5

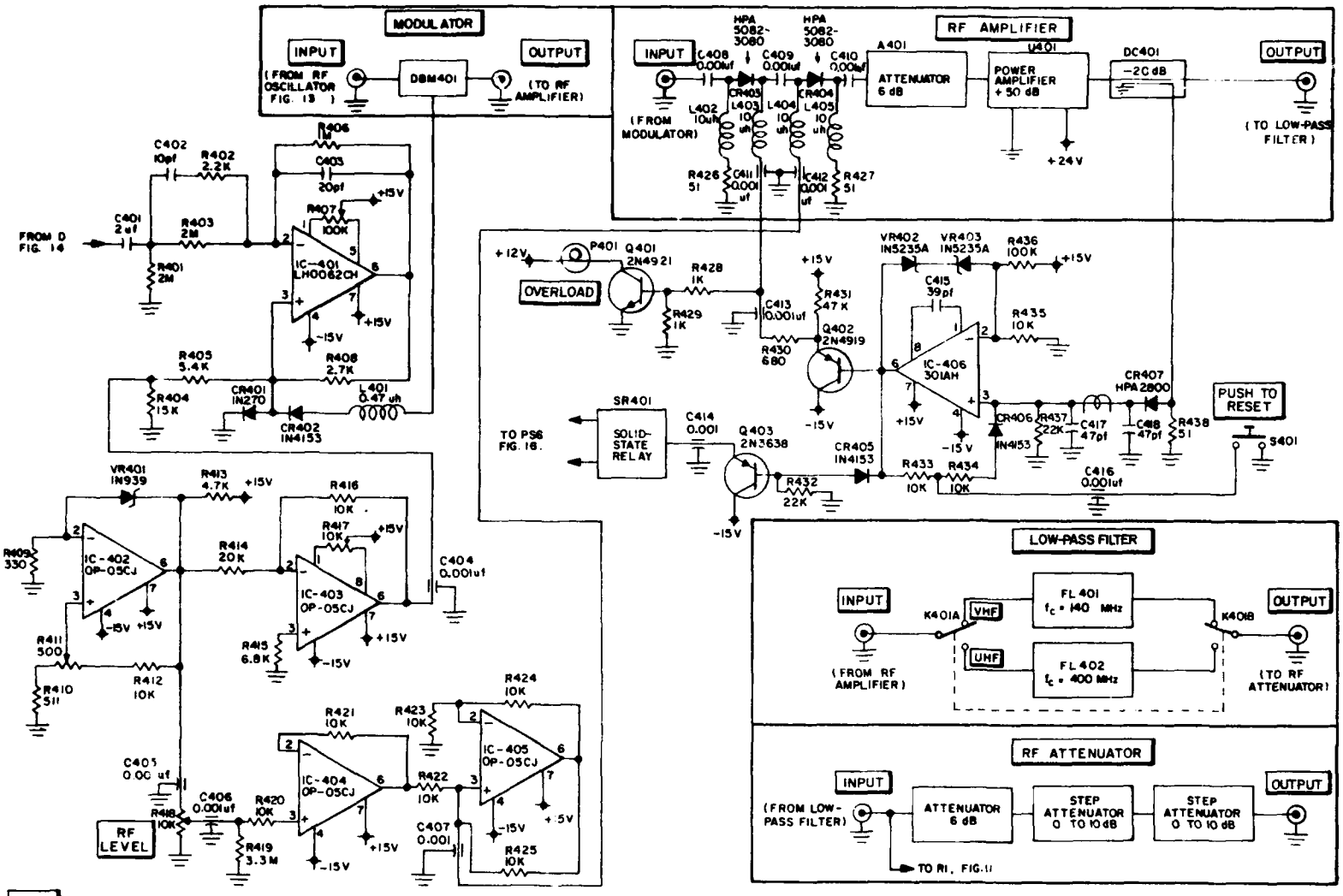

FIGURE 15. SCHEMATIC DIAGRAM OF MODULATION STANDARD. DRAWING 5 OF 5

NOTE 1:
RF OSCILLATOR (FIG. 13), MODULATOR, RF AMPLIFIER, LOW PASS FILTER, AND RF ATTENUATOR SECTIONS ARE CONNECTED IN TANDEM BY COAXIAL LINKS.

NOTE 2.
RELAY COIL WIRING NOT SHOWN.

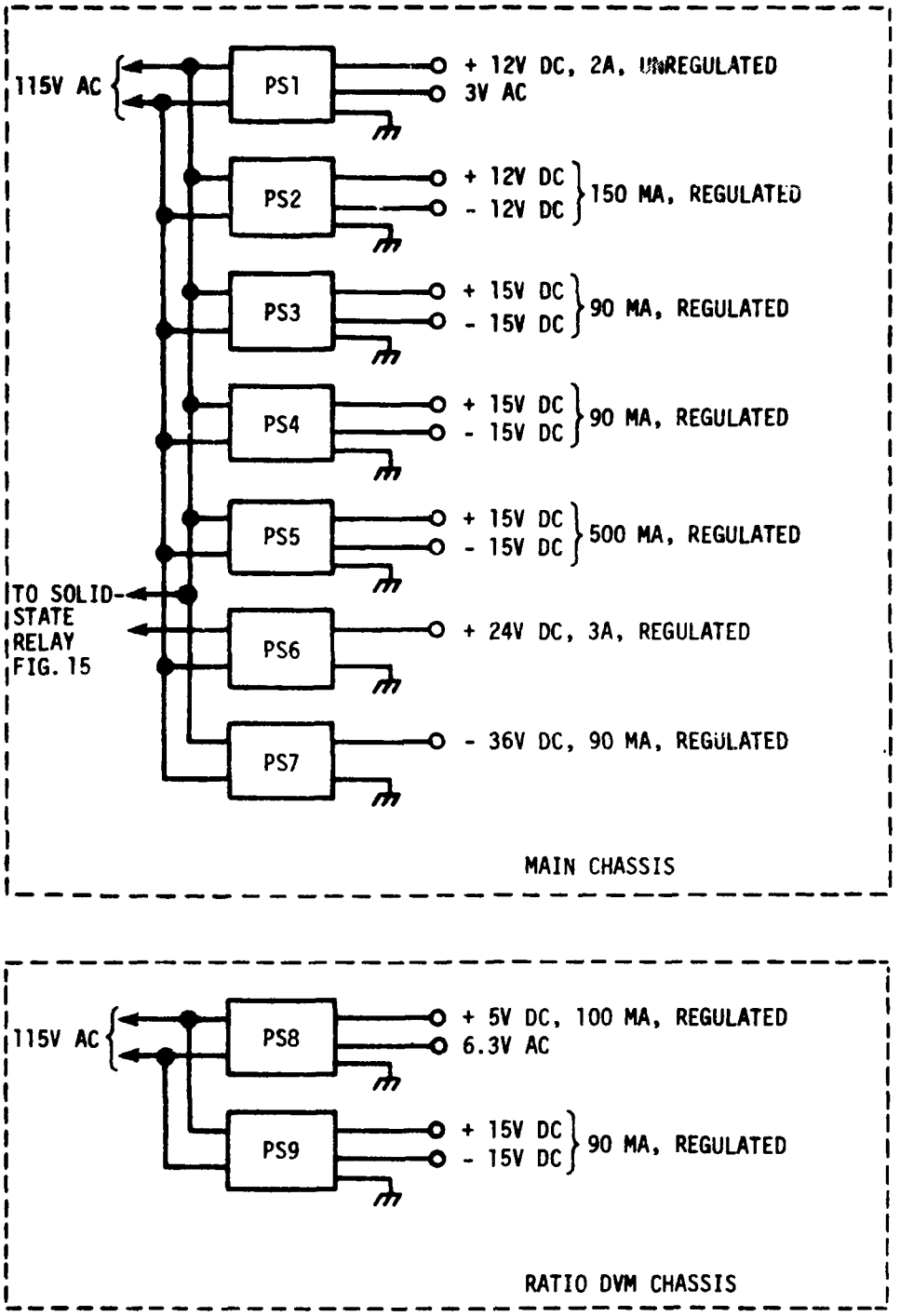

Fig. 16. Block diagram of dc power supplies

6. Measurement Errors

6.1. General Considerations

The measurement errors given in this section are the total plus-or-minus (±) limits of error for the corrected value of modulation factor. They include all known sources of error, both systematic and random. Systematic errors are calculated as plus-or-minus limits of error. Random errors are calculated as the sample standard deviation times the constant factor 1.960, which defines the confidence interval for a confidence level of 0.95. Individual error components are combined on a root-sum-square (RSS) basis to produce the total error quoted. Refer to section 7 for the error analysis.

In general, measurement errors vary with carrier frequency, modulation frequency, and modulation factor. Section 7.7 contains directions for calculating the measurement error for any signal within the range of this instrument. The total measurement error for selected ILS or VOR signals is given below. Errors for non-ILS/VOR signals can be calculated in like manner, but since there is an unlimited number of such signals, no tabulations are provided here.

Note: The measurement errors due to audiofrequency response, ac channel nonlinearity, and detector nonlinearity come from the uncertainty in the corrections for these effects that are applied to the ratio voltmeter reading (see sec. 4.2.2). Without those corrections, the measurement error would be unacceptably large. By applying the corrections, the direct errors due to these effects are removed. But the correction uncertainties remain.

6.2. ILS Signals

Total measurement errors for ILS signals, as a function of modulation factor and carrier frequency band, are shown in table 5 and figure 17. (These values also apply to all audiofrequency tones between approximately 40 Hz and 10 kHz.)

Note that the target accuracy of ±0.00125 has been exceeded.

Table 5. Total measurement error, ILS signals

Modulation factor, m	Measurement error, Δm (±) 108-118 MHz	328-336 MHz
0.1000	0.00027	0.00028
0.2000	0.00033	0.00036
0.3000	0.00041	0.00045
0.4000	0.00050	0.00054
0.5000	0.00059	0.00064
0.6000	0.00069	0.00074
0.7000	0.00079	0.00085
0.8000	0.00089	0.00097
0.9000	0.00099	0.00109

6.3. VOR Signals

Total measurement errors for VOR signals, as a function of modulation factor and audiofrequency tone, are shown in table 6 and figure 17. The errors for the 9960 Hz tone are the same as for the ILS Localizer signals. Above approximately m = 0.32 (32 percent modulation), the error for the 30 Hz tone is greater than the target accuracy set for ILS signals because of the large uncertainty in measuring the meter's ac channel gain at 30 Hz (see sec. 7.3).

Table 6. Total measurement error, VOR signals

Modulation factor, m	Measurement error, Δm ($\pm$)	
	30 Hz	9960 Hz
0.1000	0.00045	0.00027
0.2000	0.00080	0.00033
0.3000	0.00117	0.00041
0.4000	0.00154	0.00050
0.5000	0.00191	0.00059
0.6000	0.00229	0.00069
0.7000	0.00267	0.00079
0.8000	0.00305	0.00089
0.9000	0.00342	0.00099

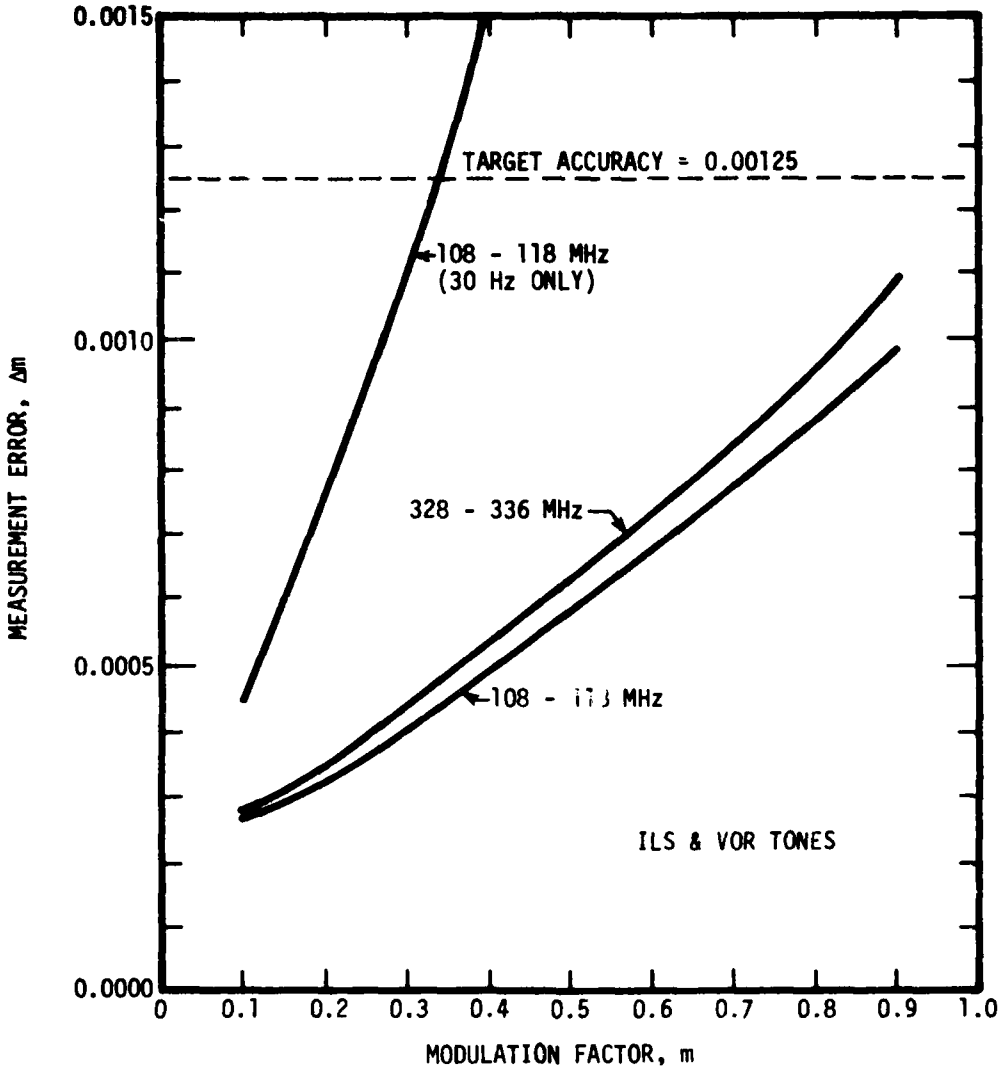

Fig. 17. Total measurement error

7. Error Analysis

7.1. Introduction

Each circuit of the modulation meter is a potential source of measurement error and has come under the scrutiny of analysis. The sources of significant error discussed in this section are the following:

a. RF detector nonlinearity
b. AC channel nonlinearity
c. Audiofrequency response
d. AC channel gain instability
e. DC channel gain instability
f. Ratio voltmeter digitizing error

Other sources have been investigated (one example is the first-order differential approximation in the Newton-Raphson method) and have been judged insignificant by comparison with those listed.

In general, errors are of two types: (1) Systematic, and (2) random [19]. For our purposes, systematic errors are those assignable to test instrument inaccuracy or to other known or controlled causes. Random errors are assignable to variations in data due to the working of a number of uncontrolled variables.

Systematic errors are expressed as the plus or minus ($\pm$) limits of error. Random errors are expressed as the sample standard deviation times the constant factor 1.960 which defines the confidence interval for a confidence level of 0.95. Both types of error are ultimately expressed in units of modulation factor, m. Errors are combined on a root-sum-square basis.

Because modulation factor is a dimensionless ratio, and the modulation meter measures m as a voltage ratio, the error-producing effects of circuit imperfections in some instances tend to be reduced. Thus, the error in the measured value of m tends to be smaller than would be the error of this same equipment used as an rf voltmeter.

7.2. RF Detector Network Error

The measurement uncertainty due to the rf detector network comes from the uncertainty in the correction that accounts for the effect of nonlinearity. (Detector bandwidth, an insignificant factor, is discussed in sec. A.4.) The correction involves three steps: (1) Modeling the detector nonlinearity, (2) determining the model parameters, and (3) computing the corrected value of m. The errors associated with these steps are discussed below.

To provide the data for this analysis, measurements of dc output voltage versus rf input voltage were made by the technique described in section A.2.1. In all, 27 sets of data were taken, consisting of nine consecutive data runs at each of three rf carrier frequencies: 30 MHz, 110 MHz, and 332 MHz. Each data run contains 45 data points. A typical set of processed measurement data is shown in the left-hand and center columns of table 7.

Table 7. Typical experimental test data

Measured data		Calculated data
RF input voltage	DC output voltage	DC output voltage, 5th degree polynomial
0.72253	9.5886	9.5871
0.70682	9.3745	9.3750
0.69119	9.1625	9.1636
0.67554	8.9508	8.9518
0.65989	8.7386	8.7398
0.64426	8.5267	8.5281
0.62878	8.3170	8.3184
0.61332	8.1076	8.1089
0.59733	7.8911	7.8922
0.58210	7.6848	7.6859
0.56632	7.4710	7.4722
0.55067	7.2592	7.2603
0.53513	7.0489	7.0500
0.51982	6.8419	6.8429
0.50399	6.6277	6.6288
0.48828	6.4151	6.4163
0.47279	6.2059	6.2070
0.45753	5.9996	6.0000
0.44166	5.7850	5.7865
0.42613	5.5753	5.5769
0.41083	5.3686	5.3703
0.39485	5.1530	5.1547
0.37924	4.9423	4.9440
0.36399	4.7366	4.7383
0.34790	4.5198	4.5213
0.33225	4.3091	4.3104
0.31727	4.1071	4.1085
0.30127	3.8919	3.8929
0.28586	3.6844	3.6853
0.26941	3.4634	3.4639
0.25525	3.2734	3.2734
0.23836	3.0466	3.0463
0.22396	2.8536	2.8528
0.21641	2.7515	2.7515
0.20056	2.5389	2.5389
0.18497	2.3302	2.3302
0.16919	2.1190	2.1191
0.15321	1.9056	1.9060
0.13713	1.6914	1.6919
0.12150	1.4838	1.4845
0.10588	1.2769	1.2778
0.09371	1.1160	1.1174
0.07544	0.8760	0.8776
0.05713	0.6376	0.6386
0.03910	0.4067	0.4049

7.2.1. Nonlinearity Model

The detector's nonlinearity characteristic is described by an algebraic polynomial (see sec. A.2) of the form

$$y = b_0 + b_1 x + b_2 x^2 + \ldots + b_i x^i + \ldots \tag{25}$$

where x and y are input and output voltage functions, respectively, and the b coefficients are constants whose values are determined by our specific detector.

To determine how many terms of eq (25) adequately characterize the detector, polynomials of degree from one through six were used to calculate output voltage values using the experimental input voltage data, and the results were compared with the experimental output voltage data. The root-mean-square (RMS) deviation of the calculated data from the measured data was used as a criterion for choosing the best polynomial degree.

From an analysis of the data, a fifth degree polynomial appears to provide an adequate representation of the detector nonlinearitry characteristic. This choice is based on the results of the following procedure:

a. From each of the nine measurement data sets at a given rf carrier frequency (a composite total of 9 x 45 = 405 data points), a set of B coefficients (see eq (A.5), sec. A.2) was calculated for polynomials of first degree through sixth degree. These coefficients for the 30 MHz, 110 MHz, and 332 MHz data are shown in tables 8, 9, and 10, respectively.

b. Using each of the six sets of B coefficients, new dc output voltage values were calculated from the measured rf input data. The right-hand column of table 7 shows these calculated values for a fifth-degree polynomial for that particular set of data. The other 161 (= [27 x 6] - 1) sets of data are similar.

c. The RMS deviations of the calculated voltages from the measured voltages were calculated by the following formula:

$$\text{RMS} = \left\{ \frac{\sum_{i=1}^{n} [V_i(\text{calc}) - V_i(\text{meas})]^2}{n - 1} \right\}^{1/2} \tag{26}$$

where n is the number of data points (n = 405). RMS deviation is a measure of how well the calculated set of voltage values represents the measured set of voltages. Table 11 and figure 18 show the RMS deviations for the 30 MHz, 110 MHz, and 332 MHz composite data.

Table 8. B coefficients, 30 MHz

Coefficient	1st degree	2nd degree	3rd degree	4th degree	5th degree	6th degree
B_0	-1.5506×10^{-1}	-1.2909×10^{-1}	-1.1565×10^{-1}	-1.0490×10^{-1}	-9.5908×10^{-2}	-8.7828×10^{-2}
B_1	10.1466×10^{-1}	10.0064×10^{-1}	9.8758×10^{-1}	9.7188×10^{-1}	9.5419×10^{-1}	9.3413×10^{-1}
B_2	--	1.3760×10^{-3}	4.4536×10^{-3}	1.0812×10^{-2}	2.1365×10^{-2}	3.7526×10^{-2}
B_3	--	--	-2.0192×10^{-4}	-1.1508×10^{-3}	-3.7658×10^{-3}	-9.5765×10^{-3}
B_4	--	--	--	4.6780×10^{-5}	3.3099×10^{-4}	1.3611×10^{-3}
B_5	--	--	--	--	-1.1211×10^{-5}	-9.9294×10^{-5}
B_6	--	--	--	--	--	2.8996×10^{-6}

Table 9. B coefficients, 110 MHz

Coefficient	1st degree	2nd degree	3rd degree	4th degree	5th degree	6th degree
B_0	-1.5602×10^{-1}	-1.2921×10^{-1}	-1.1559×10^{-1}	-1.0467×10^{-1}	-9.5679×10^{-2}	-8.7961×10^{-2}
B_1	10.1473×10^{-1}	10.0023×10^{-1}	9.8695×10^{-1}	9.7091×10^{-1}	9.5311×10^{-1}	9.3381×10^{-1}
B_2	--	1.4255×10^{-3}	4.5633×10^{-3}	1.1081×10^{-2}	2.1738×10^{-2}	3.7368×10^{-2}
B_3	--	--	-2.0633×10^{-4}	-1.1815×10^{-3}	-3.8297×10^{-3}	-9.4700×10^{-3}
B_4	--	--	--	4.8184×10^{-5}	3.3667×10^{-4}	1.3396×10^{-3}
B_5	--	--	--	--	-1.1404×10^{-5}	-9.7379×10^{-5}
B_6	--	--	--	--	--	2.8367×10^{-6}

Table 10. B coefficients, 332 MHz

Coefficient	1st degree	2nd degree	3rd degree	4th degree	5th degree	6th degree
B_0	-1.5525×10^{-1}	-1.2934×10^{-1}	-1.1394×10^{-1}	-1.0375×10^{-1}	-9.5436×10^{-2}	-8.7542×10^{-2}
B_1	10.1480×10^{-1}	10.0079×10^{-1}	9.8579×10^{-1}	9.7085×10^{-1}	9.5440×10^{-1}	9.3469×10^{-1}
B_2	--	1.3775×10^{-3}	4.9191×10^{-3}	1.0990×10^{-2}	2.0829×10^{-2}	3.6768×10^{-2}
B_3	--	--	-2.3279×10^{-4}	-1.1407×10^{-3}	-3.5843×10^{-3}	-9.3319×10^{-3}
B_4	--	--	--	4.4847×10^{-5}	3.1093×10^{-4}	1.3323×10^{-3}
B_5	--	--	--	--	-1.0515×10^{-5}	-9.8033×10^{-5}
B_6	--	--	--	--	--	2.8865×10^{-6}

Table 11. RMS deviation between measured and calculated output voltages

Degree	30 MHz data	110 MHz data	332 MHz data
1	0.00946	0.00978	0.01016
2	0.00363	0.00375	0.00521
3	0.00198	0.00212	0.00387
4	0.00112	0.00128	0.00354
5	0.00064	0.00089	0.00343
6	0.00033	0.00071	0.00339

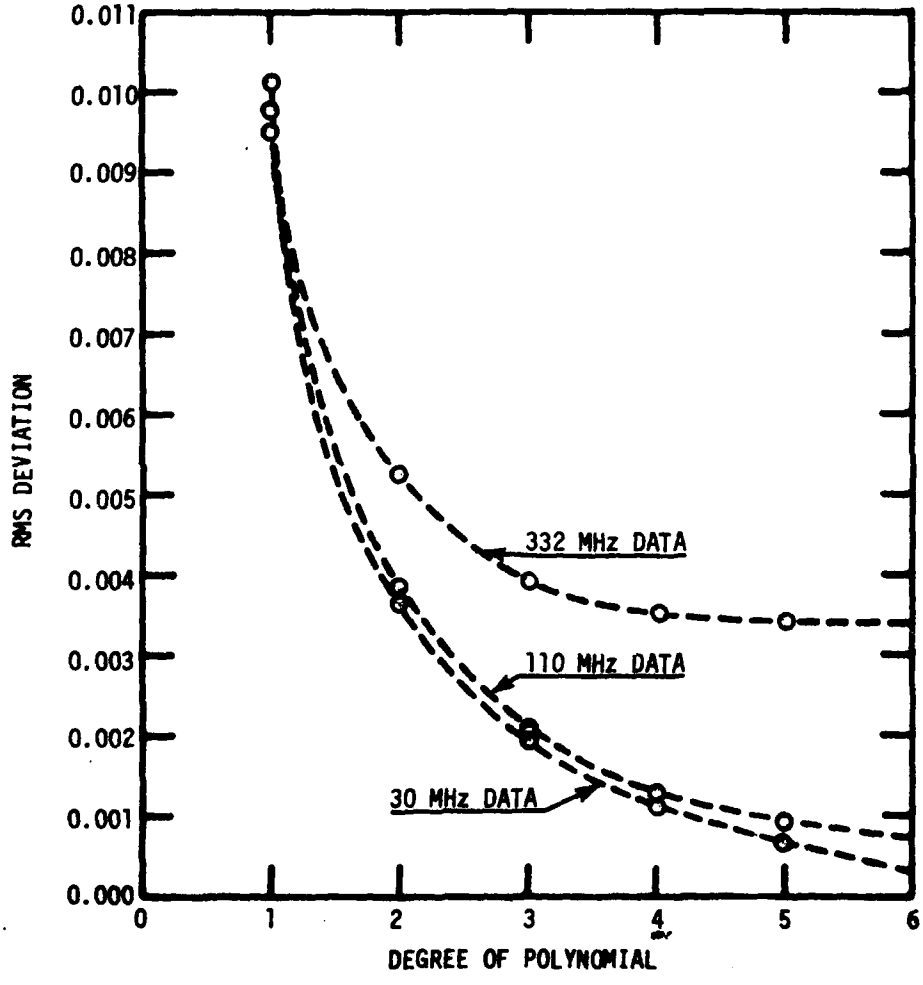

Fig. 18. RMS deviation versus degree of polynomial

It can be seen that the RMS deviation decreases as the polynomial degree increases. That is, the higher the degree of polynomial, the better its representation of the detector characteristic. However, the rate of improvement clearly decreases as the degree increases. In general, it is deceptive to believe that an even higher polynomial degree modeling results in a truly more accurate representation of a physical system [20]. Thus, either a fourth-, fifth-, or sixth-degree polynomial would be adequate in this instance.

To further support this conclusion, the effect of polynomial degree upon the calculated value of m (see sec. A.2.2) was explored. The m values varied with polynomial degree, as was expected (these results are not shown in this report); but more importantly, the amount of variation became smaller as the polynomial degree increased. Variations in m among the fourth-, fifth-, and sixth-degree polynomial computations were smaller than the error in m due to measurement uncertainties (given in sec. 7.6). And the calculated values began to cluster around a stable value. Thus, the above conclusion is reinforced.

Based on these observations, a fifth-degree polynomial has been chosen to represent the detector nonlinearity characteristic. If a fourth- or a sixth-degree polynomial had been chosen, the change in the effect of the uncertainty in the B coefficients, and subsequently on the meter's overall measurement error, would have been minor.

7.2.2. Model Parameters

Uncertainties in the B coefficients of the nonlinearity model (see sec. A.2) produce an error in the calculated value of m. These uncertainties are analyzed in two parts:
(1) Uncertainties due to instrumentation inaccuracies (systematic errors), and
(2) uncertainties due to measurement variations (random errors), including instabilities in the detector network being tested. These uncertainties and their effects on the measured value of m are discussed below.

7.2.2.1. Instrument Inaccuracy

The uncertainty in m due to instrumentation inaccuracies is evaluated by computing the spread in calculated values of m that results when test meter readings are perturbed by an amount equal to the inaccuracy specified for the meter.

Test meter inaccuracies are as follows:

a. Type II power bridge. The specified accuracy [21] is 0.03 percent for power measurement; thus, it is 0.015 percent for rf voltage measurement.

b. Digital voltmeter. The specified accuracy for a 24-hour period is as follows:

1.0 volt range: $\pm$0.001 percent of R $\pm$ 10.0μV
10.0 volt range: $\pm$0.001 percent of R $\pm$ 100.0μV

where R is the voltage reading.

Consider first the case where the measured rf input voltage values are changed by a factor equal to the power bridge specified inaccuracy, i.e., by 1.0 $\pm$ 0.015 percent, while keeping the measured dc output voltage values unchanged. This corresponds to a constant $\pm$0.015 percent error in the rf measurement and no error in the dc measurement. The effect on the calculated m values is shown in table 12. The effect is extremely small. In fact, if the error in the rf voltage data is allowed to be as large as $\pm$10.0 percent, the effect on the calculated values of m is shown in table 13.

Table 12. Effect of ±0.015 percent error in rf voltage data on the calculated values of m.

Nominal m	Change in m
0.10	<-0.000 000 04
0.20	<-0.000 000 06
0.30	<-0.000 000 07
0.40	<-0.000 000 05
0.50	<-0.000 000 03
0.60	<+0.000 000 01
0.70	<+0.000 000 04
0.80	<+0.000 000 04
0.90	<-0.000 000 04

Table 13. Effect of ±10.0 percent error in rf voltage data on the calculated values of m.

Nominal m	Change in m
0.10	<±0.000 000 05
0.20	<±0.000 000 09
0.30	<±0.000 000 10
0.40	<±0.000 000 09
0.50	<±0.000 000 05
0.60	<±0.000 000 02
0.70	<±0.000 000 07
0.80	<±0.000 000 06
0.90	<±0.000 000 06

Next, consider the case where the measured dc output voltage values are changed by an amount equal to the DVM specified inaccuracy, i.e., by ±0.001 percent of R ±0.0001 volt (10-volt range), while keeping the measured rf input voltage values unchanged. The effect on the calculated m values is shown in table 14. The effect is very small. In fact, if the error in the dc voltage data is allowed to be as large as ±1.0 percent of R ±0.0001 volt, the effect is shown in table 15.

Table 14. Effect of ±0.001 percent R ±0.0001 volt error in dc voltage data on the calculated values of m.

Nominal m	Change in m
0.10	<±0.000 002
0.20	<±0.000 004
0.30	<±0.000 006
0.40	<±0.000 008
0.50	<±0.000 010
0.60	<±0.000 012
0.70	<±0.000 014
0.80	<±0.000 016
0.90	<±0.000 018

Table 15. Effect of ±1.0 percent R ±0.0001 volt error in dc voltage on the calculated values of m

Nominal m	Change in m
0.10	<±0.000 03
0.20	<±0.000 06
0.30	<±0.000 08
0.40	<±0.000 10
0.50	<±0.000 12
0.60	<±0.000 14
0.70	<±0.000 15
0.80	<±0.000 17
0.90	<±0.000 19

Test meter inaccuracies as large as these inflated values are very improbable. Based on these calculations, it appears that the uncertainty, Δm_{dm}, in calculated m due to test instrumentation inaccuracies is insignificant.

7.2.2.2. Measurement Variations

The uncertainty in m due to data variations in the measurement of B coefficients, due to all causes, is evaluated by computing the spread in the calculated values of m from each individual data run. (Reminder: There are nine such data runs at each of three carrier frequencies.) Table 16 shows the sample standard deviation [19], s, of calculated m as a function of frequency for selected values of m.

Table 16. Sample standard deviation, s, for calculated values of m

m	30 MHz data	110 MHz data	332 MHz data
0.1000	0.4×10^{-5}	1.0×10^{-5}	4.2×10^{-5}
0.2000	0.8×10^{-5}	2.1×10^{-5}	7.7×10^{-5}
0.3000	1.0×10^{-5}	3.1×10^{-5}	10.2×10^{-5}
0.4000	1.2×10^{-5}	4.0×10^{-5}	11.5×10^{-5}
0.5000	1.2×10^{-5}	4.9×10^{-5}	12.3×10^{-5}
0.6000	1.2×10^{-5}	5.7×10^{-5}	13.7×10^{-5}
0.7000	1.3×10^{-5}	6.5×10^{-6}	16.5×10^{-5}
0.8000	1.6×10^{-5}	7.1×10^{-6}	20.3×10^{-5}
0.9000	1.9×10^{-5}	7.6×10^{-5}	24.5×10^{-5}

The sample standard deviation times the factor 1.960 defines the confidence interval in which 95 percent of the m values would fall if the variation in calculated m were random. This quantity, shown in table 17, is used as a valid measure of the uncertainty, Δm_{dv}, in calculated m due to variations in the measurement data by which the rf detector nonlinearity correction is determined.

Table 17. Uncertainty in m due to measurement instability
Δm_{dv} = 1.960s

m	30 MHz	110 MHz	332 MHz
0.1000	±0.000 008	±0.000 020	±0.000 082
0.2000	±0.000 015	±0.000 041	±0.000 152
0.3000	±0.000 020	±0.000 060	±0.000 200
0.4000	±0.000 023	±0.000 078	±0.000 226
0.5000	±0.000 023	±0.000 096	±0.000 241
0.6000	±0.000 023	±0.000 112	±0.000 269
0.7000	±0.000 026	±0.000 127	±0.000 324
0.8000	±0.000 031	±0.000 139	±0.000 398
0.9000	±0.000 037	±0.000 149	±0.000 480

7.2.3. Computation of m

The final value of m is calculated as described in section A.2.2. The procedure uses the Newton-Raphson method [22] which is an approximation method for finding a numerical solution of transcendental equations (see Appendix C). It can, by iteration, be carried to a point beyond which further improvement in m is insignificant. For our purposes, this point is reached when the change in calculated m from a previous approximation is smaller than 0.0001, the meter resolution. Beyond this point, the error introduced by the Newton-Raphson method is insignificant, and such is the case for this work (see Appendix C).

Two other sources of error may arise with the use of the Newton-Raphson method. This method requires numeric values for the B coefficients and for V_c, the dc voltage proportional to the rf carrier level. Errors in these quantities produce errors in the calculated value of m.

B coefficient errors have been dealt with in section 7.2.2. The effect of the error in V_c is found by perturbing the value of V_c by an amount equal to the voltmeter's specified inaccuracy and computing the effect on the calculated m.

The meter inaccuracy in this instance is ±0.002 percent. The resulting effect on m is shown in table 18. The effect is extremely small. In fact, if the error in V_c is allowed to be as large as ±1.0 percent, the effect is shown in table 19.

Table 18. Effect of ±0.002 percent error in V_c measurement on the calculated values of m

Nominal m	Change in m
0.10	<±0.000 000 06
0.20	<±0.000 000 11
0.30	<±0.000 000 16
0.40	<±0.000 000 21
0.50	<±0.000 000 25
0.60	<±0.000 000 29
0.70	<±0.000 000 32
0.80	<±0.000 000 36
0.90	<±0.000 000 40

Table 19. Effect of ±1.0 percent error in V_C measurement on the calculated values of m

Nominal m	Change in m
0.10	<±0.000 03
0.20	<±0.000 06
0.30	<±0.000 08
0.40	<±0.000 11
0.50	<±0.000 13
0.60	<±0.000 14
0.70	<±0.000 16
0.80	<±0.000 18
0.90	<±0.000 20

Voltmeter inaccuracy as large as 1.0 percent is very improbable. Thus, the error in calculated m due to meter error is insignificant.

7.2.4. Summary of Detector Error

The systematic errors of tables 12, 14, and 18 are combined on a root-sum-square basis, and listed in table 20. The detector's random error is as listed in table 17.

Table 20. Total detector systematic error

m	Error
0.1000	0.000 002
0.2000	0.000 004
0.3000	0.000 006
0.4000	0.000 008
0.5000	0.000 010
0.6000	0.000 012
0.7000	0.000 014
0.8000	0.000 016
0.9000	0.000 018

7.3. AC Channel Error

The measurement uncertainty attributable to the ac channel is divided into three parts: (1) Nonlinearity, (2) frequency response, and (3) gain instability. The uncertainties due to (1) and (2) come from the uncertainties in the corrections for these characteristics. These three uncertainties are discussed below.

To provide data for this analysis, measurements of dc output voltages versus ac input voltage were made by the techniques described in sections A.3.3 and A.4.1.

7.3.1. Nonlinearity

The nonlinearity correction uncertainty is comprised of two parts:

a. Decade divider accuracy
b. Measurement system instability

The decade divider's error is specified as 5 parts in 10 million when it is connected between a zero ohm source impedance and an infinity ohms load impedance. In the measurement system (see sec. A.3.3), the source impedance was 50 ohms and the load impedance was two megohms. The calculated division ratios for this case are shown in table 21. These ratios are further normalized by dividing each ratio by the maximum calculated ratio, 0.9999750. The effect of this error on the calculated m is shown in table 22.

Table 21. Decade divider ratio

Indicated ratio	Calculated ratio	Normalized ratio
0.000 0000	0.000 000 00	0.000 0000
0.100 0000	0.099 999 97	0.100 0025
0.200 0000	0.199 999 80	0.200 0048
0.300 0000	0.299 999 32	0.300 0068
0.400 0000	0.399 998 40	0.400 0084
0.500 0000	0.499 996 87	0.500 0094
0.600 0000	0.599 994 60	0.600 0096
0.700 0000	0.699 991 42	0.700 0089
0.800 0000	0.799 987 20	0.800 0072
0.900 0000	0.899 981 77	0.900 0043
1.000 0000	0.999 975 00	1.000 0000

The instabilities of the signal generator output voltage and ac channel gain were too small to be seen on the ratio voltmeter. Therefore, they must be less than $\pm$0.0001 in units of modulation factor. The effect of this uncertainty on the calculated m is also shown in table 22.

Table 22. Effect of nonlinearity measurement uncertainty on the calculated values of m

m	Systematic error	Random error
0.1000	+0.000 0025	$<\pm$0.0001
0.2000	+0.000 0048	$<\pm$0.0001
0.3000	+0.000 0068	$<\pm$0.0001
0.4000	+0.000 0084	$<\pm$0.0001
0.5000	+0.000 0094	$<\pm$0.0001
0.6000	+0.000 0096	$<\pm$0.0001
0.7000	+0.000 0089	$<\pm$0.0001
0.8000	+0.000 0072	$<\pm$0.0001
0.9000	+0.000 0043	$<\pm$0.0001

Note that the modulation meter's ratio voltmeter nonlinearity is included as part of the ac channel nonlinearity (see sec. A.3.3).

7.3.2. Frequency Response

The frequency response correction uncertainty is comprised of three parts:

a. AC voltmeter accuracy
b. DC voltmeter accuracy
c. Measurement system instability

The ac voltmeter's specified accuracy is as follows:

Frequency Range	Accuracy
20 Hz to 50 Hz	±0.38 percent
50 Hz to 10 kHz	±0.11 percent
10 kHz to 30 kHz	±0.25 percent

The dc voltmeter's specified accuracy is ±0.001 percent. This is so much better than the ac voltmeter accuracy that the combined accuracy of the two voltmeters in making the dc/ac ratio measurement is essentially equal to the ac voltmeter accuracy given above.

The effect of these voltmeter accuracies on the systematic error in the calculated m for ILS/VOR tones is shown in table 23. The effect for other af tones may be calculated as described in section 7.7.

Signal generator output voltage and ac channel gain instabilities produce variations in the measured dc/ac voltage ratio whose sample standard deviation was measured to be approximately 1.4×10^{-5}. The effect of this standard deviation multiplied by the factor 1.960 (see sec. 7.2.2.2) is to generate the random errors listed also in table 23.

Table 23. Effect of frequency response measurement uncertainty on the calculated values of m

	Systematic error			Random error
m	30 Hz	90 Hz, 150 Hz	9960 Hz	20 Hz to 10 kHz
0.1000	±0.000 38	±0.000 11	±0.000 11	±0.000 0027
0.2000	±0.000 76	±0.000 21	±0.000 21	±0.000 0053
0.3000	±0.001 14	±0.000 31	±0.000 31	±0.000 0080
0.4000	±0.001 51	±0.000 42	±0.000 42	±0.000 0107
0.5000	±0.001 89	±0.000 52	±0.000 52	±0.000 0134
0.6000	±0.002 27	±0.000 63	±0.000 63	±0.000 0160
0.7000	±0.002 65	±0.000 73	±0.000 73	±0.000 0187
0.8000	±0.003 03	±0.000 84	±0.000 83	±0.000 0214
0.9000	±0.003 41	±0.000 94	±0.000 94	±0.000 0240

7.3.3. Gain Instability

The ac channel gain relative to the dc channel gain is designed to be unity. If this relationship changes because of a gain change in either the ac or dc channels, a measurement error results. Changes in ac channel gain can be monitored and corrected by means of the calibration provision built into the modulation meter (see sec. 5.2.1.3). Gain changes are slow (e.g., <0.01 percent per hour), and the amount of change allowed by the operator is under his control. When properly adjusted, the measurement error due to ac channel gain changes can be made smaller than ±0.0001 in units of modulation factor. However, in order to allow for some uncorrected gain changes during the time of a measurement, we assign a measurement uncertainty of ±0.0002 modulation factor unit to this error source.

The effect of this uncertainty on the calculated m is a constant ±0.0002 uncertainty in each value of m.

7.4. DC Channel Error

No provision has been made for manual adjustment of dc channel gain. Tests show that gain and offset instability is no greater than ±0.012 percent. The effect of this uncertainty on the calculated m is given in table 24.

Table 24. Effect of dc channel error on the calculated values of m

m	Uncertainty
0.1000	±0.000 012
0.2000	±0.000 024
0.3000	±0.000 036
0.4000	±0.000 048
0.5000	±0.000 060
0.6000	±0.000 072
0.7000	±0.000 084
0.8000	±0.000 096
0.9000	±0.000 108

7.5. Ratio Voltmeter Error

The measurement uncertainty due to the modulation meter's ratio voltmeter consists of four parts:

1. Measurement channel nonlinearity
2. Measurement channel instability
3. Reference channel instability
4. Digitizing error

Measurement channel nonlinearity is included as part of the ac channel nonlinearity. See section 7.3.1.

Measurement and reference channel stability specifications are as follows:

Temperature:
- Range: ±0.002 percent of reading per degree centigrade
- Offset: ±0.0005 percent of full-scale reading per degree centigrade

Power Line: ±0.005 percent of reading per volt

The observed instability of this voltmeter is a change of less than ±0.0001 per day, in units of modulation factor, after a 4-hour warm-up. The voltmeter is zeroed prior to a measurement run, and its zero reading normally does not change over a 9-hour period.

The digitizing error is ±0.0001 in units of modulation factor.

In sum, the effect of all ratio voltmeter errors on the calculated m is a constant ±0.0001 uncertainty in each value of m.

7.6. Error Summary

Systematic errors for ILS and VOR tones are summarized in table 25. These apply at all rf carrier frequencies. The largest source of error is the ac channel frequency response measurement. A more accurate ac voltmeter (see sec. 7.3.2) would permit a worthwhile reduction in total systematic error, especially for af tones below 50 Hz.

Random errors for three rf carrier frequencies (30 MHz, 110 MHz, and 332 MHz) are summarized in table 26. These apply for all af modulation frequencies. Although the random error generated by the ac channel nonlinearity measurement is known to be less than ±0.0001 (see sec. 7.3.1), it is taken to be ±0.0001 in the calculation of total random error, thus making the total error a "conservative" figure.

Total measurement errors for ILS and VOR signals are summarized in tables 5 and 6, section 6. Measurement errors at other than the carrier and modulation frequencies included in these tables may be calculated by the procedure described below.

7.7. General Procedure for Calculating Measurement Error

The total measurement error for any signal that falls within the measurement ranges of this instrument may be found from the information in this report by the following procedure:

a. Find the individual systematic and random errors by the methods described below.

b. Calculate the root-sum-square (RSS) value of these individual errors.

$$RSS = \left[\sum_i (E_i)^2\right]^{1/2}, \tag{27}$$

where E_i is the ith individual error. RSS is the total measurement error for the given signal.

7.7.1. Systematic Errors

Individual <u>systematic</u> errors are found as follows:

a. RF detector nonlinearity error. This is given in table 20 for selected values of m. It is a linear function of m and may be calculated from the equation

$$\text{rf det. error} = \pm\, 2\ m \times 10^{-5}. \tag{28}$$

Table 25. Summary, systematic errors (±)

Modulation factor	RF detector nonlinearity	AC channel nonlinearity	AC channel frequency response	AC channel gain instability	DC channel gain instability	Ratio voltmeter digitizing error	Total
30 Hz							
0.1000	0.000002	0.0000025	0.00038	0.0002	0.000012	0.0001	0.00044
0.2000	0.000004	0.0000048	0.00076	0.0002	0.000024	0.0001	0.00079
0.3000	0.000006	0.0000068	0.00114	0.0002	0.000036	0.0001	0.00116
0.4000	0.000008	0.0000084	0.00151	0.0002	0.000048	0.0001	0.00153
0.5000	0.000010	0.0000094	0.00189	0.0002	0.000060	0.0001	0.00191
0.6000	0.000012	0.0000096	0.00227	0.0002	0.000072	0.0001	0.00228
0.7000	0.000014	0.0000089	0.00265	0.0002	0.000084	0.0001	0.00266
0.8000	0.000016	0.0000072	0.00303	0.0002	0.000096	0.0001	0.00304
0.9000	0.000018	0.0000043	0.00341	0.0002	0.000108	0.0001	0.00342
90/150 Hz							
0.1000	0.000002	0.0000025	0.00011	0.0002	0.000012	0.0001	0.00025
0.2000	0.000004	0.0000048	0.00021	0.0002	0.000024	0.0001	0.00031
0.3000	0.000006	0.0000068	0.00032	0.0002	0.000036	0.0001	0.00039
0.4000	0.000008	0.0000084	0.00042	0.0002	0.000048	0.0001	0.00048
0.5000	0.000010	0.0000094	0.00052	0.0002	0.000060	0.0001	0.00057
0.6000	0.000012	0.0000096	0.00063	0.0002	0.000072	0.0001	0.00067
0.7000	0.000014	0.0000089	0.00073	0.0002	0.000084	0.0001	0.00077
0.8000	0.000016	0.0000072	0.00084	0.0002	0.000096	0.0001	0.00087
0.9000	0.000018	0.0000043	0.00094	0.0002	0.000108	0.0001	0.00098
9960 Hz							
0.1000	0.000002	0.0000025	0.00010	0.0002	0.000012	0.0001	0.00025
0.2000	0.000004	0.0000048	0.00021	0.0002	0.000024	0.0001	0.00031
0.3000	0.000006	0.0000068	0.00031	0.0002	0.000036	0.0001	0.00039
0.4000	0.000008	0.0000084	0.00042	0.0002	0.000048	0.0001	0.00048
0.5000	0.000010	0.0000094	0.00052	0.0002	0.000060	0.0001	0.00057
0.6000	0.000012	0.0000096	0.00063	0.0002	0.000072	0.0001	0.00067
0.7000	0.000014	0.0000089	0.00073	0.0002	0.000084	0.0001	0.00077
0.8000	0.000016	0.0000072	0.00083	0.0002	0.000096	0.0001	0.00087
0.9000	0.000018	0.0000043	0.00094	0.0002	0.000108	0.0001	0.00097

Table 26. Summary, random errors (±)

Modulation factor	RF detector nonlinearity	AC channel nonlinearity	AC channel frequency response	AC channel gain instability	DC channel gain instability	Ratio voltmeter digitizing error	Total
30 MHz							
0.1000	0.000008	<0.0001	0.0000027	--	--	--	0.00010
0.2000	0.000015	<0.0001	0.0000053	--	--	--	0.00010
0.3000	0.000020	<0.0001	0.0000080	--	--	--	0.00010
0.4000	0.000023	<0.0001	0.0000107	--	--	--	0.00010
0.5000	0.000023	<0.0001	0.0000134	--	--	--	0.00010
0.6000	0.000023	<0.0001	0.0000160	--	--	--	0.00010
0.7000	0.000026	<0.0001	0.0000187	--	--	--	0.00010
0.8000	0.000031	<0.0001	0.0000214	--	--	--	0.00011
0.9000	0.000037	<0.0001	0.0000240	--	--	--	0.00011
110 MHz							
0.1000	0.000020	<0.0001	0.0000027	--	--	--	0.00010
0.2000	0.000041	<0.0001	0.0000053	--	--	--	0.00011
0.3000	0.000060	<0.0001	0.0000080	--	--	--	0.00012
0.4000	0.000078	<0.0001	0.0000107	--	--	--	0.00013
0.5000	0.000096	<0.0001	0.0000134	--	--	--	0.00014
0.6000	0.000112	<0.0001	0.0000160	--	--	--	0.00015
0.7000	0.000127	<0.0001	0.0000187	--	--	--	0.00016
0.8000	0.000139	<0.0001	0.0000214	--	--	--	0.00017
0.9000	0.000149	<0.0001	0.0000240	--	--	--	0.00018
332 MHz							
0.1000	0.000082	<0.0001	0.0000027	--	--	--	0.00013
0.2000	0.000152	<0.0001	0.0000053	--	--	--	0.00018
0.3000	0.000200	<0.0001	0.0000080	--	--	--	0.00022
0.4000	0.000226	<0.0001	0.0000107	--	--	--	0.00025
0.5000	0.000241	<0.0001	0.0000134	--	--	--	0.00026
0.6000	0.000269	<0.0001	0.0000160	--	--	--	0.00029
0.7000	0.000324	<0.0001	0.0000187	--	--	--	0.00034
0.8000	0.000398	<0.0001	0.0000214	--	--	--	0.00041
0.9000	0.000480	<0.0001	0.0000240	--	--	--	0.00049

It is normally so small that it may be ignored.

b. AC channel nonlinearity error. This is given in table 22 for selected values of m. It may be approximated at other values of m by interpolation. It is normally so small that it may be ignored.

c. AC channel frequency response error. This is the largest systematic errror and is given by the equation

$$\text{ac freq. resp. error} = -\frac{m\left(\frac{\Delta g}{g}\right)}{g\left(1 + \frac{\Delta g}{g}\right)}, \tag{29}$$

where g is relative gain, given in table 2, and $\Delta g/g$ is the ac voltmeter accuracy, given in section 7.3.2 as a percentage.

Example: Let

$$m = 0.30$$
$$f_m = 12{,}000 \text{ Hz}.$$

From table 2,

$$g = 1.0076.$$

From section 7.3.2,

$$\frac{\Delta g}{g} = \pm 0.25 \text{ percent}.$$

Therefore, from eq (29),

$$\text{ac freq. resp. error} = \pm \frac{0.30 \times 0.0025}{1.0076 \times (1 + 0.0025)}$$

$$= \pm 0.00074 \text{ (modulation factor units)}.$$

For af modulation tones not listed in table 2, approximate values of g may be found by interpolation.

d. AC channel gain instability error. This has been arbitrarily fixed at ± 0.0002 (see sec. 7.3.3).

e. DC channel gain instability error. This is given in table 24 for selected values of m. It is a linear function of m and may be calculated from the equation

$$\text{dc gain instability error} = \pm 1.2\, m \times 10^{-4}. \tag{30}$$

f. Ratio voltmeter digitizing error. This is fixed at ± 0.0001 (see sec. 7.5).

7.7.2. Random Errors

Individual random errors are found as follows:

a. RF detector nonlinearity error. This error has been evaluated only at 30 MHz, 110 MHz, and 332 MHz. It derives from the fluctations that occur in the measurement of the B coefficients (see sec. 7.2.2.2). Table 17 gives this error for selected values of m and carrier frequency. For values not listed, this error may be approximated by interpolation.

b. AC channel nonlinearity error. Although smaller than ± 0.0001, this error has been arbitrarily fixed at ± 0.0001 (see sec. 7.3.1).

c. AC channel frequency response error. This error is also given by eq (29), except that $\Delta g/g$ is 1.960 times the sample standard deviation, s, of the measurement data (see sec. 7.3.2). Thus,

$$\frac{\Delta g}{g} = 1.960 \times 1.4 \times 10^{-5} = 2.7 \times 10^{-5}.$$

Example: Let

$$m = 0.30$$
$$f_m = 12{,}000 \text{ Hz}.$$

From table 2,

$$g = 1.0076.$$

Therefore, from eq (29),

$$\text{ac freq. resp. error} = \pm \frac{0.30 \times 0.000027}{1.0076 \times (1 + 0.000027)}$$

$$= \pm 0.0000080 \text{ (modulation factor units)}.$$

For af modulation tones not listed in table 2, approximate values of g may be found by interpolation. This error is normally so small that it may be ignored.

d. AC channel gain instability error. This error is treated entirely as a systematic error.

e. DC channel gain instability error. This error is treated entirely as a systematic error.

f. Ratio voltmeter digitizing error. This error is treated entirely as a systematic error.

8. Acknowledgements

Those who contributed to this work are as follows: Literature search was provided by I. S. Berry. Clarification of concepts was contributed by C. M. Allred and C. H. Manney. Construction, layout, and functional testing were performed by R. F. Bailer, E. E. Baldwin, and D. G. Melquist. C. J. Roubique contributed to the design of the 90 Hz and 150 Hz signal generator section. Mathematical and programming assistance was provided by C. M. Allred, C. A. Hoer, N. T. Larsen, and P. F. Wacker. Technical management support was supplied by W. J. Anson, A. J. Estin, and C. K. S. Miller. The authors are solely responsible for the choice of design approach, design particulars, and for the performance testing and analysis of the modulation meter described herein.

Special thanks go to S. M. Etzel who typed the manuscript and put it into final form for publication.

9. References

[1] Kayton, M., and Fried, W. R., Avionics Navigation Systems, Chaps. 5 and 14 (John Wiley and Sons, Inc., New York, N.Y., 1969).

[2] Ries, F. X., National Bureau of Standards, private communication.

[3] Lathi, B. P., Signals, Systems, and Communications, Section. 11.5 (John Wiley and Sons, Inc., New York, N.Y., 1965).

[4] Van der Pol, B., and Posthumus, K., Telephone transmitter modulation measured at the receiving station, Experimental Wireless and The Wireless Engineer, 4, No. 42, 140-141 (March 1927).

[5] Jolliffe, C. B., The use of the electron tube peak voltmeter for the measurement of modulation, Proc. IRE, 17, No. 4, 660-663 (April 1929).

[6] Cooper, A. H., and Smith, G. P., A direct reading modulation meter, The Wireless Engineer and Experimental Wireless, 8, No. 99, 647 (Dec. 1931).

[7] Strafford, F. R. W., A direct reading thermal modulation meter, The Wireless Engineer and Experimental Wireless, 11, No. 129, 302-304 (June 1934).

[8] Foot, J. B. L., A simple modulation meter, Journal of Scientific Instruments, 12, No. 7, 216-217 (July 1935).

[9] Williams, F. C., and Chester, A. E., A new modulation meter, The Wireless Engineer, 15, No. 176, 257-262 (May 1938).

[10] Gunsolley, V. V., Differential modulation meter, Electronics, 13, No. 1, 18-20 (Jan. 1940).

[11] Whitehead, J. W., A simple direct-reading modulation meter, Journal of Scientific Instruments, 24, No. 10, 276 (Oct. 1947).

[12] Terman, F. E., and Pettit, J. M., Electronic Measurements, pp. 282-285 (McGraw-Hill Book Co., Inc., New York, N.Y., 1952).

[13] Oliver, B. M., and Cage, J. M., editors, Electronics Measurements and Instrumentation, pp. 639-640 (McGraw-Hill Book Co., Inc., New York, N.Y., 1971).

[14] Sorger, G. U., The accurate measurement of the modulation factor of an amplitude modulated signal, 1974 Conference on Precision Electromagnetic Measurements, IEEE Conference Publication No. 113, 306-309 (July 1974).

[15] Gaudernack, L. F., Some notes on the practical measurement of the degree of amplitude modulation, Proc. IRE, 22, No. 7, 819-846 (July 1934).

[16] (no author) Spectrum Analysis ... Accuracy Improvement, Application Note 150-8, Hewlett Packard Co., March 1976.

[17] Hudson, P. A., Ecklund, W. L., and Ondrejka, R. A., Measurement of the rf peak-pulse power by sampling-comparison method, IRE Trans. on Instrumentation, I-11, Nos. 3 and 4, 280-284 (Dec. 1962).

[18] Smith, J. I., Modern Operational Circuit Design, pp. 155-159 (John Wiley and Sons, Inc., New York, N.Y., 1971).

[19] Wilson, E. B., Jr., An Introduction to Scientific Research, Chap. 9 (McGraw-Hill Book Co., Inc., New York, N.Y., 1952).

[20] Wacker, P. F., National Bureau of Standards, private communication.

[21] Larsen, N. T., and Clague, F. R., The NBS type II power measurement system, Adv. Instrum., 25, Pt. 3, paper no. 712-70, in Proc. 25th Annu. ISA Conf., Philadelphia, Penn., Oct. 26-29, 1970.

[22] Margenau, H., and Murphy, G. M., The Mathematics of Physics and Chemistry, pp. 474-477 (D. Van Nostrand Co., Inc., New York, N.Y., 1943).

[23] Graybill, F. A., An Introduction to Linear Statistical Models, Vol. 1 (McGraw-Hill Book Co., Inc., New York, N.Y., 1961).

[24] Hoer, C. A., Roe, K. C., and Allred, C. M., Measuring and minimizing diode detector nonlinearity, IEEE Trans. on Instr. and Meas., IM-25, No. 4, 324-329 (Dec. 1976).

Appendix A. Analysis of Corrections for Nonlinearity and Frequency Effects

A.1. Introduction

The analysis of nonlinearity effects on the measured value of modulation factor is, for convenience, divided into two parts: (1) RF detector network, and (2) post-detector networks. Frequency response analysis follows the same pattern. These analyses and the measurement corrections that result therefrom are described below.

A.2. RF Detector Nonlinearity

First, consider the ideal amplitude-modulated signal, v(t), where

$$v(t) = V_c(1 + m \cos 2\pi f_m t) \cos 2\pi f_c t, \tag{A.1}$$

that is applied to an ideal detector. We define an ideal detector as one which, for an input voltage v(t), delivers an output voltage $v_o(t)$, where

$$v_o(t) = kV_c(1 + m \cos 2\pi f_m t), \tag{A.2}$$

and k is a constant. By this definition, the relationship between the output voltage, $v_o(t)$, and the envelope of the input voltage, $V_c(1 + m \cos 2\pi f_m t)$, is a linear one; that is, the factor k is independent of rf voltage level. The transfer characteristic of the ideal detector is likewise independent. Thus from eqs (A.1) and (A.2),

$$v_o(t) = (k/\cos 2\pi f_c t) \cdot v(t), \tag{A.3}$$

where the ratio $k/\cos 2\pi f_c t$ is clearly independent of voltage level.

Now consider the nonideal detector that is the same as the ideal detector with one exception; it has a nonlinear voltage transfer characteristic. Of the several mathematical forms that might be used to describe the nonlinearity characteristic, an infinite power series representation of the following form is chosen:

$$y = b_o + b_1 x + b_2 x^2 + b_3 x^3 + \ldots . \tag{A.4}$$

Thus, a general relationship between the envelope, $v_o(t)/k$, of the rf input voltage and the output voltage, $v_n(t)$, of the nonideal detector is

$$v_n(t) = B_o + B_1 v_o(t)/k + B_2[v_o(t)/k]^2 + \ldots + B_i[v_o(t)/k]^i + \ldots, \tag{A.5}$$

where B_o, B_1, B_2, etc. are constants that are characteristic of the detector. Voltage, $v_n(t)$, is comprised of a component proportional to $v_o(t)$ plus distortion products of $v_o(t)$. If the detector were ideal and produced no distortion, all terms of eq (A.5), excepting those equal to $v_o(t)$, would be zero.

Recall from figure 5 that this meter measures the ratio of the amplitude, V_m, of the $\cos 2\pi f_m t$ term to V_c, the amplitude of the dc component of the voltage $v_n(t)$. As can be seen from eqs (A.2) and (A.5), this ratio is not precisely equal to m (except when the detector is ideal). Therefore, we compute m from the measured values of V_m/V_c and V_c,

and from the measured nonlinearity characteristic of the detector network (i.e., from the B coefficients). How this is done is described in the following subsections.

A.2.1. B Coefficient Measurement

The B coefficients of eq (A.5) are calculated by a polynomial regression method [23] in which the coefficients of an nth degree polynomial are calculated using a least-squares fit of experimental data. The data, consisting of measured rf input voltage and dc output voltage values, are obtained with the measurement system diagrammed in figure A.1. This is an adaptation of one described by Hoer, et al. [24]. The principal parts of this system are as follows:

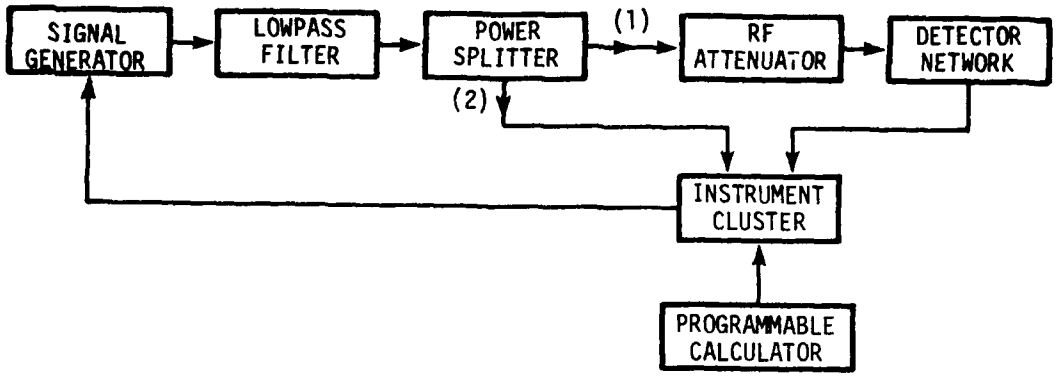

Fig. A.1. Measurement system for detector transfer coefficients

a. CW rf signal generator, whose output level is voltage controllable from the instrument cluster.

b. Lowpass filter (LPF), to assure purity of the rf test signal.

c. RF power splitter, to divide the test signal into two parts. Part (1) is the test voltage fed to the rf detector network. Part (2) is a sample voltage used to set and stabilize the level of the test voltage.

d. RF attenuator, to set the nominal level of the rf test voltage.

e. Instrument cluster, consisting of the following units:

RF bolometer
NBS Type II power bridge [21]
5 1/2 - digit digital voltmeter (DVM)
Digital-to-analog converter (DAC)
Precision dc voltage source
Input scanner

f. Programmable calculator.

The operation of the measurement system is described in reference [24]. Briefly, it is as follows:

The rf signal generator, lowpass filter, power splitter, bolometer, and power bridge comprise a leveling loop for delivering a controlled rf voltage to the rf attenuator. This loop is under the control of the programmable calculator, through which the desired rf voltage level can be selected. The DAC, in conjunction with the precision dc voltage source, provides the dc controlling voltages to the signal generator at the command of the calculator. The scanner, also under calculator control, connects the DVM to the various terminals (detector output, power bridge, etc.) at which voltages are to be measured. The DVM output data bus delivers measurement information to the calculator as requested by the program.

The measurement program, which uses BASIC computer language, steps the cw rf voltage through a range of values that corresponds approximately to the envelope voltages of a 90 percent modulated carrier. For example, if we assume a carrier amplitude of 1.00 volt, the cw test signal amplitude is stepped from 0.10 volt to 1.90 volts. Forty-five (45) data points were used to cover this range. At each data point, two voltages are measured, viz., (1) a voltage proportional to the rf voltage at the input terminals of the detector, and (2) the dc output voltage from the detector. The rf input voltage is computed from a power measurement made with the Type II bridge. Thus, the measurement sequence provides the two sets of voltages from which the B coefficients are calculated.

As stated in section 3.3, the voltage range of 0.10 to 1.90 volts is 25.58 dB. However, the bolometer's measurement range is limited to approximately 12 dB. Therefore, the measurement data are taken in three groups, each covering a range of approximately 10 dB, with an overlap of approximately 2 dB between adjacent groups. These three groups of data are subsequently merged into one continuous set of data by an interpolation process. The rf attenuator, figure A.1, is used to set the nominal rf voltage level to obtain each of the three groups of data (e.g., 16 dB for Group 1, 8 dB for Group 2, and 0 dB for Group 3).

Prior to calculating the B coefficients from the merged measurement data, the rf voltage values are multiplied by a factor, computed from the data, that forces the largest rf voltage amplitude value to be numerically equal to the largest dc output voltage value. For the data as taken in these tests, this data point corresponds to approximately 90 percent modulation. The purpose of this step is to force the B_1 coefficient to be approximately unity; this removes from the data the effect of attenuation between the detector input terminals and the point at which the rf voltage is actually measured by the Type II bridge (which is at the side arm of the power splitter). The result of this step is to produce a new set of input data values, proportional to the actual rf input voltage values, that would be numerically the same as the dc output voltage values from an ideal detector. Thus, the actual detector's nonlinearity characteristic is described in terms of how it differs from an ideal detector network.

Having obtained the two sets of data, viz., (1) the measured dc output voltage values, and (2) a set of calculated dc output voltage values that are proportional to the measured rf input voltage values, the B coefficients are calculated by the polynomial regression method [23]. A fifth degree polynomial is chosen to model the detector nonlinearity characteristic. Thus, we calculate coefficients B_0, B_1, B_2, B_3, B_4, and B_5. The reasons for truncating eq (A.5) at the fifth degree are discussed in section 7.2.1.

A.2.2. Detector Nonlinearity Correction

Having found the B coefficients of eq (A.5), truncated after the fifth degree, m is calculated from the corrected ratio voltmeter reading, M_c, and from V_c as follows:

a. First, find $[v_o(t)]^n$ algebraically from eq (A.2), where

$n = 1, 2, 3, 4,$ and 5.

b. Second, insert these algebraic terms into eq (A.5), truncated to six terms.

c. Third, collect the zero degree (dc) terms from the right hand side of eq (A.5), and set their sum equal to S_0. S_0 is a function of V_c, m, and the B coefficients. It is the algebraic representation of the denominator of M_c.

d. Fourth, collect the first degree terms in $\cos 2\pi f_m t$ from eq (A.5), and set their sum equal to S_1. S_1 is likewise a function of V_c, m, and the B coefficients. It is the algebraic representation of the numerator of M_c.

e. Finally, from the two equations in S_0 and S_1, solve for m by the Newton-Raphson method [22] of successive approximation. A detailed description of this method is given in Appendix C. To do this, we need the following information:

The numeric values of B_n
The corrected voltage ratio, M_c
The measured value of V_c

Because of its complexity, this computation is best done on a programmable computer. In practice then, with the B coefficients stored in the program, m is quickly computed by inputting the values of M_c and V_c, and running the program.

A.3. Post-Detector Nonlinearity

A.3.1. DC Channel Networks

In accordance with the design and operation of the modulation meter, the voltage applied to the dc channel is held constant at +2.50 volts (see sec. 5.2.1.1). Hence dc channel voltage nonlinearity is not a factor for which a correction must be applied.

A.3.2. AC Channel Networks

Input voltage levels to the ac channel range from 0.25 volt peak at m = 0.10 to 2.25 volts peak at m = 0.90. This is a dynamic range of approximately 19 dB. AC channel gain over this range is not constant, thus causing an error in the measurement of the ratio, V_m/V_c. The correction for this effect is developed as follows.

Let g be the ratio of the ac channel gain to the dc channel gain. First, assume that g is manually adjusted to unity when the ac input peak voltage is 2.50 volts. (Provision for this adjustment is included in the instrument.) Then the dc output voltage from the precision ac rectifier is equal to the output voltage from the dc channel. If for some other sinusoidal input voltage of peak amplitude, V_u, the relative voltage gain is g_u, then the dc output voltage, $V_{d,u}$, is

$$V_{d,u} = g_u V_u, \tag{A.6}$$

and the voltage ratio, $M(V_u)$, at the ratio voltmeter input is

$$M(V_u) = \frac{V_{d,u}}{V_c} = \frac{g_u V_u}{V_c}, \tag{A.7}$$

where g_u is a function of V_u. In general, g_u may be less than or greater than unity, depending upon the nonlinearity characteristic of the ac channel.

If g_u were constant and equal to unity,

$$M(V_u) = \frac{V_u}{V_c}, \tag{A.8}$$

and no correction to $M(V_u)$ would be needed. Otherwise, the error, δm_n, in the measured ratio is

$$\delta m_n = \frac{g_u V_u}{V_c} - \frac{V_u}{V_c}. \tag{A.9}$$

The nonlinearity correction, Δm_n, to be added to the measured ratio, $M(V_u)$, is therefore

$$\Delta m_n = M(V_u) \cdot \frac{1 - g_u}{g_u} . \tag{A.10}$$

This correction is measured by the method described below.

A.3.3. AC Channel Nonlinearity Measurement

Figure A.2 shows a block diagram of the system for measuring the ac channel nonlinearity correction, Δm_n. The principal parts of this system are as follows:

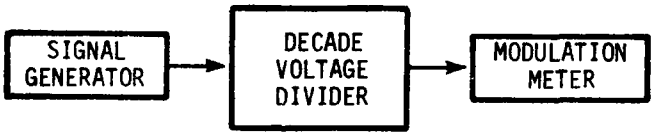

Fig. A.2. Measurement system for ac channel nonlinearity

a. Stable audiofrequency signal generator

b. Precision autotransformer-type decade voltage divider

The measurement procedure is as follows:

a. The decade divider's output port is connected to the input port of the ac channel immediately following the detector diode.

b. The signal generator frequency and the af bandpass filter in the modulation meter are adjusted to the test frequency.

c. With the decade divider's ratio set at 1.0000000, the generator's output voltage is adjusted to produce a reading of 1.0000 on the modulation meter's ratio voltmeter. The

relative gain of the ac channel is previously set to unity at the test frequency and at this (maximum) voltage level.

d. The decade divider's ratio is stepped from 1.0000000 to 0.0000000 in steps of 0.1000000, and the modulation meter's ratio voltmeter reading is recorded at each step.

e. The reading error, δm_n, due to nonlinearity, is calculated from the equation,

$$\delta m_n = \text{Voltmeter Reading} - \text{Decade Divider Reading}. \tag{A.11}$$

The nonlinearity correction, Δm_n, is the negative of δm_n.

$$\Delta m_n = \text{Decade Divider Reading} - \text{Voltmeter Reading}. \tag{A.12}$$

Table 3, section 4.2.2.2., gives Δm_n for selected values of M as a function of test frequency. For the unfiltered case, the test frequency was 1020 Hz.

Notice that the corrections to be applied when the bandpass filters are in use are generally larger (except at 9960 Hz) than when no filter is inserted. Tests show that the gains of these particular filters (30 Hz, 90 Hz and 150 Hz) are input voltage dependent. (The 9960 Hz filter is of a different type, being comprised of separate high pass and lowpass filters in cascade.) The small nonlinear behavior of the unfiltered configuration at low voltages is caused by the characteristics of the active circuits in the precision ac rectifier network.

Because these measurements pertain to the complete ac channel from the detector output port to the ratio voltmeter output display, any nonlinearity in the ratio voltmeter is included in the correction, Δm_n.

A.4. Frequency Response Correction

If the rf detector and the ac channel transfer characteristics are not constant with modulation frequency, f_m, the measured value of V_m, and hence of the ratio, V_m/V_c, will vary with f_m. The correction for this effect is calculated as follows:

Let $g(f_m)$ be the ratio of (1) the detector-plus-ac-channel gain at frequency f_m to (2) the detector-plus-dc-channel gain at zero frequency. Then the voltage ratio, $M(f_m)$, at the ratio voltmeter input, is

$$M(f_m) = \frac{V_m g(f_m)}{V_c} . \tag{A.13}$$

If $g(f_m)$ were unity and independent of f_m, no correction would be needed; otherwise, the error, δm_f, in the measured ratio is

$$\delta m_f = \frac{V_m g(f_m)}{V_c} - \frac{V_m}{V_c} . \tag{A.14}$$

The frequency response correction, Δm_f, to be added to the measured ratio, $M(f_m)$, is the negative of δm_f.

$$\Delta m_f = M(f_m) \cdot \frac{1 - g(f_m)}{g(f_m)} \qquad (A.15)$$

To evaluate the relative gain factor, $g(f_m)$, it was separated into two parts; viz., the detector part and the ac channel part. The detector frequency response was not measured, but calculations based upon an analysis of the circuit (which is a resistance-capacitance lowpass filter configuration) show the relative gain to be between unity and 0.99999 at frequencies from zero to 100 kHz. Thus, the detector frequency response should contribute no significant measurement error within this audiofrequency range. The ac channel unfiltered frequency response was measured by the method described below.

A.4.1. Audiofrequency Response Measurement

Figure A.3 shows a block diagram of the system for measuring ac channel frequency response. The principal parts are as follows:

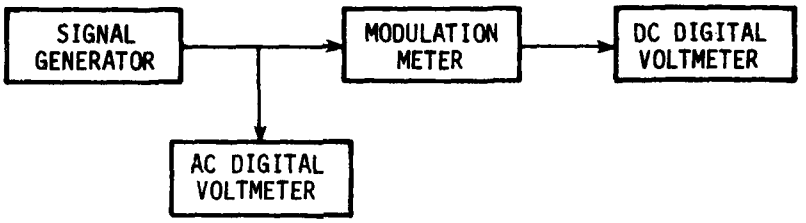

Fig. A.3. Measurement system for ac channel frequency response

a. Stable audiofrequency signal generator
b. 6 1/2 - digit ac digital voltmeter
c. 6 1/2 - digit dc digital voltmeter

The signal generator's output port is connected to the input port of the ac channel immediately following the detector diode. The ac channel's dc output voltage is measured at the signal input port of the ratio voltmeter. The signal generator's output voltage is held approximately constant as its frequency is varied from 20 Hz to 20 kHz. The ac channel absolute gain is calculated as the ratio of the dc output voltage to the ac input voltage. Relative gain, $g(f_m)$, is calculated by normalizing the data to unity at 100 Hz; this is given in table 2 and plotted in figure 6, section 4.2.2.1.

Appendix B. Alternative Detector Circuits

B.1. Introduction

Three alternative approaches for improving detector linearity were explored during the course of this work. Each involves the addition of a correction network between the output port of the envelope detector, figure 9, and the following filter networks. The correction network modifies the detector diode output voltage to produce a waveform that is more closely similar to the rf envelope waveform.

The three approaches are: (1) Modulated subcarrier feedback technique, (2) baseband feedback technique, and (3) quadratic technique. Each has different strengths and weaknesses. The first technique has been incorporated in the modulation standard along with the detector described in section 5.2.1.1, and can be utilized after a simple wiring change. The other techniques were carried to various stages of development, but work on them was not completed. Each is described below.

B.2. Modulated Subcarrier Feedback Technique

The modulated subcarrier feedback network described in this section can be used only when the modulation frequency is between approximately 20 Hz and 1000 Hz. However, within this range the measurement accuracy is comparable to that achieved by the detector described in section 5.2.1.1 without any need to correct for detector nonlinearity (as in sec. 4.2.2.3).

A block diagram of the subcarrier feedback network, including the rf signal detector (diode No. 1), is shown in figure B.1. The heart of the technique is the use of a second

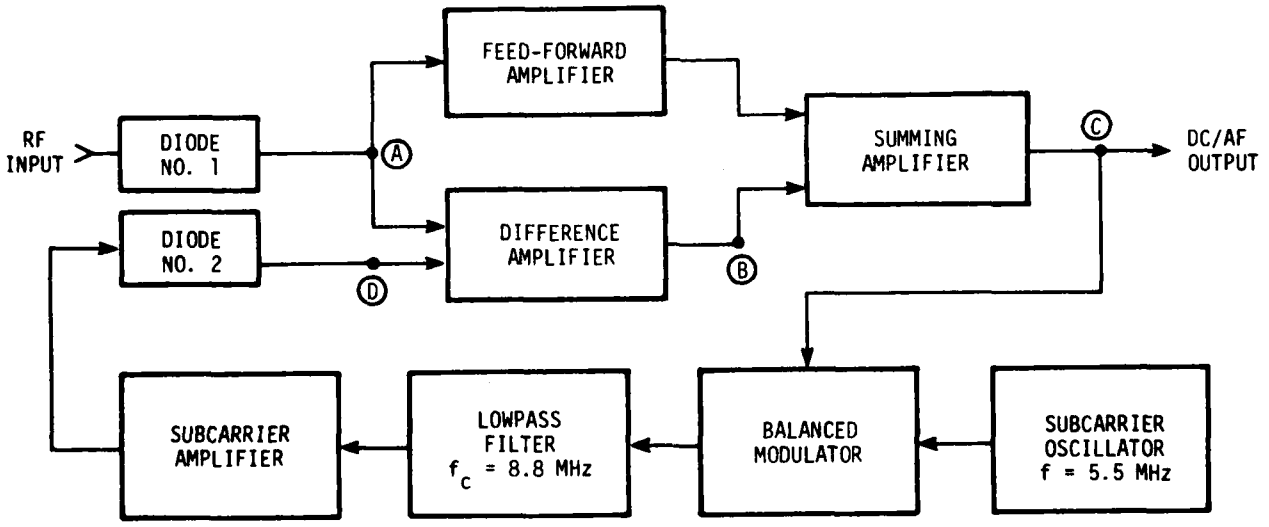

Fig. B.1. Block diagram of modulated subcarrier feedback detector

diode (diode No. 2) whose transfer characteristic is closely similar to that of the detector diode. Ideally, the two diodes would be identical. Diode No. 1 detects the amplitude-modulated rf signal whose modulation factor is to be measured. Diode No. 2

detects an amplitude-modulated 5.5 MHz subcarrier signal whose envelope (i.e., its modulation waveform) is closely similar to (ideally, the same as) that of the rf input signal. This envelope is produced from the output voltage of diode No. 1 at point A by the action of the networks between point A and point C, and is available at point C as a low-distortion replica of the rf input signal envelope.

B.2.1. Overview Circuit Description

This section describes the general operating principles of the modulated subcarrier feedback detector. Section B.2.2 will describe the circuit in more detail.

Consider first the circuit of figure B.1 without diode No. 1 and the feed-forward amplifier. See figure B.2. This has the configuration of a conventional negative feedback

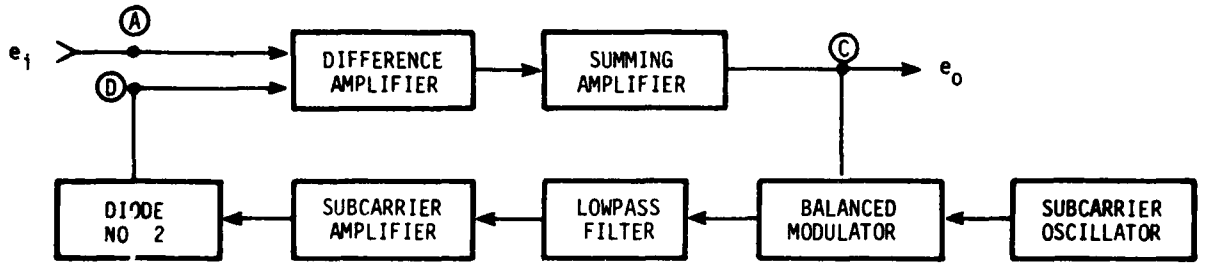

Fig. B.2. Amplifier with feedback

circuit, but the feedback branch from point C to point D involves a frequency translation to radiofrequency (5.5 MHz), and back to dc-audiofrequency. From feedback amplifier theory,

$$e_o = \frac{A_1 A_2}{1 + A_1 A_2 B} e_i, \tag{B.1}$$

where

A_1 = Difference amplifier gain,
A_2 = Summing amplifier gain,
B = Feedback branch gain.

The voltage at point D is Be_o. From eq (B.1),

$$Be_o = \frac{A_1 A_2 B}{1 + A_1 A_2 B} e_i. \tag{B.2}$$

If $A_1 A_2 B \gg 1$, then

$$Be_o \simeq e_i, \tag{B.3}$$

and the voltage at point D is essentially a replica of the voltage at point A. This is the characteristic of a negative feedback amplifier circuit that is exploited in this technique. For, if the open loop gain, A_1A_2B, were infinite, and if the two diodes of figure B.1 responded identically to the two rf input voltages, then the envelope of the subcarrier voltage input to diode No. 2 would be equal to the envelope of the input to diode No. 1. And, if the subcarrier modulation process were linear, the voltage waveform at point C would be identical to the modulation waveform of the rf input voltage to diode No. 1.

In practice, the loop gain A_1A_2B must be kept small to prevent oscillation because of phase shifts. Therefore, additional gain outside the loop is provided by the feed-forward amplifier shown in figure B.1. In this case,

$$e_o = \frac{A_2(A_1 + A_3)}{1 + A_1A_2B} e_i, \tag{B.4}$$

where

A_3 = feed-forward amplifier gain.

If gain A_3 is set equal to the value

$$A_3 = \frac{1}{A_2B}, \tag{B.5}$$

then, from eqs (B.4) and (B.5),

$$Be_o = e_i \tag{B.6}$$

without the necessity of having gains A_1 or A_2 be large.

The circuit of figure B.1 has certain problems in practice. First, diodes No. 1 and No. 2 cannot be exactly matched over their full operating voltage and frequency ranges. Second, the subcarrier feedback branch, particularly the balanced modulator, is not perfectly linear. Modulator leakage introduces additional linearity problems. Finally, loop phase shifts, primarily in the 8.8 MHz bandpass filter, limit the audiofrequency bandwidth over which the circuit will work as described. For stability, the difference amplifier frequency response has been specifically designed to be nearly constant only from approximately 3 Hz to 500 Hz, above which it rapidly declines. For all these reasons, the voltage at point C is a less than perfect replica of the rf input voltage envelope.

In spite of these difficulties, this detector performs well for the lower audiofrequency modulation tones, as discussed in section B.2.3. As improved balanced modulators and operational amplifiers become available, this circuit could conceivably be used for modulation tones up to 10 kHz or higher.

B.2.2. Detailed Circuit Description

The subcarrier feedback detector circuit is comprised of the additional networks shown in figure B.3 that are connected to the networks of figure 11 at points A, B, and C. These points correspond to the points so marked in figure B.1. Through these connections, operational amplifier IC-1 of figure 11 becomes the feed-forward amplifier and amplifier IC-2 becomes the summing amplifier of figure B.1. Resistor R8, figure 11, adjusts the gain of IC-1 to produce zero (or minimum) ac voltage at point B in fulfillment of eqs (B.5) and (B.6).

Referring to figure B.3, the 5.5 MHz subcarrier voltage is generated in oscillator Q501 and amplified in stages Q502 and Q503 through Q506. The output voltage is applied directly to balanced modulator DBM501 which is a double-balanced mixer of the same type as described in section 5.2.2.3. The voltage-to-current converter, IC-501, is similar to that described in section 5.2.2.3 except that frequency compensating capacitors and the shunt output diode are omitted. Also, both dc and audiofrequency voltages from IC-2 are applied to the same input port, pin 2.

The modulated subcarrier is filtered by lowpass filter FL501 which has a cutoff frequency of 8.8 MHz. It is designed to have maximum rejection at the third harmonic frequency, 16.5 MHz, which is the most prominent spurious component from the balanced modulator.

Amplifier stages Q507 through Q510 and driver amplifier IC-502 provide closely the same rf voltage level across load resistor R538 as is present at input resistor R1 of figure 11. The circuit associated with subcarrier detector diode CR502 is designed and built to be as nearly like its counterpart in figure 11 as possible. In addition, diodes CR1 and CR502 are thermally coupled together in a heavy brass housing. One important difference between the two diode circuits is that the polarities of CR502 and constant-current source transistor Q511 are opposite to their counterparts in figure 11. This produces the 180-degree phase reversal required in the negative feedback circuit. Output voltage from CR502 is summed through resistor R541 with the output voltage from CR1 (through R540) at pin 2 of operational amplifier IC-503, thus accomplishing the difference amplifier function shown in figure B.1.

Resistors R548 through R552 provide feedback around IC-503 to produce a gain of approximately 300 in this stage for dc and near-zero frequencies. Additionally, capacitors C531 and C532 provide a nearly constant gain of 14 from approximately 3 Hz to 500 Hz. Above 500 Hz, gain falls gradually until at approximately 3.3 kHz and above, it is decreasing at the rate of 6 dB per octave. Potentiometer R551 permits gain adjustment for optimum compromise between maximum gain and adequate margin for amplifier stability.

The output voltage from IC-503 is summed through resistors R553 and R554 with the output voltage from IC-1 (through R9, fig. 11) at pin 2 of IC-2. The output voltage from IC-2 connects through resistor R512 to modulator-driver IC-501. This closes the feedback loop of the subcarrier detector circuit.

Potentiometer R554 permits the dc voltage at pin 6 of IC-503 to be set to zero in the absence of input voltage on pin 2.

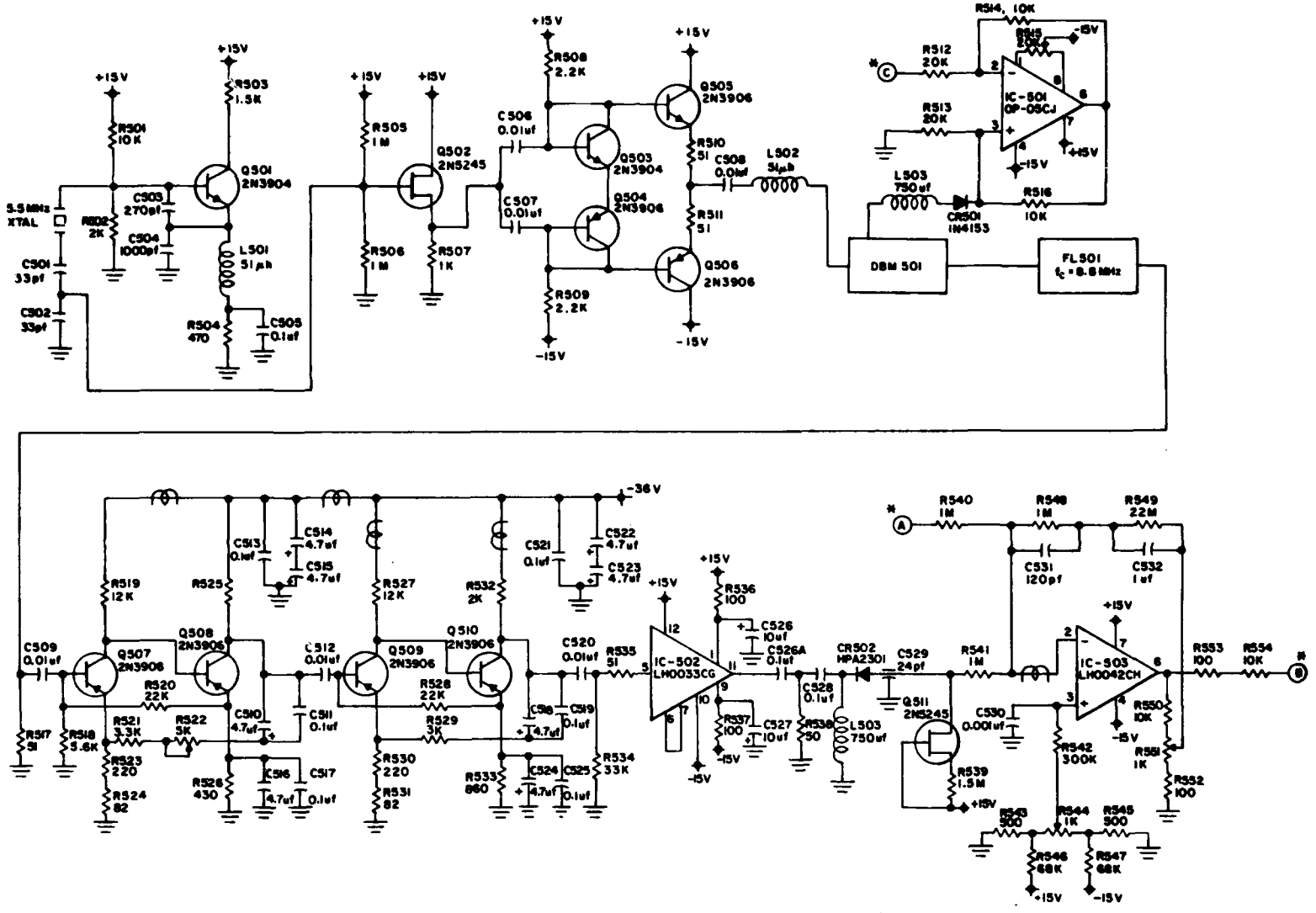

FIGURE B.3 SCHEMATIC DIAGRAM OF ADDITIONAL CIRCUITS FOR SUBCARRIER FEEDBACK DETECTOR .

* = SEE FIG. 11.
= FERRITE BEAD

B.2.3. Feedback Detector Accuracy

An error analysis of the type described in section 7 has not been made for the subcarrier feedback detector circuit. However, its measurement accuracy can be inferred by measuring the same amplitude-modulated signal with both detectors and comparing the results.

Tables B.1 through B.4 show the results of several sets of such measurements. The first two columns of figures are the original measurement data as read from the ratio voltmeter. The modulation factor of the rf signal was adjusted to produce exact readings at 0.1000 intervals from 0.1000 to 0.9000 as measured with the subcarrier feedback detector. Then the detector was quickly switched to the conventional configuration described in section 5, and the ratio voltmeter reading was recorded. Columns three and four show the corrected readings. Post-detector nonlinearity corrections were applied to both sets of data, and detector nonlinearity corrections were applied to only the conventional detector data. The frequency response correction was applied only for the 9960 Hz data.

Column five shows the differences between the corrected subcarrier feedback detector readings and the corrected conventional detector readings. Except at 9960 Hz, these differences are comfortably smaller than the target accuracy of $\pm$0.00125 (see sec. 2.3.2). At 9960 Hz the feedback loop gain is very small, and detector linearity suffers appreciably. Also note that the maximum modulation factor that could be measured at 9960 Hz with the subcarrier feedback detector was approximately 0.75. Above this point, slew-rate limiting in addition to phase shifts causes severe distortion of the waveform in the feedback branch, and the network output voltage drops precipitously.

Column six shows the measurement uncertainty for the conventional detector configuration (from sec. 6.2 and sec 6.3).

Additional measurements were made at a modulation frequency of 1020 Hz to indicate detector performance for non-ILS/VOR signals. The results are shown in tables B.5 and B.6 for filtered and unfiltered conditions, respectively. They indicate that the subcarrier feedback detector linearity is still quite good at 1020 Hz despite the decrease of loop gain above 500 Hz. The upper frequency limit for acceptable performance was not determined; but clearly from the data of tables B.4 and B.6, it must lie between 1 kHz and 10 kHz.

Table B.1. Comparison of detector measurements
110 MHz carrier frequency
30 Hz modulation frequency

Ratio voltmeter readings		Corrected readings			Measurement uncertainty of conventional
Feedback det.	Conventional det.	Feedback det.	Conventional det.	Reading difference	detector
0.1000	0.1036	0.1005	0.1006	-0.0001	0.00045
0.2000	0.2070	0.2003	0.2004	-0.0001	0.00080
0.3000	0.3103	0.2971	0.2973	-0.0002	0.00117
0.4000	0.4131	0.3953	0.3953	0.0000	0.00154
0.5000	0.5164	0.4954	0.4952	-0.0002	0.00191
0.6000	0.6196	0.5967	0.5965	-0.0002	0.00229
0.7000	0.7223	0.6979	0.6976	-0.0003	0.00267
0.8000	0.8247	0.7990	0.7988	-0.0002	0.00305
0.9000	0.9269	0.8955	0.9001	-0.0006	0.00342

Table B.2. Comparison of detector measurements
110 MHz carrier frequency
90 Hz modulation frequency

Ratio voltmeter readings		Corrected readings			Measurement uncertainty of conventional
Feedback det.	Conventional det.	Feedback det.	Conventional det.	Reading difference	detector
0.1000	0.1036	0.1000	0.1002	-0.0002	0.00027
0.2000	0.2071	0.1999	0.2001	-0.0002	0.00033
0.3000	0.3108	0.2998	0.3004	-0.0006	0.00041
0.4000	0.4140	0.3997	0.4001	-0.0004	0.00050
0.5000	0.5170	0.4996	0.4998	-0.0002	0.00059
0.6000	0.6202	0.5997	0.6000	-0.0003	0.00069
0.7000	0.7230	0.6998	0.7002	-0.0004	0.00079
0.8000	0.8255	0.7999	0.8005	-0.0006	0.00089
0.9000	0.9271	0.9000	0.9008	-0.0008	0.00099

Table B.3. Comparison of detector measurements
110 MHz carrier frequency
150 Hz modulation frequency

Ratio voltmeter readings		Corrected readings			Measurement uncertainty of
Feedback det.	Conventional det.	Feedback det.	Conventional det.	Reading difference	conventional detector
0.1000	0.1036	0.1004	0.1005	-0.0001	0.00027
0.2000	0.2070	0.2008	0.2009	-0.0001	0.00033
0.3000	0.3105	0.3009	0.3011	-0.0002	0.00041
0.4000	0.4137	0.4010	0.4011	-0.0001	0.00050
0.5000	0.5167	0.5010	0.5009	+0.0001	0.00059
0.6000	0.6200	0.6009	0.6010	-0.0001	0.00069
0.7000	0.7272	0.7008	0.7009	-0.0001	0.00079
0.8000	0.8252	0.8006	0.8009	-0.0003	0.00089
0.9000	0.9272	0.9003	0.9011	-0.0008	0.00099

Table B.4. Comparison of detector measurements
110 MHz carrier frequency
9960 Hz modulation frequency

Ratio voltmeter readings		Corrected readings			Measurement uncertainty of
Feedback det.	Conventional det.	Feedback det.	Conventional det.	Reading difference	conventional detector
0.1000	0.1015	0.1002	0.0983	+0.0019	0.00027
0.2000	0.2030	0.2002	0.1965	+0.0037	0.00033
0.3000	0.3043	0.3001	0.2944	+0.0057	0.00041
0.4000	0.4053	0.4001	0.3920	+0.0081	0.00050
0.5000	0.5060	0.5000	0.4895	+0.0105	0.00059
0.6000	0.6056	0.6000	0.5862	+0.0138	0.00069
0.7000	0.6943	0.7000	0.6724	+0.0276	0.00079
0.8000	0.7412	0.8000	0.7181	+0.0819	0.00089
0.8700	0.7676	0.8700	0.7439	+0.1261	0.00099

Table B.5. Comparison of detector measurements
110 MHz carrier frequency
1020 Hz modulation frequency, filtered

Ratio voltmeter readings		Corrected readings			Measurement uncertainty of
Feedback det.	Conventional det.	Feedback det.	Conventional det.	Reading difference	conventional detector
0.1000	0.1035	0.0991	0.0992	-0.0001	0.00027
0.2000	0.2068	0.1982	0.1982	0.0000	0.00033
0.3000	0.3103	0.2973	0.2974	-0.0001	0.00041
0.4000	0.4136	0.3968	0.3968	0.0000	0.00050
0.5000	0.5167	0.4964	0.4964	0.0000	0.00059
0.6000	0.6197	0.5964	0.5964	0.0000	0.00069
0.7000	0.7225	0.6968	0.6968	0.0000	0.00079
0.8000	0.8248	0.7975	0.7975	0.0000	0.00089
0.9000	0.9263	0.8986	0.8986	0.0000	0.00099

Table B.6. Comparison of detector measurements
110 MHz carrier frequency
1020 Hz modulation frequency, unfiltered

Ratio voltmeter readings		Corrected readings			Measurement uncertainty of
Feedback det.	Conventional det.	Feedback det.	Conventional det.	Reading difference	conventional detector
0.1000	0.1036	0.1002	0.1004	-0.0002	0.00027
0.2000	0.2070	0.2002	0.2003	-0.0001	0.00033
0.3000	0.3103	0.3001	0.3002	-0.0001	0.00041
0.4000	0.4138	0.4001	0.4003	-0.0002	0.00050
0.5000	0.5169	0.5001	0.5001	0.0000	0.00059
0.6000	0.6199	0.6000	0.6000	0.0000	0.00069
0.7000	0.7227	0.7000	0.7001	-0.0001	0.00079
0.8000	0.8253	0.8000	0.8004	-0.0004	0.00089
0.9000	0.9270	0.9000	0.9007	-0.0007	0.00099

B.3. Baseband Feedback Technique

A block diagram of the baseband feedback detector circuit is shown in figure B.4. Like the previous technique (sec. B.2), two matched diodes are used, one as the rf rectifier and the other in the feedback loop around an operational amplifier. The feedback forces the voltage at point B toward zero. If the waveform distortion caused by diode No. 2 is

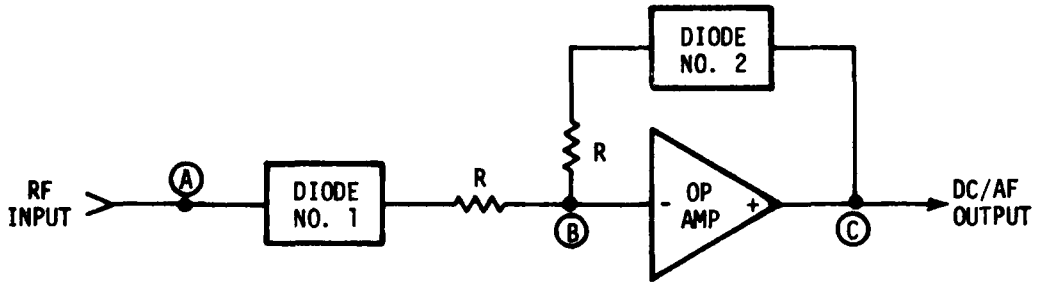

Fig. B.4. Block diagram of baseband feedback detector circuit

closely similar to that caused by diode No. 1, the waveform at point C (the input to diode No. 2) will be closely similar to the envelope of the waveform at point A (the input to diode No. 1).

In practice, even though the voltage at B is forced toward zero, the voltage at C does not replicate the envelope at A because the detailed waveform at A is at radiofrequency and that at C is at zero and audiofrequency. This causes the currents that flow in the two diodes to differ from each other, producing differences in their transfer characteristics.

Even so, the circuit of figure B.4 is more linear than a conventional detector without the diode feedback branch. The measurement results of an experimental detector circuit in which the feedback path could be either opened or closed are shown in table B.7. These results are expressed in terms of the calculated measurement error, Δm, as a function of modulation factor, m, caused by detector nonlinearity. The feedback detector error ranges from 13 percent to 21 percent of the conventional detector error.

It must be emphasized that the above results are preliminary. They obtain from unmodulated rf voltage measurements and calculations based on an assumed circuit model. However, because its modulation bandwidth capability may be quite large, this circuit may warrant further development.

Table B.7. Comparison of conventional and baseband feedback detectors
350 MHz carrier frequency

Modulation factor	Measurement error, Δm		Error ratio
	Conventional det.	Feedback det.	
0.10	-0.0017	0.00035	0.21
0.20	-0.0033	0.00063	0.19
0.30	-0.0048	0.00094	0.20
0.40	-0.0066	0.00125	0.19
0.50	-0.0080	0.00151	0.19
0.60	-0.0094	0.00171	0.18
0.70	-0.0107	0.00185	0.17
0.80	-0.0119	0.00188	0.16
0.90	-0.0129	0.00162	0.13

B.4. Quadratic Technique

A block diagram of the quadratic technique is shown in figure B.5. The envelope detector output voltage, v_n, is applied to two networks: (1) The quadratic network, and (2) one input to the difference amplifier.

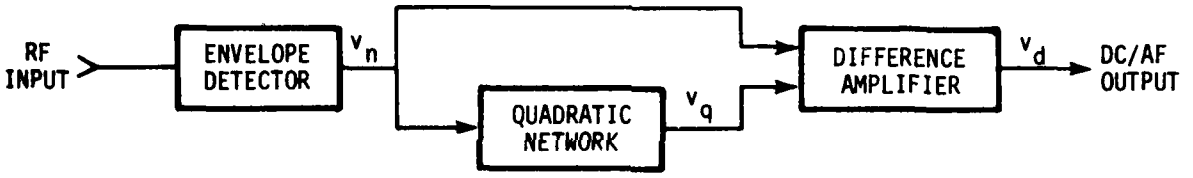

Fig. B.5. Block diagram of quadratic technique

The output voltage of the quadratic network, v_q, is given by the equation,

$$v_q = A + Bv_n + Cv_n^2, \tag{B.7}$$

where A, B, and C are constants. Voltage v_q is subtracted from v_d by the difference amplifier. If constants A, B, and C are chosen such that v_q is closely similar to the envelope distortion produced by the detector, then the difference amplifier output voltage, v_d, will be closely similar to the envelope of the rf input voltage.

The constants of eq (B.7) are determined as follows: First, the detector transfer characteristic is measured by the procedure described in section A.2.1. This procedure produces a set of input-voltage/output-voltage data pairs, $\{v_o, v_n\}$, over the range of the detector. (Refer also to eq (A.5).) Each data pair is inserted into the equation,

$$v_n - v_o = A + Bv_n + Cv_n^2. \tag{B.8}$$

By eq (B.8), we are attempting to represent the voltage difference, $v_n - v_o$, (i.e., the detector distortion) by a quadratic model. Using the set of equations obtained by inserting the set of data pairs v_o, v_n into eq (B.8), the constants are calculated by the polynomial regression method [23].

Using these values for A, B, and C, voltage v_q simulates the detector distortion voltage, $v_n - v_o$. That is,

$$v_q \simeq v_n - v_o. \tag{B.9}$$

Then,

$$v_d = v_n - v_q \tag{B.10}$$

$$\simeq v_o, \tag{B.11}$$

where v_o is the envelope voltage of the rf input signal.

The above procedure was applied to the baseband feedback detector of figure B.4, yielding the following constant values:

A = 0.0188 volt
B = -0.0136
C = 0.0012 per volt-squared.

A block diagram of the quadratic network is shown in figure B.6. Constant A is a voltage source. Constants B and the square root of C are set by the gains of operational amplifiers. An analog multiplier produces the quadratic term. The three terms are combined in the summing amplifier as shown.

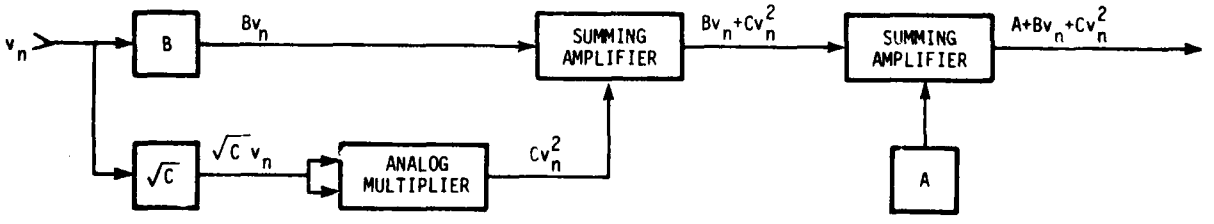

Fig. B.6. Block diagram of the quadratic network

The measurement results of an experimental quadratic network used in conjunction with the baseband feedback detector described in section B.3 are shown in table B.8. These results are expressed in terms of the calculated measurement error, Δm, as a function of

modulation factor, m, caused by detector nonlinearity. This quadratic network improved the measurement accuracy mostly in the range between 50 and 90 percent modulation. However, the measurement error overall was comfortably less than the target accuracy of 0.00125.

Table B.8. Comparison of the quadratic technique, applied to the baseband feedback detector, and the baseband feedback detector alone

Modulation factor	Measurement error, Δm		Error ratio
	Feedback det.	Quadratic tech.	
0.10	0.00035	0.00029	0.82
0.20	0.00063	0.00055	0.87
0.30	0.00094	0.00076	0.81
0.40	0.00126	0.00088	0.70
0.50	0.00151	0.00088	0.58
0.60	0.00171	0.00072	0.42
0.70	0.00185	0.00038	0.21
0.80	0.00188	-0.00012	-0.06
0.90	0.00162	-0.00090	-0.56

It must be emphasized that the above results are preliminary. They obtain from unmodulated rf voltage measurements and calculations based on an assumed circuit model.

The primary limitation on the quadratic technique is the linearity and bandwidth of the analog multiplier. A high speed (5 MHz) multiplier was used in this work, but its characteristics in this network were not fully evaluated.

A network based on a quadratic equation, eq (B.7), may not provide a sufficient simulation of the detector distortion in some applications. A more powerful network, from the standpoint of circuit modeling, is shown in figure B.7. This is an infinite power series network whose input/output relationship is given by the equation,

$$v_y = D + \frac{Ev_x + Fv_x^2}{1 - Gv_x} . \qquad (B.12)$$

It has four degrees of freedom, compared with three for the quadratic network, and can be assembled from the same types of network components as used in figure B.6. This network was not investigated during this work.

$$v_y = D + \frac{Ev_x + Fv_x^2}{1 - Gv_x}$$

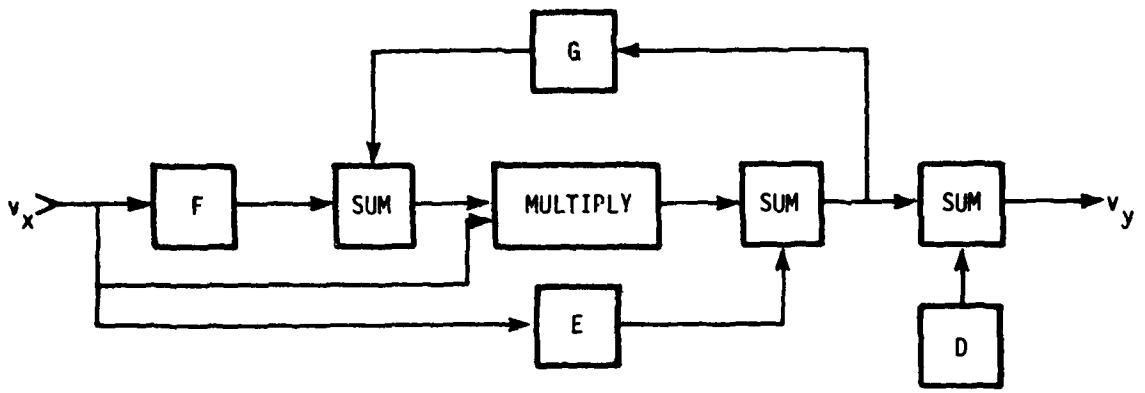

Fig. B.7. Block diagram of the infinite power series network

Appendix C. The Newton-Raphson Method

No general method exists for finding the exact roots of transcendental equations such as the equations for S_0 and S_1 discussed in section A.2.2. (These are eqs (C.10) and (C.11), given below.) Several approximation methods are available [22], one of which is the Newton-Raphson method described here.

When the derivative, $f'(x)$, of a function, $f(x)$, is easily evaluated numerically, the real roots of $f(x) = 0$ may be determined as follows: Let x_0 be an approximate value of one of the roots. Then an improved value, x_i, of the root is given by

$$x_i = x_0 - \frac{f(x_0)}{f'(x_0)}. \tag{C.1}$$

The next approximation is found by substituting x_i in place of x_0 to get a new value of $f(x_0)/f'(x_0)$, continuing in this way as long as necessary. In practice, after a few approximations the value of the derivative will change very little with succeeding values of x_i, and hence f' need not be recomputed further.

In the application of the Newton-Raphson method in section A.2.2, the derivative typically changes by a few parts in one billion, or less, after two improved values of x_i are computed. Thus, the convergence to an acceptably accurate value is very quick.

The basic method outlined above is applied as follows. Begin with eq (A.2):

$$v_o(t) = kV_c(1 + m \cos 2\pi f_m t) \tag{A.2}$$

For simplicity of notation, set

$$2\pi f_m t = \emptyset \tag{C.2}$$

and

$$kV_c \approx A, \tag{C.3}$$

so that (A.2) becomes

$$v_o(\emptyset) = A(1 + m \cos \emptyset). \tag{C.4}$$

Then,

$$[v_o(t)]^2 = A^2[1 + \tfrac{1}{2}m^2 + 2m \cos \emptyset + \tfrac{1}{2}m^2 \cos 2\emptyset], \tag{C.5}$$

$$[v_o(t)]^3 = A^3[(1 + \tfrac{3}{2}m^2) + (3m + \tfrac{3}{4}m^3) \cos \emptyset + \tfrac{3}{2}m^2 \cos 2\emptyset + \tfrac{1}{4}m^3 \cos 3\emptyset]. \tag{C.6}$$

$$[v_o(t)]^4 = A^4[1 + 3m^2 + \frac{3}{8}m^4) + (4m + 3m^3)\cos \emptyset +$$

$$+ (3m^2 + \frac{1}{2}m^4)\cos 2\emptyset + m^3\cos 3\emptyset + \frac{1}{8}m^4\cos 4\emptyset], \quad (C.7)$$

and

$$[v_o(t)]^5 = A^5[(1 + 5m^2 + \frac{15}{8}m^4) + (5m + \frac{15}{2}m^3 + \frac{5}{8}m^5)\cos \emptyset +$$

$$+ (5m^2 + \frac{5}{2}m^4)\cos 2\emptyset + (\frac{5}{2}m^3 + \frac{5}{16}m^5)\cos 3\emptyset +$$

$$+ \frac{5}{8}m^4\cos 4\emptyset + \frac{1}{16}m^5\cos 5\emptyset]. \quad (C.8)$$

Substituting eqs (C.3) through (C.8) into (A.5), truncated after the fifth degree term, gives

$$v_n(t) = B_o t + B_1 V_c[1 + m\cos \emptyset] +$$

$$+ B_2 V_c^2[(1 + \frac{1}{2}m^2) + 2m\cos \emptyset] + B_3 V_c^3[(1 + \frac{3}{2}m^2) + (3m + \frac{3}{4}m^3)\cos \emptyset] +$$

$$+ B_4 V_c^4[(1 + 3m^2 + \frac{3}{8}m^4) + (4m + 3m^3)\cos \emptyset] +$$

$$+ B_5 V_c^5[(1 + 5m^2 + \frac{15}{8}m^4) + (5m + \frac{15}{2}m^3 + \frac{5}{8}m^5)\cos \emptyset] +$$

plus higher degree terms in cos 2$\emptyset$, cos 3$\emptyset$, cos 4$\emptyset$, and cos 5$\emptyset$. (C.9)

The sum of the terms in eq (C.9) that do not include cos n$\emptyset$ is extracted and set equal to S_o. This sum represents the dc part of voltage, $v_n(t)$, and is written out as eq (C.10).

$$S_o = B_o + B_1 V_c + B_2 V_c^2(1 + \frac{1}{2}m^2) + B_3 V_c^3(1 + \frac{3}{2}m^2) +$$

$$+ B_4 V_c^4(1 + 3m^2 + \frac{3}{8}m^4) + B_5 V_c^5(1 + 5m^2 + \frac{15}{8}m^4). \quad (C.10)$$

The sum of the terms in eq (C.9) that are coefficients of cos $\emptyset$ is extracted and set equal to S_1. This sum represents the amplitude of the ac component of $v_n(t)$ of frequency f_m, and is written out as eq (C.11).

$$S_1 = B_1 V_c m + 2B_2 V_c^2 m + B_3 V_c^3 (3m + \frac{3}{4} m^3) +$$

$$+ B_4 V_c^4 (4m + 3m^3) + B_5 V_c^5 (5m + \frac{15}{2} m^3 + \frac{5}{8} m^5). \qquad (C.11)$$

Equations (C.10) and (C.11) contain ten quantities: m, V_c, B_0, B_1, B_2, B_3, B_4, B_5, S_0, and S_1. The six B coefficients are determined experimentally as described in section A.2.1. S_0 and S_1 are measured by the modulation meter (see next paragraph below). This leaves the two quantities, m and V_c, as unknowns to be found by the Newton-Raphson method.

The numeric value of S_0 is measured by the modulation meter's RF CARRIER LEVEL voltmeter (see fig. 5). The numeric value of S_1 is found by measuring the voltage ratio, S_1/S_0, with the modulation meter's ratio voltmeter (see fig. 5) and multiplying by S_0.

Now, <u>calculate</u> a numeric value, S_{0n}, of S_0 by substituting into eq (C.10) the values of the six B coefficients and the <u>first approximate values</u> of V_c and m. The measured value of S_0 is a suitable first approximate value of V_c, and the measured voltage ratio, S_1/S_0 (called the ratio voltmeter reading, M, in sec. 4.2.2), is a suitable first approximate value of m.

Similarly, calculate a numeric value, S_{1n}, of S_1 by substituting S_0 and M into eq (C.11).

From differential calculus, the difference, ΔS_0, between S_0 and S_{0n} is, to a first order approximation, given by

$$\Delta S_0 \doteq \frac{\partial S_0}{\partial V_c}\bigg|_{V_c,m} \cdot \Delta V_c + \frac{\partial S_0}{\partial m}\bigg|_{V_c,m} \cdot \Delta m. \qquad (C.12)$$

In words, eqs (C.10) and (C.12) say, "Given S_0 as a function of V_c and m, and given S_{0n} as an estimate of S_0, the difference between S_0 and S_{0n} (i.e., the "error" in S_{0n}) is, to a first approximation, the slope $\partial S_0/\partial V_c$, of the function at point $[V_c, m]$ times the "error", ΔV_c, in V_c, plus the slope, $\partial S_0/\partial m$, of the function at point $[V_c, m]$ times the "error", Δm, in m."

Similarly, the difference, ΔS_1, between S_1 and S_{1n} is given approximately by

$$\Delta S_1 \doteq \frac{\partial S_1}{\partial V_c}\bigg|_{V_c,m} \cdot \Delta V_c + \frac{\partial S_1}{\partial m}\bigg|_{V_c,m} \cdot \Delta m. \qquad (C.13)$$

The partial derivatives in eqs (C.12) and (C.13) are found analytically from eqs (C.10) and (C.11) (see below). ΔV_c and Δm are then found by solving eqs (C.12) and (C.13) as simultaneous equations. This is facilitated by the matrix operations as follows. Let

$$[\partial] = \begin{bmatrix} \left.\frac{\partial S_o}{\partial V_c}\right|_{V_{c,m}} & \left.\frac{\partial S_o}{\partial m}\right|_{V_{c,m}} \\ \left.\frac{\partial S_1}{\partial V_c}\right|_{V_{c,m}} & \left.\frac{\partial S_1}{\partial m}\right|_{V_{c,m}} \end{bmatrix} \tag{C.14}$$

$$[\Delta] = \begin{bmatrix} \Delta V_c \\ \Delta m \end{bmatrix} \tag{C.15}$$

and

$$[\delta] = \begin{bmatrix} \Delta S_o \\ \Delta S_1 \end{bmatrix} \tag{C.16}$$

Then, from eqs (C.12) and (C.13),

$$[\partial] \cdot [\Delta] = [\delta] \tag{C.17}$$

$$[\partial]^T \cdot [\partial] \cdot [\Delta] = [\partial]^T \cdot [\delta] \tag{C.18}$$

and

$$[\Delta] = ([\partial]^T \cdot [\partial])^{-1} \cdot [\partial]^T \cdot [\delta]. \tag{C.19}$$

The partial derivatives in eqs (C.12) and (C.13), obtained from eqs (C.10) and (C.11), are as follows:

$$\frac{\partial S_o}{\partial V_c} = B_1 + 2B_2V_c(1 + \frac{1}{2}m^2) + 3B_3V_c^2(1 + \frac{3}{2}m^2) +$$

$$+ 4B_4V_c^3(1 + 3m^2 + \frac{3}{8}m^4) + 5B_5V_c^4(1 + 5m^2 + \frac{15}{8}m^4) \tag{C.20}$$

$$\frac{\partial S_o}{\partial m} = B_2V_c^2m + 3B_3V_c^3m +$$

$$+ 6B_4V_c^4(m + \frac{1}{4}m^3) + 10B_5V_c^5(m + \frac{3}{4}m^3) \tag{C.21}$$

$$\frac{\partial S_1}{\partial V_c} = B_1 m + 4B_2 V_c m + 9B_3 V_c^2 (m + \frac{1}{4}m^3) +$$

$$+ 16B_4 V_c^3 (m + \frac{3}{4}m^3) + 25B_5 V_c^4 (m + \frac{3}{2}m^3 + \frac{1}{8}m^5) \qquad (C.22)$$

$$\frac{\partial S_1}{\partial m} = B_1 V_c + 2B_2 V_c^2 + 3B_3 V_c^3 (1 + \frac{3}{4}m^2) +$$

$$4B_4 V_c^4 (1 + \frac{9}{4}m^2) + 5B_5 V_c^5 (1 + \frac{9}{2}m^2 + \frac{5}{8}m^4) \qquad (C.23)$$

ΔV_c and Δm are, to a first approximation, the changes in V_c and m that account for the difference, ΔS_0, between S_0 and S_{0n}, and the difference, ΔS_1, between S_1 and S_{1n}, simultaneously. Having found ΔV_c and Δm by eq (C.19), second (improved) approximations of V_c and m are computed by adding ΔV_c and Δm to the first approximation. The computational process is repeated until successive values of ΔV_c and Δm become acceptably small. The resulting approximations are the desired values of V_c and m.